DEGRADATION AND RECOVERY OF POLYDIMETHYLSILOXANE (PDMS) BASED COMPOSITES USED AS HIGH VOLTAGE INSULATORS

by

TECLESENBET ABRAHAM BERHANE

Thesis presented in partial fulfilment of the requirements for the degree of Master of Science (Polymer Science)

at the

University Stellenbosch

Study leader

Dr. P. E. Mallon

Stellenbosch

December 2004

Declaration

I, the undersigned, hereby declare that the work contained in this thesis is my original work and that I have not previously in its entirety or in part submitted it at any university for a degree.

Signature Date

VAK: .....

TITELNR.: 632588.....

DATUM: .....

SKENKER/HERKOMS: .....

.....

BESIT: .....

DUPLIKAATOPNAME: .....

HANDTEKENING: .....

BESTEMMING: .....

Abstract

Polydimethylsiloxane (PDMS) compounds are utilized in outdoor high voltage insulation due to their low weight, vandalism resistance, better anti-contamination performance and their superior hydrophobic nature. Under severe environmental conditions and over prolonged service time, however, the hydrophobic surface can gradually become hydrophilic and then recover with adequate resting period.

In this study, room temperature vulcanized (RTV) PDMS samples were prepared with different formulations and then exposed to corona discharge to evaluate its effect. The influence of different additives, such as different types and amount of fillers and additionally added low molar mass silicone oils, on the hydrophobicity recovery of the material was investigated. The effects of two types of corona treatment were also evaluated.

Hydrophobicity recovery of corona and UV-C aged PDMS samples was evaluated by means of static contact angle measurements.

Positron annihilation spectroscopy (PAS) gave important information on the micro structural change after corona treatment of RTV PDMS as well as naturally aged high temperature vulcanized (HTV) PDMS samples. The different formulations of the RTV PDMS samples and the effect of the additives were studied with this technique. The formation of a thin, highly crosslinked inorganic silica-like (SiO_X) layer was confirmed even at the early stage of degradation. It was also possible to estimate the thickness of the silica-like layer formed during corona exposure that is responsible for the loss and recovery of hydrophobicity.

The surface hardness and hydrophilicity change of PDMS samples due to corona treatment were studied simultaneously with force distance measurements by atomic force microscopy (AFM). The adhesive force calculated from the pull-off force-distance curves showed that the adhesive force between the probe and the sample decreased with increasing corona treatment time, indicating hydrophobicity recovery. In addition to this, the increase in hardness after corona exposure provides indirect evidence of the formation of a silica-like layer. In all cases the hydrophilicity and the surface hardness of the PDMS samples increased directly after corona treatment and recovered with time. Two types of FTIR spectroscopy were used to analyse the surface of the polymer.

Opsomming

Polidimetielsiloksaan (PDMS) word in buitelug hoogspanninginsulasie gebruik as gevolg van sy lae massa, weerstand teen vandalisme, verbeterde anti-kontaminasie werkverrigting en superieure hidrofobiese karakter. Die hidrofobiese oppervlakte kan egter gelydelik hidrofillies word onder uiterste omgewingsomstandighede en oor langdurige dienstyd. PDMS materiaal herstel egter nadat dit genoeg rustyd toegelaat is.

Kamertemperatuur-gevulkaniseerde (KTV) PDMS met verskillende formulasies is in hierdie studie voorberei, aan korona ontlading blootgestel, geëvalueer en vergelyk. Die invloed van bymiddels soos verskillende tipes en hoeveelhede vuller, asook addisionele lae molekulêre massa silikoonolie, op die herstel van hidrofobisiteit van die materiaal is ondersoek. Twee verskillende metodes van korona behandeling is ook geëvalueer.

Die herstel van hidrofobisiteit van korona en UV-C verouderde PDMS monsters is met statiese kontakhoekmeting geëvalueer.

Positronvernietigingspektroskopie (PVS) is 'n kragtige tegniek wat belangrike inligting oor die mikrostrukturele verandering van korona behandelde van KTV PDMS sowel as natuurlik-verouderde hoë temperatuur gevulkaniseerde (HTV) PDMS monsters gee. Die verskillende formulasies van die KTV PDMS monsters, sowel as die effek van die vullers, is met behulp van hierdie tegniek ondersoek. Die vorming van 'n dun, hoogs-kruisgebinde, anorganiese silika-agtige (SiO_x) laag op die PDMS oppervlak, selfs tydens die vroeë stadium van degradasie, is bevestig. Dit was ook moontlik om die dikte van die silika-agtige laag wat gedurende die korona blootstelling gevorm het, en wat verantwoordelik is vir die verlies aan hidrofobisiteit, te bepaal.

Die oppervlakhardheid en hidrofilisiteit verandering van PDMS monsters as gevolg van korona behandeling, was gelyktydig met krag-afstand metings deur middel van atoomkragmikroskopie (AKM) bestudeer. Die kleefkrag, soos bereken van aftrek krag-afstandkurwes, dui daarop dat kleefkragte tussen die taster en die monster afneem met toenemende korona behandelingstyd, wat beduidend is op die herstel van hidrofobisiteit. Daarbenewens is die toename van oppervlakhardheid na korona blootstelling 'n indirekte bewys van die formasie van 'n silika-agtige laag. In alle gevalle het die hidrofilisiteit en die oppervlakhardheid van die PDMS monsters toegeneem direk na afloop van korona behandeling en gevolglik herstel met tyd. Twee tipes IR

spektroskopie metodes is gebruik vir die chemiese-oppervlak analises.

Acknowledgements

I wish to express my sincere gratitude and appreciation to the following persons and institutions that provided me with invaluable support during my study:

Dr P. E. Mallon for his guidance generously shared his knowledge, time, energy, continued advice and fruitful comments on my work as well as for his friendly attitude. I always thank for his willingness and always having time for discussion

Dr M. Meincken for recording AFM results and for valuable discussions

Ms C. J. Greyling for sharing her knowledge with me

Dr Margie Hundall for taking such care trying to correct my grammar and for her fruitful suggestions. Thanks for all your time and effort.

Eritrean Human Resources Development (EHRD), for giving me an opportunity to study at the University of Stellenbosch and for the financial support

Eskom for the financial support of this project

The positron annihilation spectroscopy group of University of Missouri Kansas City for the positron analysis

The University of Stellenbosch, in particular the Department of Chemistry and Polymer Science is acknowledged

Thanks for all polymer science students, especially Ms V. Cloete who translated the abstract to Afrikaans

My family for their love and encouragement

Finally I wish to extend my appreciation to all my friends, here in Stellenbosch and all over, for their motivation and intellectual stimulation.

My acknowledgement of gratitude expressed here goes beyond the limits of the brief way in which it is recorded.

Dedicated to my mother

List of Abbreviations

AFM	Atomic force microscopy/microscope
ATH	Aluminium tri-hydrate
ATR-FTIR	Attenuated total reflection - Fourier transform infrared
DBA	Dry-band arcing
DCA	Dynamic contact angle
EDAX	Energy depressive X-ray analysis
EPDM	Ethylene propylene diene monomer
EPM	Ethylene propylene monomer
ESCA	Electron spectroscopy for chemical analysis
FTIR	Fourier transform infrared
HTV	High temperature vulcanized
HV	High voltage
KeV	Kilo electron volt
KIPTS	Koeberg insulator pollution test site
KV	Kilo volt
LMW	Low molecular weight
mA	mili-Ampere
NCI	Non ceramic insulators
o-Ps	Ortho-positronium
PAL	Positron annihilation lifetime spectroscopy
PAS	Positron annihilation spectroscopy
Pas	Photoacoustic spectroscopy
Ps	Positronium
PDMS	Polydimethylsiloxane
rms	Root mean square value of an alternative voltage or current

RTV	Room temperature vulcanized
SCA	Static contact angle
SEM	Scanning electron microscopy/microscope
SIR	Silicone rubber
SiO_X	Silicone oxide where X is bonded to 3 or 4 oxygen atoms
US	Ultrasonic bath
UV	Ultraviolet
XPS	X-ray photoelectron spectroscopy

Table of Contents

List of Figures

List of Tables

Chapter One

Introduction and Objectives

1.1. Introduction

Ceramic materials such as porcelain and glass have been used in outdoor high voltage insulation for many years and are still widely used for this purpose because of their excellent durability, specifically their ability to withstand heat and dry-band arcing. They are inert and stable to substantial amounts of arcing without serious surface degradation [1]. However, these materials are highly wettable when exposed to wet conditions like fog, drizzle, dew and rain, because of their high surface energy. When these materials are both contaminated and wet, leakage current develops which may lead to flashover and may be followed by a power system outage.

Recently, there has been a tremendous growth in the application of non-ceramic composite polymeric insulators in place of the conventional inorganic ceramics in high voltage insulation [2-4]. Silicone rubbers, mainly polydimethylsiloxane (PDMS), have received much attention as substitutes for the heavy and wettable porcelain and glass, especially in areas of high pollution. PDMS offers several significant advantages when compared to the traditional glass and porcelain. These advantages are: low weight, good electrical properties, better performance under conditions of wet and severe pollution and, above all, excellent water repellence and comparable or even better ability to withstand high voltage compared to porcelain or glass insulators [5]. PDMS is also thermally stable and performs over a wide temperature range. Polydimethylsiloxane compounds are used as the bulk material in the construction of the sheds of high voltage insulators as well as a coating for porcelain and glass to improve their hydrophobic behaviour under wet conditions. In South Africa, Eskom is currently employing PDMS elastomers both as high voltage composite suspension insulators as well as coatings on porcelain line and sub-station insulators.

As mentioned above, PDMS polymer has the unique property that it is hydrophobic in environmentally wet conditions. However, under severe environmental conditions and after prolonged service, the hydrophobic surface gradually becomes hydrophilic due to electrical discharge. The resulting hydrophilic polymer promotes spreading of water on its surface, which becomes conductive due to the formation of dissolved pollutants, and this may lead to flashover, which is the main cause of material damage [6].

The hydrophilic surface of PDMS (silicone rubber) created by partial discharge regains its hydrophobic nature partially or fully after a certain time, once the partial discharge is removed. The unique performance of the PDMS composite-based insulators is directly attributed to the ability of these materials to maintain and recover their surface hydrophobicity in the presence of severe contamination and under wet conditions. It is due to this low wettablity and the ability to recover that PDMS insulators are utilized and perform exceptionally well in extremely polluted environments [7].

The underlying processes for the hydrophobicity recovery suggested by various researchers are:

1) Diffusion of the low molecular weight (LMW) silicones from the bulk to the surface [8-10]

2) The re-orientation, by conformational change of the molecule in the surface region to the bulk [11-12]. The LMW silicone oils that migrate to the surface of the polymer could arise from:

- ✧ Incomplete curing
- ✧ Addition of silicone liquids as processing aids
- ✧ Breakdown of the PDMS polymer molecule (*in-situ*).

In addition to PDMS, other important non ceramic insulators (NCIs) that are widely used in high voltage insulation are: ethylene propylene diene monomer rubber (EPDM), ethylene propylene monomer (EPM), and cyclo aliphatic and aromatic epoxys. Additionally, for low voltage in outdoor or indoor applications, high-density propylene (HDPE), polyurethane and polytetrafluoroethylene (PTFE) are used. Most polymeric materials display good anti-contamination performance only in the early stages of service. Silicone rubber insulators, however, maintain their high hydrophobicity even after long-term outdoor use.

As mentioned above, the chief advantages of non ceramic insulators over conventional porcelain and glass insulators are:

- Light weight,
- Superior to vandal resistance (non-shattering) and
- They exhibit better anti-contamination performance [13, 14]. A 90% reduction in weight is achieved when employing PDMS insulators. The light weight of the composite

PDMS insulator strings permits an increase in the clearance distance between conductors to ground and an increase in the phase-to-phase distance, in order to reduce the electric and magnetic fields. The light weight of the PDMS composite insulators also makes them easier to handle and install and this saves on insulation costs. More importantly, they are preferable to other types of insulators due to the hydrophobicity of the surface of the material that contributes to the suppression of leakage current. PDMS insulators tend to form droplets rather than a film on a wet surface.

One drawback of PDMS insulators compared to inorganic porcelain or glass insulators is that they are subjected to material ageing with time upon exposure to discharge and arcing. Other environmental factors such as ultraviolet radiation from sunlight, acid rain, temperature and flammability also contribute to the degradation of the material.

The main disadvantages of polymeric insulators are: [1, 2, 15-16]

- They are subjected to chemical change on the surface due to weathering and from electrical discharging (dry band arcing)
- They suffer from erosion and tracking, which may lead to failure of the insulation
- Faulty insulators are difficult to detect
- Life expectancy is difficult to evaluate, because of relatively little experience with such insulators to date.

The silicone rubber in PDMS insulators is not passive, but reacts actively with its environment. Many different physical and chemical processes occur, and most of them are not well understood. For this reason, it is difficult to evaluate how long the insulator surface will be hydrophobic, or how long it will take to recover its hydrophobicity.

Different fillers may be added to PDMS to increase the mechanical values and tracking performance of the insulators. For a given material, the higher the filler content the higher the tracking performance will be [17], but lower hydrophobic properties are also probable. The challenge lies in determining a well-balanced system of filler and other formulations. Therefore, it is important to gain a good understanding of the influence of different formulations of the PDMS insulators on their performance, as well as to correlate results of the field aged and accelerated laboratory-aged samples.

1.2 Koeberg insulator pollution test station (KIPTS)

The Koeberg insulator natural ageing test station is situated along the Western Cape coast (South Africa), about 50 meters from the sea. The site is generally recognized as a severe coastal test station for determining the pollution and ageing performance of outdoor insulators. At the KIPTS test site various types of energized insulators have been exposed to the environment. The test station consists of test bays for 11, 22, 33, 66 and 132 KV as well as a complete control room for environmental monitoring, a pollution monitoring station and leakage current logger system [7]. The test station was established in 1994 to evaluate the performance of different types of insulators and is financially supported by the South African National Energy Council, Eskom.

The climatic conditions at KIPTS are characterized by dry summers with high winds, mist banks and heavy marine and industrial pollution. According to an environmental survey done by W. L. Vosloo in the Koeberg area [7], the suggested sources of pollution are marine, industrial and agricultural, originating mainly from:

- The Atlantic Ocean which lies to the west of the test station, where wave action, sea breezes/winds and periodic mist banks are the cause of an influx of moisture and salt particles in the vicinity of the test station
- The breakwater wall at the Koeberg Nuclear plant north of KIPTS that causes local salt mist bank to occur
- Pollution from the eastern agricultural area, caused by ploughing, harvesting and crop spraying
- An industrial area emits burnt diesel, coal and heavy oil from the north east
- Nearby heavy industries such as a fertilizer and a lime plant and an oil refinery are the main causes of severe particle emissions.

The pollution index at KIPTS is in the order of 2000 μs/cm, which is classified as very high. The test site has both marine and industrial pollution condensation, which makes it an ideal environment in which to evaluate insulator products. The climate at KIPTS is generally similar to that of Cape Town. KIPTS is situated 20 km north of Cape Town, on the Southwestern tip of Africa, and the climate of the region is classified as a Mediterranean climate. The long-term average annual rainfall is 400 mm and the rainy season is in winter. Koeberg generally has an ambient temperature with moderate variations especially when the wind is onshore. The west coast is liable to have a

considerable amount of fog due to cooling of moisture over the Benguela current. Most of the time, the fog forms at sea and drifts inland on a light westerly breeze. The fog persists until sunrise if the ground is cold. It is believed that the wind, the speed of which can be extremely high, is the main carrier of pollution at KIPTS. The westerly wind brings marine pollution and the south-easterly wind brings industrial pollution, the north-easterly wind brings rain and the easterly wind tends to be hot.

1.3 Objectives

The overall aim of this research was to contribute to the fundamental understanding of the polydimethylsiloxane material used in high voltage insulators. It is mainly focused on the mechanisms of degradation of the material and evaluation of the loss and recovery of hydrophobicity. Gaining a greater understanding of the fundamental mechanisms and processes involved in the material degradation can contribute to the prediction of the life-term performance of PDMS insulators in-service. This fundamental understanding will also allow for a better understanding of the processes that lead to the failure of in-service insulators. It should assist in determining the exact mechanisms of material degradation that may have lead to failure in these insulators.

One objective was to determine the role of the various components of PDMS in terms of material performance, especially the different types and proportions of polymers and fillers used, including the externally added low molecular weight silicone oils. The study includes consideration of the laboratory-prepared PDMS samples with controlled formulations as well as commercially available samples of HTV PDMS.

A further objective was to draw a correlation between the laboratory aged and naturally aged samples. This part of study includes an investigation into the effect of cleaning of the pollution of the naturally aged sample before analysis to eliminate interference of the pollutants during the analysis. The naturally aged samples were in service at Koeberg insulation pollution test site for one year.

Yet other objective was to investigate the effectiveness of the many existing surface analysis techniques to track the material degradation as well as to investigate and possibly develop new techniques and methods to evaluate the material degradation. This included the use of positron annihilation spectroscopy and AFM.

1.4 Structure of the thesis

This thesis is organized into and presented in five chapters.

Chapter 1 provides a general introduction to the subject and the basic theory of insulator pollution, as well as background information on the Koeberg insulator pollution test site. The research aim and objectives are set out.

In Chapter 2, gives a brief background to insulators. The historical and theoretical background of non ceramic insulators (NCI) is also discussed. It includes a literature survey of the existing research relevant to this study.

Chapter 3 describes the experimental work carried out. It includes the preparation of the moulded materials to be studied and a discussion of the basic theory of instrumentation used for material analysis.

Chapter 4 describes the result of the above and a discussion of the findings.

Chapter 5 contains conclusions derived from this study and presents recommendations for future studies.

1.5 References

1. S. H. Kim, E. A. Cherney and R. Hackam, IEEE Trans. on Elect. Insul., Vol. 27, 1065-1072, 1992.
2. R. Hackam, IEEE Trans. Diel. Elect. Insul., Vol. 6, 556-585, 1999.
3. J. Kim, M. K. Chaudhury, M. J. Owen and T. Orbeck, J. Colloid Interface Sci. Vol. 244, 200-207, 2001.
4. J. K. Kim and I. H. Kim, J. Appl. Polym. Sci., Vol. 79, Issue 12, 2251-2257, 2001.
5. J. F. Hall, IEEE. Trans. on Power Delivery, Vol. 8, 376-384, 1993.
6. S. Kumagai, X. Wang and N. Yoshimura, IEEE, Trans. Diel. Elect. Insul., Vol.5, 281-289, 1998.
7. W. L. Vosloo, A comparison of the performance of high voltage insulator materials in a severely polluted coastal environment, PhD dissertation, University of Stellenbosch, 2002.
8. H. Hillborg, S. Karlsson and U. W. Gedde, Polymer, Vol. 42, 8883-8889, 2001.
9. H. Hillborg and U. W. Gedde, Polymer, Vol. 39, 1991-1998, 1998.
10. H. Janssen, A. Herden and H. C. Kärner, The loss and recovery of hydrophobicity

on silicone rubber surfaces, 10th International Symposium on High Voltage Engineering, Montreal, Canada, 1997.

11. M. Morra, E. Occhiello, R. Marola, F. Garbassi, P. Humphrey and D. Johnson, J Colloid Interface. Sci., Vol. 137, 11-24, 1990.
12. S. H. Kim, E. A. Cherney and R. Kackam, IEEE Trans. on Power Delivery., Vol. 6, 1549-1556, 1991.
13. T. G. Gustavsson, S. M. Gubanski, H. Hillborg, S. Karlsson and U. W. Gedde, IEEE Trans. Diel. Elect. Insul., Vol. 8, 1029-1039, 2001.
14. S. H. Kim, E. A. Cherney, R. Hackam and K. G. Rutherford, IEEE Trans. Diel. Elect. Insul., Vol. 1, 106-122, 1994.
15. H. Janssen, A. Herden and H. C. Kärner, Contact angle measurement on clean and polluted high voltage polymer insulators, 10th International Symposium on High Voltage Engineering, Montreal, Canada, 1997.
16. H. Büchner, F. Schmuck, A. Zanetti, R. Bärsch, H. Jahn, J. Lambrecht, CIGRE regional meeting for the African continent, Cairo, Egypt, 1997.
17. S. Kumagai and N. Yoshimura, IEEE, Trans. Diel. Elect. Insul., Vol. 8, 679-686, 2001.

Chapter Two

Historical and Theoretical Background of Non Ceramic Insulators

2.1 History of non ceramic insulators

The first and most commonly used materials in outdoor insulators were made from glass and porcelain. These traditional inorganic insulators were widely used in the field of high voltage electrical application until the 1980s. Since then, composite non-ceramic insulators have gained greater acceptance and are replacing porcelain and glass, especially in polluted environmental areas. Even though the history of polymeric insulators began in the late 1940s, when organic insulating materials were manufactured for use in indoor electrical insulators from epoxy resins, it is only in the past 30 years that there has been a dramatic increase in the utilization of new polymeric materials in the outdoor high voltage insulator market [1].

The first non ceramic insulators were manufactured on a commercial basis in the United States more than four decades ago and were composed of epoxy resins [2]. Many units were installed but they failed after a short period in outdoor environments. This is because they suffered from severe tracking and erosion. The failure was also associated with lack of proper design. As a result, some manufacturers were not encouraged to continue with their production. The first generation of today's polymeric insulators first appeared in Europe during the 1960s. These insulators were made of porcelain and supported by an epoxy resin fiberglass rod [3]. These first composite insulators were, however, not widely used because of the subsequent development of lighter weight polymeric insulating materials.

2.2 Comparison of ceramic vs. non ceramic insulators

Ceramic insulators	Non ceramic insulators
➢ Made from inorganic materials	Made from organic materials
➢ Do not age	Age
➢ > 80 years experience	>30 years experience (latest < 10 years)
➢ Wettable	Non wettable
➢ Better resistance to heat and dry-band arcing (DBA)	Better pollution performance

Polymeric insulators for transmission lines began to be manufactured in Europe and

USA in the mid 1970s and beyond. The early development of modern polymeric insulators for transmission lines can be illustrated by the work of the German manufacturer Rosenthal since 1964 [3]. In 1977, Hydro-Quebec in Canada installed a 16 km section of a 735 KV_{rms} transmission line, comprising 282 composite insulators made by three different manufacturers [3]. This experimentation was later extended to other lines and/or voltage levels and has continued to date. The early utility experimentation done with the first generation of polymeric insulators has led to mixed results. One insulator that featured silicone rubber housing and a construction that avoided joints in the housing showed good electrical performance. However, due to low tear resistance the sheds of room temperature vulcanized (RTV) silicone rubber were later replaced by high temperature vulcanized (HTV) silicone rubber, which is mechanically more resistant to electrical discharge.

Ethylene propylene diene monomer (EPDM) rubber shed sections used on other insulator types provided good housing material performance. However, shed bonds degraded in these early insulators when exposed to coastal environments. The manufacturer who first used ethylene propylene rubber (EPM) for its shed sections has since developed an alloy of EPDM with silicone fluid to provide surface hydrophobicity.

During the late 1970s Eskom, South Africa's largest electricity supplier, started experimenting with insulators by replacing existing inorganic insulators with NCI materials. Silicone rubber and EPDM test insulators were installed on a 400 kV line near the Koeberg Nuclear Power Station and the results showed that the silicone rubber insulator performed better than the EPDM counterpart did [4]. The latter showed heavy discharge and had to be removed within one year because of radial cracks at the bottom shed.

The wider application of modern NCI materials was restricted to distribution lines until about two decades ago, due to the lack of an adequate understanding of how the materials would perform in higher voltage applications. A few years later, manufacturers in West Germany, the USA, France, England and Italy introduced the first generation of present day non-ceramic transmission line (high voltage) insulators [2]. All of these insulators had a core composed of a fiberglass rod, surrounded by polymer watersheds. Polymeric transmission line insulators offer significant advantages over porcelain and glass insulators, especially for ultra-high voltage transmission lines. Their low weight

allows tower designs that porcelain and glasses do not. They can be used as phase spacers on compact lines to control galloping and to limit conductor motion.

Today there is a pronounced interest in using non-ceramic insulator systems and they are increasingly capturing a large share of the high voltage insulator market. Currently, in the United States, non-ceramic insulators form between 60% to 70% of all the new HV insulators [5] and their market share is anticipated to grow at a steady rate. Kikuchi *et. al.* [6] showed in their survey on the current status of non-ceramic composite insulators that about 80% of the responding utilities answered that they would actively increase their use of non ceramic insulators in the future. It is therefore anticipated that the market will expand significantly. The main reasons for expanding of the use of NCIs are: simple and easy installation, light weight, vandalism resistance, better anti-contamination, easy maintenance and reasonable cost.

In some cases, however, power utilities are still reluctant to use composite insulators because of the remaining uncertainty regarding their long-term reliability. The prime concern is the ageing of the insulators and the corresponding degradation in performances, both electrical and morphological, over the long-term. Other concerns are quality control during manufacturing and the maintenance problem i.e. being able to detect defective units in service, and the unknown life expectance.

2.3 Polydimethylsiloxane (PDMS)

Polydimethylsiloxane (PDMS), $[SiO(CH_3)_2]_n$, is the most common silicone rubber polymer and the one used exclusively in high voltage outdoor insulation applications. PDMS has an extremely low surface tension. It spreads over solid surfaces and forms a tenacious film which is hydrophobic and water-repellent. PDMS elastomers are used both as high voltage composite suspension insulators, as well as coatings on porcelain line and sub-station insulators. PDMS is the basic polymer for silicone oil and silicone rubber. It consists of an inorganic backbone with alternating silicone and oxygen atoms, and two methyl groups attached to the silicone atoms, forming the repeat unit in the polymer. (See Figure 2.1)

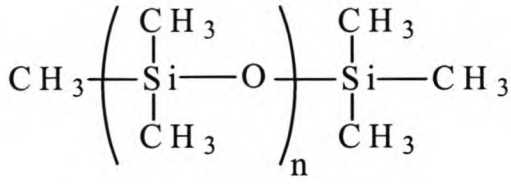

Figure 2.1: Chemical formula of PDMS

PDMS has a variety of characteristics that makes it particularly suitable to HV application. These include its grease-like nature, which enables the coating of existing insulators such as porcelain and glass, its low weight, high UV resistance, good electrical performance and, most importantly, its low surface energy. The polymer is able to maintain its hydrophobicity on the surface of the material in the presence of severe contamination and under wet conditions. Under severe environmental conditions, however, electrical discharge can eventually cause loss of this hydrophobicity. The initial hydrophobic surface becomes progressively hydrophilic when exposed to electrical discharge. After a relatively short period of time with no discharge activity, however, the PDMS insulator surface regains its initial hydrophobic nature. This "self-healing" is often referred as the "hydrophobicity recovery".

2.3.1 Properties of PDMS of special interest

PDMS has the following important characterstics:-

- Low surface energy
- Hydrophobic, water insoluble
- Forms LMW silicones
- Low glass transition temperature
- Weak intermolecular forces
- Good dielectric properties
- High thermal and oxidative stability
- Low reactivity, toxicity and combustibility.

There are four fundamental properties of PDMS which account for the above behaviors and these are [7, 8]:-

- Low intermolecular force between methyl groups
- Partial ionic nature of the siloxane bond
- Unique flexibility of the siloxane backbone
- High strength of the siloxane bond.

The low surface tension of liquid PDMS is due to the closely packed methyl groups in the surface. Furthermore, the interfacial tension to pure water is low in comparison with hydrocarbons. In the case of PDMS the Pauling electro-negativity difference of 1.7 between the silicone and the oxygen atoms makes the siloxane bond 41% polar in character [7]. Since oxygen is more electronegative, it attracts electon density from the silicone atom. The positively polarized silicone atom has an electron-withdrawing nature from the attached carbon atom because of the electronegativity difference between them. The polar nature of the siloxane bond, therefore, makes it susceptible to hydrolysis under acidic or basic conditions. Thus, the methyl groups in the PDMS behave differently to those in hydrocarbon polymers. These groups have high thermal and oxidative stability compared to the methyl attached to hydrocarbon polymers.

2.3.2 Thermal stability

Compared to other hydrocarbon polymers, PDMS is more thermally stable and performs well over a wide temperature range. Silicone rubbers in the absence of acidic or basic catalysts are exceptionally stable [9]. Stable silicone products can be heated in air at $200\,^{0}C$ for a year without an appreciable change in properties, and even at $300\,^{0}C$ for a short period. This high thermal stability contributes to making PDMS a material of choice in the field of non-ceramic high voltage applications.

It is well known that the thermal degradation of PDMS in an inert atmosphere and under vacuum results in de-polymerization at 400-$650\,^{0}C$, yielding cyclic oligomers [10]. Polyphenylsiloxanes are stable even at higher temperatures. Extra energy is necessary to dissociate the substantially stable siloxane bonds.

Low molecular weight (LMW) oligomers of PDMS are formed by the high heat generated from dry-band arcing. The tendency of silicone rubber to form LMW PDMS oligomers (silicone fluid) as a result of heat generated by dry-band arcing in wet conditions is probably due to bond scission [11]. Since dry-band arcing can increase the temperature at the surface of insulator to very high levels, it may instantaneously burn the surface and cause dissociation of chemical bonds. This will result in the formation of smaller molecule contaminants and crosslinking of the remaining body of the polymer may take place at the surface.

2.3.3 Oxidative stability

PDMS elastomers are reasonably resistant to oxidation by ozone and oxygen (insensitive to ozone). The methyl groups in PDMS have higher oxidative stability than the methyl groups attached to hydrocarbon chains such as in propylene. This is due to the polar nature of the siloxane bond that is electron withdrawing, polarizing the methyl group and thus rendering it less susceptible to radical attack [8]. Although some loss of silicone elastomer tensile strength is seen overtime in outdoor insulation, and which may be ascribed both to hydrolysis and/or oxidation, the resistance to oxidation is one of the bases for utilizing PDMS in HV insulation applications.

Despite these very high oxidative stabilities under very aggressive environmental conditions, as well as electrical discharges such as dry-band arcing and corona, oxidation and crosslinking of the polymer remains a possible phenomena .

2.3.4 UV radiation stability

Outdoor insulators in service are exposed to UV radiation from sunlight as well as UV produced in the plasma from corona discharge. PDMS has high UV stability in comparison to other polymeric materials such as EPDM. This is due to the high dissociation energy of the siloxane bond Si-O, which is 445K J/mol [8], whereas the energy of sunlight at 300nm is 393K J/mol. PDMS does not absorb light in the near UV wavelength range (300 to 400 nm). However, the dissociation energy for C-C bond energy like EPDM is 346 KJ/mole [7]. Therefore, the extra energy required for breaking the bond between silicone and oxygen makes PDMS more stable to UV radiation.

Although results from literature suggest that PDMS is highly resistant to UV-radiation from sunlight, a study carried out by Vasilets [12], using AFM and XPS, on the effect of vacuum UV-radiation (147nm), i.e. an extremely small wavelength in the presence of air, revealed that the surface roughness of PDMS decreases.

2.4 Preparation of PDMS

The basic starting materials for the preparation of silicone polymers are dialkyldichlorosilanes, normally dichlorodimethylsilane, which are prepared by the direct process of oxidative addition of an alkylhalide to Si, to give R_2SiX_2.

$$2RCl + Si \xrightarrow[250\text{-}280^{\circ}C]{Cu} R_2SiCl_2 \qquad (1)$$

There are many synthetic methods for the preparation of organo-silicone compounds. The Grignard reaction is the classic method of preparing organosiloxanes and was the first commercially important route. [13]

$$RMgCl + SiCi_4 \longrightarrow RSiCl_3 + MgCl_2 \quad (2)$$

$$RMgCl + RSiCl_3 \longrightarrow R_2SiCl_2 + MgCl_2 \quad (3)$$

2.5 Vulcanization (crosslinked network)

Linear PDMS is usually manufactured from dimethyldichlorosiloxane, which is produced by the reaction of powdered silicone with methylchloride. A mixture of cyclic (c) and linear (l) PDMS oligomers are formed by hydrolysis of the dimethyldichlorosilane, followed by a condensation reaction.

$$(CH_3)_2SiCl_2 + H_2O \longrightarrow [(CH_3)SiO]_C + HO[(CH_3)_2SiO]_lH \quad (4)$$

High molar mass polymers are then produced by anionic or cationic ring-opening polymerization of the cyclic oligomers or polycondensation of the silanol end-blocked linear oligomers [7].

There are a number of possible routes by which crosslinking can be achieved. However, the most commonly used one are:-

1) The incorporation of tri-or tetra-functional silanes that can react under ionic conditions
2) The use of organic residues on the silicone polymer (methyl, vinyl, H groups) to form a network [8, 9].

In the former case a pure silicone containing a Si-O linkage is formed while in the latter case organic spacers link the silicone polymer.

Depending on the temperature of vulcanization there are different categories of crosslinked PDMS: [14].

- Room temperature vulcanized (RTV)
- Low temperature vulcanized (LTV) and
- High temperature vulcanized (HTV).

These categories differ not only in their curing temperature but also by the pressure at which the vulcanization is achieved and by the curing agent used. HTV, for example,

requires high pressure. Vulcanization is the process whereby chemical bonds are formed between the polymer chains.

2.5.1 High temperature vulcanization

In high temperature vulcanized (HTV) silicone rubbers, crosslinking of PDMS occurs in the presence of organic peroxides, such as benzoyl peroxide, m-chlorobenzoyl peroxide and di-butyl peroxide. The curing requires the application of high temperature (usually above $100\,^{0}C$) and pressure, so that the peroxide decomposes to form free radicals [9, 12]. The formed free radicals then initiate the curing by reacting with the methyl groups, by abstraction of a hydrogen atom or, more easily, with unsaturated bonds (vinyl groups). It is therefore possible to use less reactive peroxides to form crosslinked silicones from vinyl-substituted silicones. The temperature needed to generate the free radical species depends on the peroxide structure. Generally, the onset temperature of radical generation of acyl peroxide is lower than that of alkyl peroxide. A typical initial radical generation step due to high temperature is shown below.

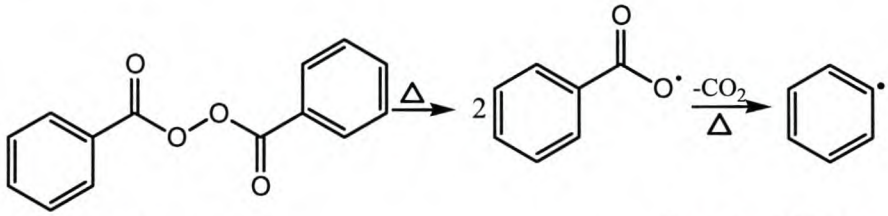

Benzoyl peroxide Reaction initiator radical (5)

The free radicals generated along the polymer chain recombine and forms crosslinks between the siloxane chains. The remaining residual volatile decomposition products in the HTV silicone rubber are removed by a post-cure step, which involves heating the sample at atmospheric pressure.

2.5.2 Room temperature vulcanization

Two-component silicone rubber compounds can be cured (vulcanized) by two different chemical mechanisms, each of which greatly affects the processing properties and the service properties of the final elastomers [8, 9].

2.5.2.1 Condensation cure

This involves the reaction of silanol groups to form siloxane bonds. The reaction involves the liberation of water and it is an equilibrium process, catalyzed by acids or

bases. Such reactions take place at room temperature and yield RTV silicone.

$$\equiv SiOH + \equiv SiOH \xrightarrow{\text{acid / base}} \equiv SiOSi\equiv + H_2O \qquad (6)$$

In general, hydroxyl-terminated polydimethylsiloxane [$HO(Si(CH_3)_2O)_nH$] is formed by reacting relatively small quantities of tri- and tetra-functional silanes ($RSiX_3$ or SiX_4). The reaction occurs at room temperature, and hence the term room temperature vulcanized (RTV) is associated with the process. The preferred crosslinking agents are the methoxy and ethoxysilanes, such as $RSi(OR)_3$, because they are easily converted to silanol by hydrolysis, and then condensation occurs. The choice of crosslinker is not only dictated by the rate of curing but also the nature of the by-product that forms.

2.5.2.2 Hydrosylation cure (addition cure)

Addition of silane with vinyl groups is also another means of preparing RTV PDMS. It is a widely used process for the preparation of silicone elastomers. The crosslinking is essentially the same as the above (2.5.2.1) except that here two complementary polymers must be used. One siloxane-containing vinyl end group Si-CH=CH_2 can react with a siloxane containing a Si-H group in the presence of suitable catalyst. The reaction occurs rapidly under mild conditions (from ambient temperature to 100^0C). A platinum catalyst is most commonly used in the hydrosylation cure. The reaction takes place at a temperature below 100^0C. It is preferable to post-cure the material at a higher temperature. This should be by raising the temperature slowly, to avoid de-polymerization. This second crosslinking reaction is very specific and the crosslinking density can be controlled very accurately by this method.

2.6. The use of silicone rubber in high voltage applications

It is well known that the main problem with porcelain and glass insulators is that water readily forms a film on their surfaces, along with airborne contaminants. Natural contaminants such as wind-blown sea salt and human-made pollutants such as electrolytic precipitants found in many industrial settings aggravate the condition. These deposits encourage leakage current development, which may lead to dry-band arcing, or flashover. To help prevent such problems in the disruption of power systems due to insulator contamination, regular insulator washing and cleaning is needed. However, such practices are costly and time consuming. Therefore, in order to overcome such problems, power utilities have recently shown considerable interest in RTV silicone fluid

coatings for porcelain [15-17].

Room temperature vulcanized coatings prevent water filming on the virgin surface. However, this water repellency gradually deteriorates with time due to physical and chemical changes, which arise from heavy surface discharge. Nevertheless, the lost hydrophobicity recovers completely after a certain period without electrical discharge [18-19]. As a result, RTV coatings have gained acceptance as suitable coatings for porcelain insulators; they lead to improved performance under polluted conditions. The role of RTV coatings on inorganic insulators in-service is to transfer the hydrophobic nature to them and to therefore suppress the leakage current. The use of ATH filler in the RTV coating also improves the tracking and erosion resistance.

RTV coatings can be easily handled and applied as a paint-on coating for porcelain insulators to impart good anti-contamination performance under polluted conditions [20], while HTV insulators, which display better mechanical properties than RTV coatings, are used exclusively in the construction of outdoor composite insulators. According to a study done by Gubanski [21], the silicone rubber housing used in composite insulators preserves the ability to recover hydrophobicity even better than the RTV coating does.

Coating with RTV PDMS is an effective way to suppress leakage current and to enhance the performance of ceramic insulators. Insulators coated with RTV PDMS can withstand exposure to severe weather condition for up to three years without considerable damage [22].

2.7 Hydrophobicity

PDMS is known to possess exceptional hydrophobic character. This hydrophobicity is a result of two phenomena [9]:

1) The methyl groups provide hydrophobic characteristics to the polymer and
2) The flexibility of the silicone polymer chain permits the rearrangement of the polymer backbone such that the methyl groups may orient themselves at an interface. That is, the fluid nature of the silicones allows them to readily re-orientate from the bulk to the surface, presenting a layer of hydrophobic methyl groups at the surface.

The high chain flexibility arises from the very large bond angle of the Si-O-Si linkage in the siloxane backbone (135-180°), with an energy minimum at 145°, which makes it relatively easy for the methyl group to reorient from the bulk to the surface [23].

A hydrophobic surface is defined as a surface which is not readily wettable. Hydrophobic ("water hating") materials have little or no tendency to adsorb water and water tends to bead on their surfaces (i.e. discrete droplets are formed instead). Hydrophobic materials possess low surface tension values and lack active groups in their surface chemistry for the formation of "hydrogen-bonds" with water. The intermolecular attraction that causes surface tension results from a variety of intermolecular forces. Most of these forces, such as London dispersion and the hydrogen bonding forces, are functions of the specific chemical nature of a substance. London dispersion exists in all types of matter and always gives an attractive force between adjacent atoms or molecules [24]. In PDMS, the London dispersion force is much larger than the hydrogen bonding force and it is this dispersion force that makes PDMS hydrophobic [18].

Hydrophobicity is a most useful property for outdoor insulation. It prevents the formation of water films between the ends of an insulator, which could otherwise lead to surface discharges destroying the polymeric material. If the surface of a high voltage insulator is hydrophobic then the leakage current as well as surface discharge activities will be reduced significantly.

When a water droplet is in contact with a solid surface then an angle, termed the contact angle is formed. The shape of the droplet depends on the solid material and the physical and chemical state of the surface. The surface hydrophobicity of a solid is determined by its free surface energy and the higher the surface free energy is the more easily it is wetted. A surface with a lower surface free energy does not allow water to spread over it in a continuous film. In the interfacial region between PDMS and water, the methyl groups are attracted toward the bulk of PDMS by the intermolecular or attractive forces along the normal to the surface [18] and thus make it hydrophobic. A surface can be considered as hydrophilic if the contact angle is $<90°$ and as hydrophobic if the contact angle is $>90°$. If the sample and the droplet are at rest, a static contact angle is obtained.

A system at rest may be in a stable equilibrium (the lowest energy state), or in a metastable equilibrium (an energy trough separated from neighbouring state by energy barriers). Stable equilibrium will be obtained only if the solid surface is ideally smooth, homogeneous, planar and nondeformable, and the angle formed is the equilibrium

contact angle, θ_e. On the other hand, if the solid surface is rough or compositionally heterogeneous, then the system may reside in one of the metastable states and the angle formed is the metastable contact angle. The amount of mechanical energy in a liquid drop, i.e. water (such as vibrational energy) determines which metastable state is to be occupied. Therefore, metastable contact angles vary with drop volume, external mechanical energy and how the angle is formed (whether by advancing or receding the liquid front on the solid).

Many real surfaces, like the NCI sheds, are rough or heterogeneous and a liquid resting on such a surface may reside either in a stable or in the metastable state [25]. In the case of NCIs it is known that with ageing they become rougher and more heterogeneous with time of outdoor exposure. In the cases of EPDM and cycloaliphatic insulators, the roughness is known to be caused by erosion and cracking of the surface and the accompanying exposure of filler. In the cases of silicone rubber based NCIs and coatings, the pollutants which settle on the surface become coated in a thin layer of low molecular weight (LMW) silicone fluids, effectively permanently "gluing" them to the surface and yielding an extremely rough, yet chemically homogenous, surface. For these reasons a high variation in contact angles on the aged NCIs can be expected.

The aim of carrying out hydrophobicity tests on NCI shed materials is to evaluate the wettability of the surfaces. This parameter is believed to be the most dominant characteristic in determining the performance of NCIs in regions of high industrial and marine pollution and at times of high humidity and light wetting. If a solid layer of moisture, with dissolved conducting pollutants, is able to form over the insulator surface, then the consequence is either high leakage currents (associated with localized heating and material degradation) or possible flashover.

2.7.1 Contact angle measurements

When a water droplet is in contact with a solid surface, the angle formed between them is referred to as the contact angle, as shown in Figure 2.2 below. Contact angle measurement is the ideal method to characterize surface wettablity and probably the most widely utilized technique to study of loss and recovery of surface hydrophobicity [13, 24, 26].

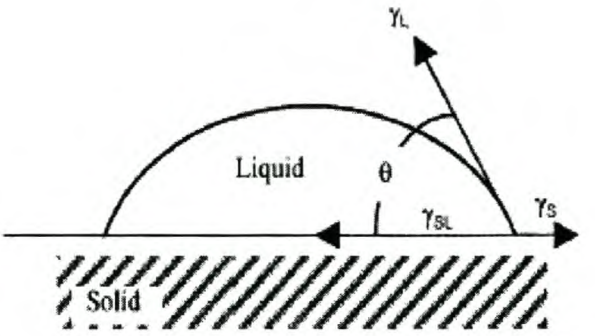

Figure 2.2: Wetting of droplet on the surface of a solid [27]

In general, the lower the surface free energy is, the higher the contact angle and the stronger the hydrophobicity. Contact angle as a wetting phenomenon was originally defined some two hundred years ago for solid, non-porous, non-absorbent surfaces, for which the contact angle readings were taken at equilibrium. The surface contact angle of a solid material is quantitatively related to Young Depru's equation [27, 28]:

$$\gamma s = \gamma sl + \gamma l \cos\theta \qquad (2.1)$$

The contact angle θ is dependent on the interfacial forces of the three boundaries, where θ is the static contact angle on a horizontally placed sample and γs, γsl and $\gamma l \cos\theta$ are the surface free energies per unit of the solid, liquid and solid-liquid interfacial surfaces. If the adhesion energy of the liquid and the solid are known, then the contact angle can be calculated.

Generally, the accuracy of contact angle measurement is not limited by the experimental technique, but by the reproducibility of the surfaces investigated. Instruments that measure to an accuracy of 1° are usually adequate [28]. Usually there is good agreement between the results obtained by various methods if appropriate precautions are taken.

2.7.1.1 Static contact angle

The classical method used to characterize the hydrophobicity of a surface, usually used in laboratories, is the static contact angle (SCA). To measure this static contact angle, a droplet of water is placed on a level surface of the material using a syringe and the dimension of the droplet is measured by a goniometer or with the assistance of a microscope or zoom photography.

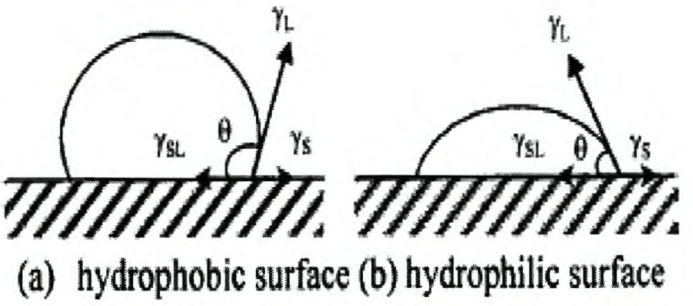

Figure 2.3: Comparing the SCA of hydrophobic and hydrophilic surfaces [27].

The contact angles of NCI sheds can be determined by measuring the dimensions of a liquid drop. The most critical factors for accurate SCA determination identified in literature have been noted as:

- Droplet volume
- SCA measurement technique (direct angle vs drop dimension measurements)
- Number of measurements averaged
- Time of measurement after droplet placement.

It was shown by Souheng [28] that the size of the droplet has a significant effect on the value of the contact angle. Larger droplets have a gravity effect. For very small drops, of the order of 10^{-4} ml, the distorting effect of gravity is negligible, and the drop takes the form of a spherical segment. Time of measurement after placing the drop onto the surface is also crucial and it is best if it is done within 2 minutes after placing the drop on the surface, as suggested by Janssen and Stietzel [25]. This is to avoid any evaporation.

The contact angle θ can be determined by measuring the dimensions of the liquid droplet and applying the formula below to calculate the angle:

$$Tan(\theta/2) = h/r \qquad (2.2)$$

Where: - h is the drop height
- r is the radius of the drop base.

The drop height is usually smaller than the base radius and is more difficult to measure.

2.7.1.2 Dynamic contact angle

Dynamic contact angle (DCA) measurements based on the Wilhelmy plate method can be used to evaluate time variation of loss and recovery of hydrophobicity of the material. This technique can determine both advancing and receding contact angles of a plate sample and evaluate, in a very short time, variation of the surface properties.

The tensiometeric method for measuring contact angles measures the force that is present when a sample of solid is brought into contact with a test liquid. If the force of interaction, geometry of the solid and surface tension of the liquid are known, then the contact angle can be calculated.

The wetting force on the solid is measured as the solid is immersed in or withdrawn from a liquid of known surface tension.

$$\text{Wetting force} = \gamma_l \rho \cos\theta \qquad (2.3)$$

Where γ_l is the surface tension of a liquid, *?* is the perimeter of the plate and θ is the contact angle of the sample.

2.7.2 Loss of hydrophobicity of PDMS

It is well known that the hydrophobic surface of PDMS loses this property when exposed to prolonged electrical discharge under wet conditions. An investigation carried out by Hollan and Carlson in 1970 [29] revealed that the hydrophobic surface properties of silicone rubber can be lost by oxidation during exposure to corona discharges in air and radio-frequency plasma treatments. Since then many researchers have employed corona and oxygen plasma to treat silicone rubber and investigate the loss and recovery of hydrophobicity. Exposure to severe corona treatment also causes both physical and chemical damage to the silicone rubber insulators that may reduce some of the properties desirable for insulator service.

Other factors that also lead to the loss of hydrophobicity are surface pollution and long-term submersion in water. As Hackam [3] mentioned in his review, 100 hours of immersion of silicone rubber in water leads to a decrease in the contact angle measured, from 80° to 45°, which indicate the loss of hydrophobicity. This could be due to hydrolysis of the siloxane bonds and the creation of hydrophilic end groups at the surface.

Analyses by different analytical techniques such as EDAX, ESCA and XPS have shown that surface oxidation causes a decrease in the carbon content and an increase in the oxygen content of the surface [3, 19, 30]. This increase in the average oxygen content is due to highly oxidized surface layers (oxygen bonded to the silicone atom). It has also been suggested that a crosslinked, brittle, silica-like structure may form. Polar hydroxyl groups are also formed. Both these factors can cause an increase in the hydrophilicity of the surface.

Surface oxidation by electrical discharges such as dry-band arcing and corona is aggravated in the presence of water and air-borne natural contaminations like sea salt and man-made pollutants [31]. It has been suggested that oxidation of the insulator surface results in the formation of an inorganic silica-like (SiOx) structure, i.e. a silicone atom bonded to more than two oxygen atoms, which increases the hydrophilicity of the surface. However, PDMS insulators recover their original hydrophobicity after a certain time of rest and this recovery allows them to continue suppressing leakage current in high voltage insulators.

2.7.3 Hydrophobicity recovery mechanism

The change in PDMS insulator surfaces from hydrophilic to hydrophobic is referred to as the hydrophobicity recovery. It is usually explained as being due to one of the following mechanisms [23, 32]:-

a) Diffusion of pre-existing low molecular weight (LMW) silicone fluid from the bulk to the surface
b) Re-orientation of polar groups from the surface to the bulk phase or reorientation of the nonpolar group from the bulk to the surface
c) Condensation of the surface hydroxyl groups
d) Migration of *in situ* created LMW species during discharge to the surface.

It is not well known which of these factors is responsible for the long-term stability of hydrophobicity recovery. Several researchers [33-37] have suggested that surface re-orientation and diffusion of LMW species are the main mechanisms. Toth *et. al.* [33] suggested that the diffusion-controlled migration of LMW species plays a more major role in the recovery process than the reorientation of the newly formed hydrophilic groups in the bulk. They concluded that 2/3 of the recovery is due to diffusion of LMW PDMS oligomer and 1/3 is due to reorientation. Morra *et. al.* [34] on the other hand

proposed that the hydrophobic recovery is due to burial of the polar groups into the bulk, accompanied by the condensation of surface silanol and consequent crosslinking in the contact angle-probed layer. Although several mechanisms have been proposed to account for recovery, many agree that migration of low molar mass PDMS oligomers to the surface is the dominant mechanism [11, 35 36]. The extreme flexibility of the siloxane chain and the low intermolecular forces between the methyl groups, which result in the low glass transition temperature and high free volume of PDMS, allow PDMS to reorient its surface readily. It has the most mobile surface of all common polymers. Likewise, the LMW component that is usually present in most commercial PDMS materials provides an ample reservoir of diffusible material, even if such un-reacted components have not been deliberately added. The same factors that permit facile reorientation will allow ready diffusion of such species.

It has been reported that the LMW species that migrate to the surface of PDMS are primarily cyclic in nature [37]. Janssen [35] reported that both linear and cyclic LMW species are responsible for hydrophobicity recovery. RTV insulators contain cyclic PDMS whereas HTV insulators contain both linear and cyclic oligomers. This is supported by results of the investigation done by Hant and George [38] showed that the cyclic oligomers are more abundant than the linear oligomer. The predominance of the cyclic over the linear is attributed to the more compact shape of the cyclic oligomers and their known higher diffusivity.

Recovery rates have been found to be highly dependent on the applied voltage that causes the electrical discharge. It was observed that the initial recovery rate increases with increasing corona exposure time. Kim *et. al.* [39] concluded that the LMW species produced *in situ* as a result of high voltage corona treatment and their subsequent migration to the surface are responsible for the hydrophobicity recovery rate and the added fillers have no major effect. Due to the high voltage, enough LMW species are formed and dominate the recovery rate by diffusion from the bulk to the surface.

The rate of hydrophobicity recovery of PDMS is also dependant on mechanical stresses on the material and temperature. Hillborg and Gedde [19] found that the hydrophobicity recovery of an untouched specimen was markedly slower than the hydrophobicity recovery of a mechanically deformed one. The suggested reason for such a difference is that a brittle, silica-like layer that formed during corona treatment could delay the

recovery of hydrophobicity on the undeformed surface by inhibiting the transport of LMW PDMS to the surface. The SiOx layer is formed by oxidation, in the presence of oxygen in the surroundings or in dissolved form in the polymer.

In the undeformed state the silica-like layer prohibits fast diffusion, while mild bending or deformation of the material causes cracks in the brittle silica layer and hence a more rapid migration of low molar mass PDMS species through the cracks to the surface. The rate of recovery is also strongly dependent on the temperature of storage [40], i.e. the higher the storage temperature the higher the rate of recovery. This may be associated with the higher diffusion of low molecular weight species when the storage temperature is higher.

Surface reorientation can still be an important factor in the recovery of the silicone insulator surfaces that do not develop a highly crosslinked silica-like layer. The recovery is a so-called conformational change; the methyl groups turn over from the bulk to the surface, or the silanol group, which is hydrophilic, turns toward the bulk, and the surface becomes hydrophobic. However, the highly crosslinked silica-like SiO_X cannot readily re-orient between hydrophilic and hydrophobic [7]. In such cases diffusion of LMW oligomers of silicon oil are more important for the rate of recovery.

2.8 Possible mechanisms that can lead to PDMS degradation in HV insulators

Compared to most other NCI materials PDMS insulators have better thermal stability and resistance to UV radiation because of their strong Si-O bond and excellent water repellence due to low intermolecular forces. One important property of PDMS relevant to HV insulation is its stability to oxidative degradation when compared to other polymeric insulators. The surface of silicone is, however, more prone to long-term degradation during outdoor use when compared to porcelain and glass. In general, the causes of ageing in PDMS insulators could include: electrical impact, including partial discharge caused by leakage current, dry-band arcing and corona, or environmental attack such as thermal degradation, ultraviolet-initiated polymer degradation, acidic attack and chemical attack from salt contamination [30].

2.8.1 Thermal degradation

As mentioned, the superior thermal stability of PDMS makes it attractive for use in HV insulation. Although PDMS based insulators are frequently used in demanding

temperature environments due to their greater thermal stability compared to other polymeric insulators, high temperatures, usually above $300^{0}C$, can lead to degradation and ageing [10, 33, 41]. It is well known that the thermal degradation of PDMS in an inert atmosphere leads to de-polymerisation and the formation of predominantly cyclic (mainly D3 and D4) oligomers. Camino *et. al.* [10] explained that PDMS thermally decomposes to cyclic oligomers through Si-O bond scission in chain-folded cyclic conformation, energetically favoured by the overlapping of empty d-orbitals with orbitals of the oxygen and the carbon atoms.

During degradation the PDMS polymer decomposes to form lower molar mass oligomers. There are also a number of possible reactions which PDMS can undergo to change the polymer network, such as siloxane bond interchange and hydrolysis of siloxane bonds [11]. Since thermal degradation of PDMS is only significant at temperatures above $300^{0}C$, it is not expected that this mode of degradation will be significant for in-service materials, except in the case of dry-band arcing where there can be extremly high localized temperatures during the discharge.

2.8.2 UV radiation

Due to the general behaviour of polymeric insulators toward UV radiation, UV radiation has become an important factor and an accepted concern for various materials. Analysis of insulator materials such as EPDM show micro-cracks after a certain period of outdoor exposure, mainly traced back to the UV radiation [42]. These micro-cracks lead to spreading of moisture and EPDM insulators become hydrophilic. To date, no decrease in hydrophobicity due to UV radiation has been reported for silicone rubber insulators although there is a surface discoloration.

It has been assumed that UV radiation from the sun has a negligible impact on the service of PDMS based outdoor insulators, since silicone rubber is much more resistant to UV radiation when compared to other material such as EPDM monomer. Kumagai and Yoshimura [43] have however suggested that the UV component in sunlight can cause chain scission and crosslinking in the molecules of the polymer. Therefore, even though the probability of main chain scission is low, crosslinking reactions can take place in the positions where Si-C and C-H bonds are broken by UV radiation. The chemical and morphological changes due to UV radiation and the nature of the LMW silicone fluid can have an effect on the hydrophobic behaviour of PDMS material. The

amount of LMW chains, especially the very short chains (with n=3 to 5 repeat units), would decrease or increase [30]. The UV components believed to play a role in the PDMS insulator degradation are the UV radiation from sunlight as well as UV produced in the plasma from corona discharge.

Reports from field tests on the other hand, indicate that UV enhances hydrophobicity and its recovery [44]. Insulators aged at the Anberge field station in Sweden were found to be less hydrophobic during the wet and less sunny weather than they were during the summer [44]. This may be due to the wet and sunny environmental conditions. The silicone insulators were less hydrophobic on the parts of the sheds that were shielded from the sunlight. It has also been reported that hydrophobicity of both HTV and RTV materials increased steadily during the first year in a tropical climate [8]. This increase in hydrophobicity could be due to (as some researchers suggest) an increase in LMW oligomers formed by UV radiation [45].

2.8.3 Corona discharge

Electrical activities (corona, arcing or oxidative plasma) are most widely recognized as the primary cause of non ceramic insulator ageing. The high electric field at the edge of HV insulators or gaps between water drops on the hydrophobic surface can produce corona discharges [33]. This corona discharge can lead to a loss of hydrophobicity and subsequently lead tor further ageing.

Exposure to severe corona treatment is both physically and chemically damaging to the silicone elastomers. Cracking of the surface and an increase of wettability by water are the usual manifestations of corona discharge. A PDMS insulator exposed to corona discharge or oxygen plasma undergoes not only oxidation and chain scission, but also crosslinking and the suggested formation of an inorganic, silica-like surface layer, which retards the hydrophobicity recovery. Hillborg *et. al.* [46] found an evidence of the formation of a thin, oxidised surface layer of silicone bonded to 3 or 4 oxygen atoms by XPS after oxygen plasma treatment.

Corona discharge generates: UV radiation, heat, gaseous by-products like O_3 (ozone) and NO_2 [5, 22]. During exposure to corona, NCIs are subjected to the effects of simultaneous energy inputs. The mechanical impact of electrons and/or ions, UV light, and ozone all act on the NCI surface during corona exposure. Through

secondary reactions, highly oxidizing species and hydrated versions of nitrogen oxides are generated and which, in the presence of moisture, can lead to formation of acidic water which is highly corrosive. Corona discharge produces both positive and negative ions that will be accelerated toward the surface of the insulator and cause material ageing, depending on the polarity of the ions [22].

The main effects of corona and plasma on silicone rubber are: [8]

1) An increase in oxygen content in the surface
2) Degradation of the network structure, resulting in the formation of mainly LMW cyclic and medium to high LMW linear PDMS
3) The suggested formation of a glassy SiO_x surface layer.

Continuous exposure of the insulator to corona discharge certainly causes chemical and morphological change, leading to ageing. However, since cyclic silicone oligomers are formed as by-product of corona, there is quick hydrophobicity recovery.

2.8.4 Dry-band arcing

Tracking and erosion of polymeric materials occur due to the high temperatures caused by dry-band arcing (DBA). The heat generated by DBA causes hydrolysis, scission and interchange of the siloxane bonds [30]. Kim *et. al.* [11] suggested that the interchanging of backbone chains and oxidation of CH_3 groups produces short backbone chains of PDMS, which are the components of silicon fluid. This was supported by Kumgai *et. al.* [47]. They showed that DBA causes the silicone polymer to decompose, forming a solid residue. Dry-band arcing is one of the multiple stresses of electrical and thermal impacts on the performance of silicone insulators. If the resultant temperature is above the boiling point of the silicone oligomer, which contributes to the recovery of hydrophobicity, it can remove the required groups for the recovery by evaporating the volatile linear and cyclic silicone oils.

Dry-band arcing at currents from 1 to 20 mA may be responsible for surface erosion of non ceramic insulators. Tracking and erosion are serious degradation modes for NCIs that considerably reduce their insulating property and mechanical strength by accelerating thermal degradation [39, 48]. Fillers are used in housing insulators to improve the tracking and erosion of silicone insulators by electrical discharge.

2.9 Role of fillers

Fillers added to silicone rubber insulators play a very important role in the service life performance of the insulators, as well as in the processebility during manufacturing. To compensate for their poor mechanical properties silicone rubbers have to be reinforced by the incorporation of reinforcing materials. Therefore, in high voltage insulation, the main purpose of using fillers is to improve the mechanical properties of the insulator material.

Fumed silica and aluminium tri-hydrate (ATH) ($Al_2O_3.3H_2O$) are the most commonly used reinforcing fillers for silicone polymers. Strong polymer-filler interaction is responsible for improvement of the mechanical strength of the filled silicone rubber. The hardness of the insulator is increased and, as a result, the tracking resistance is also increased.

As mentioned earlier, tracking and erosion of the polymeric insulators occur with thermal degradation as a result of high temperatures caused by dry-band arcing. Thermal degradation behaviour at elevated temperature may be closely related to the resistance of tracking and erosion [49]. Incorporation of filler into the silicone rubber insulator is therefore crucial for tracking resistance. High temperature vulcanized silicone rubbers filled with ATH fillers are being increasingly used for the housing of non ceramic insulators. Ageing resistance is increased by the addition of ATH filler and it prevents degradation of the material by dry-band arcing, not only of HTV but also of RTV PDMS materials.

The combination of silicone polymers and fillers provides an arc resistant elastomer with the long term ability to limit leakage current and reduce the risk of flashover [19, 50]. A satisfactory level of ATH for outdoor service of HTV-SIR has been determined to be between 40% and 60% by weight, based on electrical tests such as outdoor exposure and laboratory salt-fog tests. The suspension of tracking and erosion of HTV-SIR with ATH is based on the flame retarding mechanisms that have been linked primarily to carbon chain polymers [49]. One of the main advantages of using ATH as filler in polymer insulators results from its decomposing to water and aluminium at high temperature. However, the conclusion drawn by Kim *et. al.* [51] indicates that even though fillers are effective in suppressing the leakage current, higher levels of filler were observed to slow down the migration of silicone fluids from the bulk to the surface of

insulators during the recovery period following dry-band arcing. A longer time is necessary for the lost hydrophobicity to recover after the specimen has been exposed to corona and dry-band arcing.

As it has been explained previously, the addition of ATH filler is a key factor in determining the service life of insulating materials. The lifetime of ATH-filled RTV coatings depends strongly on the size of the ATH particles [3, 31]. Generally, coatings with a smaller particle size have a longer life, except in the case of very small particle sizes, when the dispersion becomes less effective. The best performance, resulting in lower leakage current, lower current pulse count and the longest time to failure of the coating, was observed with 4.5-13 μm size ATH particles. This is because more silicone fluid is able to diffuse to the surface, allowing for quicker recovery of water repallency.

The role that the ATH particle size plays in determining the life of RTV coatings is also associated with the roughness of the surface. Generally, the surface roughness increases with increasing ATH particle size. Larger particle sizes lead to higher leakage current as well as higher temperature development at the rough surface due to their poorer thermal conductivety when dry-band discharge occurs. Subsequently, this high temperature removes more silicone fluid from the surface, and this leads to a more rapid loss of water repellence [31].

2.10 Effect of the addition of silicone fluid

As already mentioned, the highly mobile LMW linear and cyclic oligomers play a vital role in restoring the hydrophobicity temporarily lost by electrical and environmental effects. It is obvious therefore that one can expect the presence of externally added LMW silicon fluid in the silicone rubber insulators to play an important role in maintaining the hydrophobic nature for quite a long period of time [8, 47, 52]. This is because the added silicone fluid enriches the LMW oligomers, which are responsible for restoring the hydrophobicity by diffusion from the bulk to the surface. Kim *et. al.* [32] reported that corona treated samples containing added LMW PDMS exhibit faster recovery than the extracted samples. The presence of sufficient LMW silicone fluid in the HTV insulators as well as in the bulk of the coating is a critical factor in both the recovery of hydrophobicity and its long-term maintenance under wet and polluted conditions.

The addition of extra silicone oils to the insulator was observed to improve the overall performance of the insulator by the suppression of the leakage current, although oligomer diffusion initially leads to an adhesion of pollutant [8]. However, the investigation by Deng and Hackam [52] reveals that the addition of 10% silicone fluid by weight to the formulation of RTV- SIR adversely affected the electrical performance. The more abundant silicone fluid on the surface retards the conduction of heat, generated by dry-band arcing to the bulk, due to its lower thermal conductivity. In this case, higher temperatures at the silicone fluid layer will produce more damage and a rough surface, which leads to a higher leakage current.

As the study by Kim, Chaudhury and Owen [39] reveals, at high voltage enough LMW species are formed and dominate the recovery process, with the external added fluid having no major effect. The recovery is mainly due to the *in situ* produced LMW species. However, at low discharge voltage, there is less generation of LMW and thus the added fluid could play a role in maintaining the hydrophobicity.

2.11 Impact of pollution on insulators service

Pollution has a severe effect on the in-service life of insulators. Harsh environments that include desert, marine and industrial pollution, along with high ambient temperatures, have a severe effect on the life performance of insulators. The presence of a conducting electrolyte layer on the surface of an insulator can be a cause of pollution flashover [14, 53]. The contaminants most responsible for causing contamination flash over are: sea salt, cement, fertilizer, road salt, lime stone, emissions from the paint industry and paper mills, bird droppings, sulphate, phosphate rock crusher etc.

The use of silicone rubber (PDMS) insulators appears to be the most promising solution for the prevention of pollution flashover because of their generally acknowledged superior pollution performance. The pollution that covers the silicone insulator surface causes an indirect loss of the LMW silicones. This is because low molecular weights of silicone oligomers migrate to the surface of the insulator and maintain the hydrophobicity of the material. However, the LMW silicones may be removed from the surface by certain effects, such as rain. This means that pollution has the effect of decreasing the LMW silicone content on the insulator surface. In addition to this, the electrolytic pollutants are conductive and lead to flashover. A coastal environment and highly industrialised areas are the most common sources of pollution in many

industrialised countries.

Under actual service conditions, the surface of polymer insulators and hollow insulators are subjected to heavy deposition contaminants. Some researchers have suggested that the thick pollutant layer plays a role in reducing the UV radiation from the sun. Hirano *et. al.* [54] estimated that the normal contamination deposit of 0.49 mg/cm^2 reduces UV exposure by 24%, which means that because of the effect of the contaminant layer in reducing the UV rays, sheds covered with such a layer age slower than uncontaminated sheds.

The potential presence of contaminants on the surface of in-service insulators can also clearly affect any analysis of these insulators after service.

2.12 References

1. J. F. Hall, IEEE. Trans. on Power Delivery, Vol. 8, 376-384, 1993.
2. H. M Schneider, J. F. Hall, G. Karady and J. Rendeowden, IEEE. Trans. on Power Delivery, Vol. 4, 2214-2219, 1989.
3. R. Hackam, IEEE Trans. Diel. Elect. Insul., Vol. 6, 556-585, 1999.
4. W. L. Vosloo, A comparison of the performance of high voltage insulator materials in a severely polluted coastal environment, PhD Dissertation, University of Stellenbosch, 2002.
5. V. M. Moreno, R. S. Gorur and A. Kroese, IEEE. Trans. Diel. Elect. Insul., Vol. 10, 80-95, 2003.
6. T. Kikuchi, S. Nishimura, M. Nagao, K. Izumi, Y. Kubota, and M. Sakata, IEEE. Trans. Diel. Elect. Insul., Vol. 6, 548-555, 1999.
7. J. Kim, M. K. Chaudhury and M. J. Owen, IEEE. Trans. Diel. Elect. Insul., Vol. 6, 695-702, 1999.
8. H. Hillborg and U. W. Gedde, IEEE. Trans. Diel. Elect. Insul., Vol. 6, 703-716, 1999.
9. M. A. Brook, *Silicon in organic, Oganometalic and polymer chemistry*, John Wiley & sons. Inc., Canada, 2000.
10. G. Camino, S. M Lomakin and M. Lazzari, Polymer, Vol. 42, 2395-2402, 2001.

11. S. H. Kim, E. A. Cherney, R. Hackam and K. G. Rutherford, IEEE. Trans. Diel. Elect. Insul., Vol.1, 106-122. 1994.

12. V. N. Vasilets, K. Nakamura, Y. Uyama, S. Ogata and Y. Ikada, Polymer, Vol. 39, 2875-2881, 1997.

13. J. P. Critchley, G. J. Knight and W. W Wright, *Heat resistant polymers technological useful materials*, Plenum press, London, 1982.

14. J. P. Renders, I. R. Jandrell and S. M. Reynders, IEEE. Trans. Diel. Elect. Insul., Vol. 6, 620-631, 1999.

15. R. S. Gorur, J. Mishra, R. Tay and R. McAfee, IEEE. Trans. Diel. Elect. Insul., Vol. 3, 299-306, 1996.

16. E. A. Cherney and R. S. Gorur, IEEE. Trans. Diel. Elect. Insul., Vol 6, 605-611, 1999.

17. S. H. Kim, E. A. Cherney and R. Hackam, IEEE. Trans. on Power Delivery, Vol. 5, 1491-1498, 1990.

18. S. H. Kim, E. A. Cherney and R. Hackam, IEEE. Trans. Diel. Elect. Insul., Vol. 27, 610-621, 1992.

19. H. Hillborg and U. W. Gedde, Polymer, Vol. 39, 1991-1998, 1998.

20. H. Homma, T. Kuroyagi, K. Izumi, C.L Mirley, J. Ronzello and S.A Boggs, IEEE. Trans. Diel. Elect. Insul., Vol. 15, 2000.

21. S. M. Gubanski, IEEE. Trans. on Elect. Insul., Vol. 27, 374-381, 1992.

22. M. Abdel-salam, H. Anis, A. Ei-Morshedy and R. Radwan, *High voltage engineering theory and practice*, 2nd edition , Marcel Dekker, Inc., New York, 2000.

23. T. G. Gustavsson, *Silicone Rubber Insulators*, PhD. Dissertation, University of. Chalmers, 2002.

24. T. W. Graham Solomons and C. B. Fryhle, *Organic chemistry*, 7th ed, John Wiley & sons, Inc. New York, 2002.

25. H. Janssen and U. Stietzel, 10th International Symposium on High Voltage Engineering, Montreal, Canada, 1997.

26. S. M. Gubanski and A. E. Vlastós, IEEE. Trans. Diel. Elect. Insul., Vol 5, 1527-

1535, 1990.

27. J. K. Kim, and I. H. Kim, J. Appl. Polym. Sci., Vol. 79, Issue 12, 2251-2257, 2001.
28. W. U Souheng, *Polymer interface and adhesion*, Marcel Dekker, Inc, New York, 1982.
29. J.R. Hollahan and G.L. Carlson, J. Appl. Polym. Sci., Vol. 14, 2499-2508, 1970.
30. N. Yoshimura, S. Kumagai and S. Nishimura, IEEE. Trans. Diel. Elect. Insul., Vol 6, 632-649, 1999.
31. H. Deng, R. Hackam and E. A Cherney, IEEE. Trans. on Power Delivery, Vol.10, 1012-1024, 1995.
32. J. Kim, M. K. Chaudhury, M. J. Owen and T. Orbeck, J. Colloid Interface Sci., Vol. 244, 200-207, 2001.
33. A. Toth, I. Bertoti, M. Blazso, G. Banhegyi, A. Bognar and P. Szaplonczay, J. Appl. Polym. Sci., Vol. 52, 1293-1307, 1994.
34. M. Morra, E. Occhiello, R. Marola, F. Garbassi, P. Humphrey and D. Johnson, J Colloid Interface Sci., Vol.137, 11-24, 1990.
35. H. Janssen, A. Herden and H. C. Kärner, The loss and recovery of hydrophobicity on silicone rubber surfaces, 10th International Symposium on High Voltage Engineering, Montreal, Canada, 1997.
36. R.S. Gorur, J.W. Chang and O.G. Amburgey, IEEE. Trans. on Power Delivery, Vol. 5, 1923-1928, 1990.
37. H. Hillborg, S. Karlsson and U. W. Gedde, Polymer, Vol. 42, 8883-8889, 2001
38. S. M. Hunt and G. A. George, Polym. Int., Vol. 49, 633-635, 2000.
39. J. Kim, M. K. Chaudhury and M. J. Owen, J. Colloid Interface Sci., Vol. 226, 231-236, 2000.
40. H. Jahn, R. Bärsch and E. Wendt, IEEE conference on electrical insulating and dielectric phenomena (CEIDP), 2000.
41. G. Camino, S. M Lomakin and M. Lazzari, Polymer, Vol. 43, 2011-2015, 2002.
42. A. E. Vlastós and S. M. Gubanski, IEEE. Trans. on Power Delivery, Vol. 6, 888-900, 1991.

43. S. Kumagai, and Y. Yoshimura, IEEE. Trans. Diel. Elect. Insul., Vol.18, 506-515, 2003.

44. T. Sörqvist and A. E. Vlastós, IEEE. Trans. on Power Delivery, Vol. 12, 1041-1048, 1997.

45. S. Siegel and H. Judeikis, J. Chem. Phys., Vol. 43, 343-351, 1965.

46. H. Hillborg, J. F Ankner, U. W. Gedde, D. D. Smith, H. K. Yasuda and K. Wikstrom, Polymer, Vol. 41, 6851-6863, 2000.

47. S. Kumagai, X. Wang and N. Yoshimura, IEEE, Trans. Diel. Elect. Insul., Vol. 5, 281-289, 1998.

48. S. Kumagai and N. Yoshimura, IEEE, Trans. Diel. Elect. Insul., Vol. 8, 203-211, 2001.

49. S. Kumagai and N. Yoshimura, IEEE, Trans. Diel. Elect. Insul., Vol. 8, 679-686, 2001.

50. H. Büchener, F. Schmuck, A. Zanetti, A. Zingg, 10th International Symposium on High Voltage Engineering, Montreal, Canada, 1997.

51. S. H. Kim, E. A. Cherney and R. Hackam IEEE Trans. on Elect. Insul. Vol. 27, 1065-1072, 1992.

52. H. Deng and R. Hackam, IEEE, Trans. Diel. Elect. Insul., Vol. 8, 84-94, 1998.

53. G. G. Karady, IEEE, Trans. Diel. Elect. Insul., Vol. 6, 718-723, 1999.

54. Y. Hirano, T. Inohara, M. Toyoda, H. Murase and M. Kosakada, IEEE, Trans. Diel. Elect. Insul., Vol. 8, 97-103, 2001.

Chapter Three

Experimental and Instrumentation

3.1 Preparation of crosslinked polydimethylsiloxane

Samples of room temperature vulcanized PDMS with different formulations were prepared (polymerized) in accordance with the instructions supplied by Wacker Chemie, Germany.

The weight ratios of reagents used to prepare polymers of different formulations and crosslinking agents (100 g quantities) were mixed as shown in Table 3.1. The polymer component contains a Si-H end group whereas the crosslinking agent has a vinyl end group. These two components, different quantities and types of fillers (mainly silica and ATH), inhibitors and LMW of silicone oils were mixed in the presence of catalyst as tabulated below. The catalyst was added while stirring to avoid cluster formation prior to polymerization. All the components were mixed by means of a static mixer for 5 minutes. The catalyst employed was a Pt compound.

After mixing, the air bubbles were removed by degassing under vacuum in desiccator. This was done to avoid any subsequent void formation in the product that may aggravate degradation during the electrical discharge. After mixing and degassing, the components were placed in a steel mould on Teflon sheets in the presence of a mould releasing agent. Samples of 6 mm thickness and 5.6 cm length and width were cured in the mould for 10 minutes at $100\,^{0}C$. The samples were then placed in a vacuum oven at $100\,^{0}C$ for an hour for post-cure purposes.

Table 3.1: Different formulations of PDMS samples, prepared for this study in 100 gram quantities

Sample ID	Crosslink agent (g)	Fillers (g)		Inhibitor (g)	Catalyst (g)	AK 35 oil (g)
		Silica	ATH			
A Polymer 200	15	-	-	0.08	0.1	-
B "	15	-	-	0.08	0.1	5.76
C Polymer 7,000	3.2	-	-	0.07	0.1	-
D "	3.2	-	-	0.07	0.1	5.17
E "	3.2	15.48	-	0.08	0.1	-
F "	3.2	15.48	-	0.08	0.1	5.94
G "	4	-	26	0.07	0.17	-
H "	4	-	26	0.07	0.17	6.51
I "	4	15.48	26	0.07	0.19	-
J "	4	15.48	26	0.07	0.19	7.29
K Polymer 1,000	1.4	-	-	0.07	0.1	-
L "	1.4	-	-	0.07	0.1	5.08
M (commercial)*	HTV					

* Sample M has the same formulation as sample I.

AK 35 is a low molecular weight, externally added silicone oil, which has a molecular weight of about 2500 g/mole and corresponds to an oligomer of between 4-5 units long. This oil was selected since Hillborg *et. al.* [1] had found that the low molar mass species produced in crosslinked polydimethylsiloxane on exposure to corona discharges were mainly cyclic oligomers with 4-9 repeating units. The externally added LMW oils could have a positive effect on the hydrophobicity recovery.

3.2 Accelerated ageing techniques used

The insulator material was artificially aged by different methods in order to correlate the field-aged and the laboratory-aged samples and to obtain a better understanding of the mechanisms of ageing.

3.2.1 Corona exposure

Two different types of corona discharger were used to treat samples of different formulations. These are the desktop corona and the French cell type corona. Several

other researchers had also used different types of corona discharger and it was considered important to compare the effects of the different types of corona treatment.

3.2.1.1 Desktop corona

The PDMS samples were cut to the desired dimensions for the different analytical techniques. A sample was then rinsed with acetone prior to exposure to corona to prevent any surface contamination during cutting. After rinsing, the sample was dried and then placed at the bottom of a one-litre glass beaker and then exposed to a very high frequency of corona discharge in air at room temperature and normal atmospheric pressure for various times.

A model BD-20 AC high-frequency laboratory corona treater, supplied by Electro-Technic product, USA, was used. A schematic diagram of the desktop corona discharger is shown in Figure 3.1. This needle electrode has high ion bombardment which can have a serious effect on the degradation of the material.

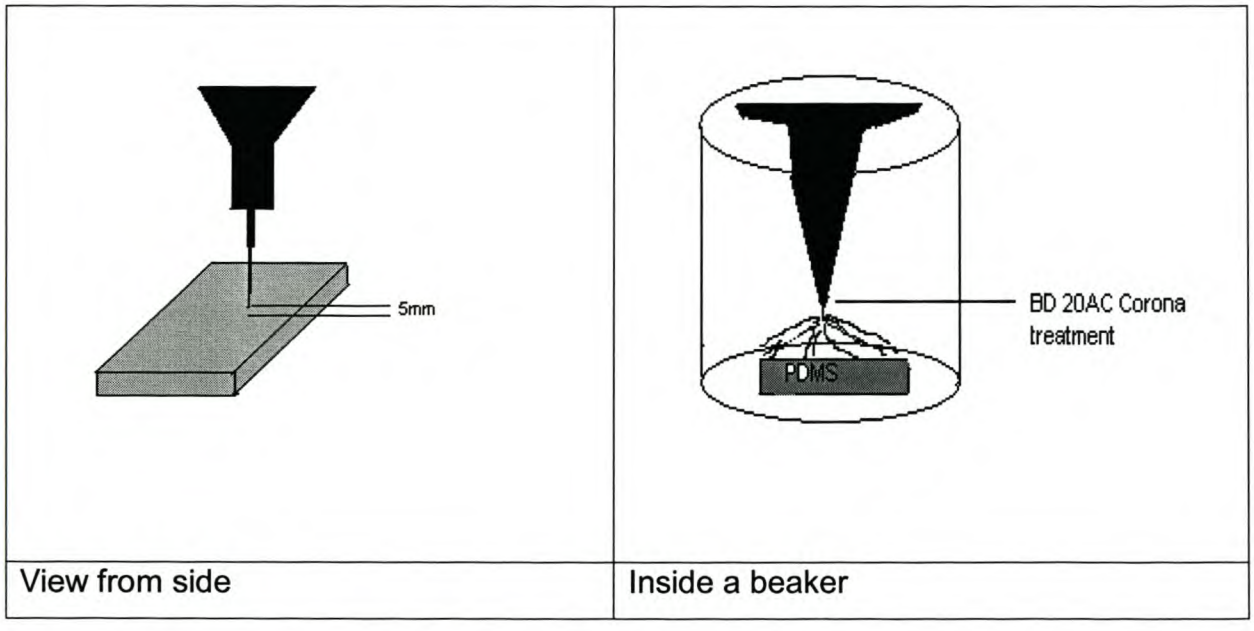

Figure 3.1: Schematic diagram of desktop corona discharger.

The distance between the surface of the PDMS sample and the stationary tip of the corona discharger needle was 5 mm. A spark of visible glow generated by the laboratory corona treater impinged to the surface of the PDMS sample for the required period of time. The nature of the corona formed in the needle electrode corona treater was similar to the corona ageing of real insulators in service. Care was taken to move

the sample onto a backing plate for the static contact angle measurement and all other sample analyses without deformation. Samples were covered when transported to avoid any contamination before analysis.

3.2.2.2 French cell type corona

The construction of this type of corona is based on a design that was developed in France, and hence termed French cell corona [2].

This type of corona discharge ageing was done at the high voltage laboratory in the Department of Electrical Engineering, University of Stellenbosch, using standard safety precautions, including a safety cage and ventilation to remove the ozone generated during the corona treatment. Before the corona treatment of the different PDMS formulations the relative permittivity of the samples was determined since the air gap is dependent on it. Samples having the same permittivity and thickness were aged in one experiment. This was done to ensure that each sample was exposed to exactly the same surface stresses.

A schematic diagram of the French cell type corona is shown in Figure 3.2. The glass casing was constructed in an attempt to control the amount of ozone that the surfaces were exposed to, by improved control of the outflow through the cell.

In the figure, *e* is the relative permittivity and L_1 is thickness of the glass, L_2 is the air gap and L_3 is the thickness of the sample. With the following formula it is possible to vary the air gap and voltage, depending on the relative permittivity and thickness of the sample, to ensure that all samples are treated in exactly the same manner.

$$V = E_2(\varepsilon_2 / \varepsilon_1 L_1 + L_2 + \varepsilon_2 / \varepsilon_3 L_3 + \varepsilon_3 / \varepsilon_4 L_4) \quad (3.1)$$

E_2 is the field strength and V is the voltage applied

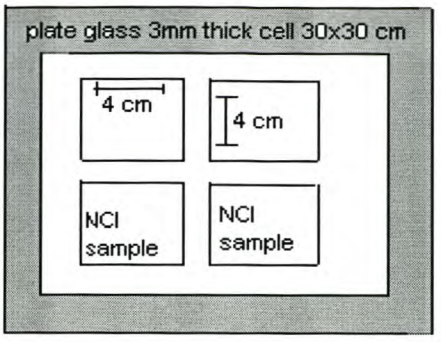

View from top

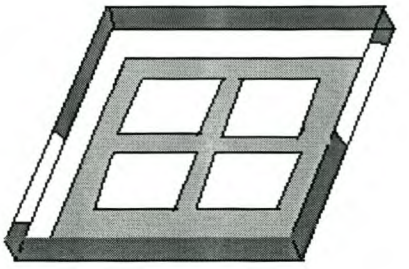

Side view showing open side for air/ozone flow

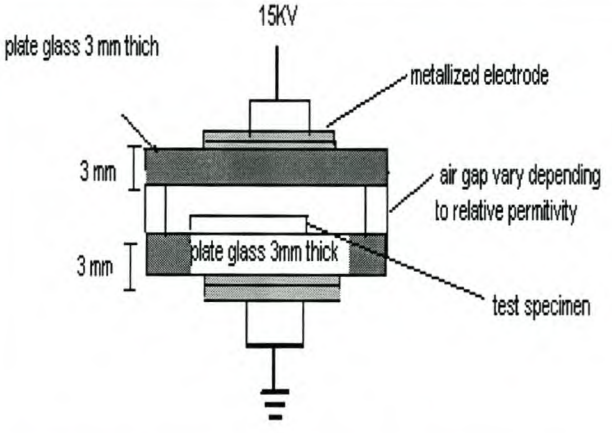

Sample in French cell under glass

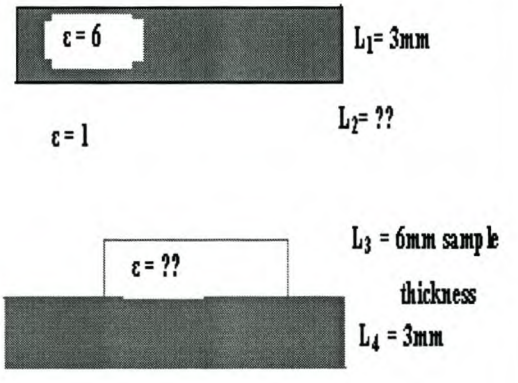

Calculation of the air-gap

Figure 3.2: Schematic representation of different views of the French cell type corona discharger.

3.2.2 UV-C exposure

A significant amount of UV light is produced during corona discharge [3, 4]. This UV radiation can play a role in the degradation of insulator materials. It is well known that the PDMS material is highly resistant to the effect of UV-A (340 nm) and UV-B (313 nm). Therefore, the aim of this study was to determine if the short wavelength UV-C light, which is believed to be produced during corona discharge, will have an influence on the material degradation.

In order to study the possible effect of UV-C, HTV Wacker Chemie-formulated PDMS samples were exposed to a UV-C lamp for different periods of time. The samples were placed inside a box 2 cm distant from the UV-C lamp. The xenon UV-C lamp had an

intensity maximum at a wavelength of 254 nm.

3.2.3 Naturally aged PDMS insulators

Three naturally aged HTV PDMS samples from the KIPTS test station were also included in this study as part of the investigation to determine the effect of cleaning of the insulator surface prior to analysis. This study was considered necessary since pollution and other surface contamination on the naturally aged samples can lead to misleading results. The pollution and contaminants present on the sample surface could be a significant problem since most of the analytical techniques are surface specific. The samples used here were specified as blue, light grey and dark grey, and are shown in Figure 3.3.

A number of different cleaning techniques were investigated and the one decided upon was as follows: The samples were first heated at $200^{0}C$ for 30 minutes and then allowed to cool to an ambient temperature. After 30 min they were cleaned in an ultrasonic bath with 10 ml chloroform for 5 minutes. This was repeated with fresh solvent subsequently. The samples were dried for 15 min in an oven of $40^{0}C$ to eliminate the chloroform.

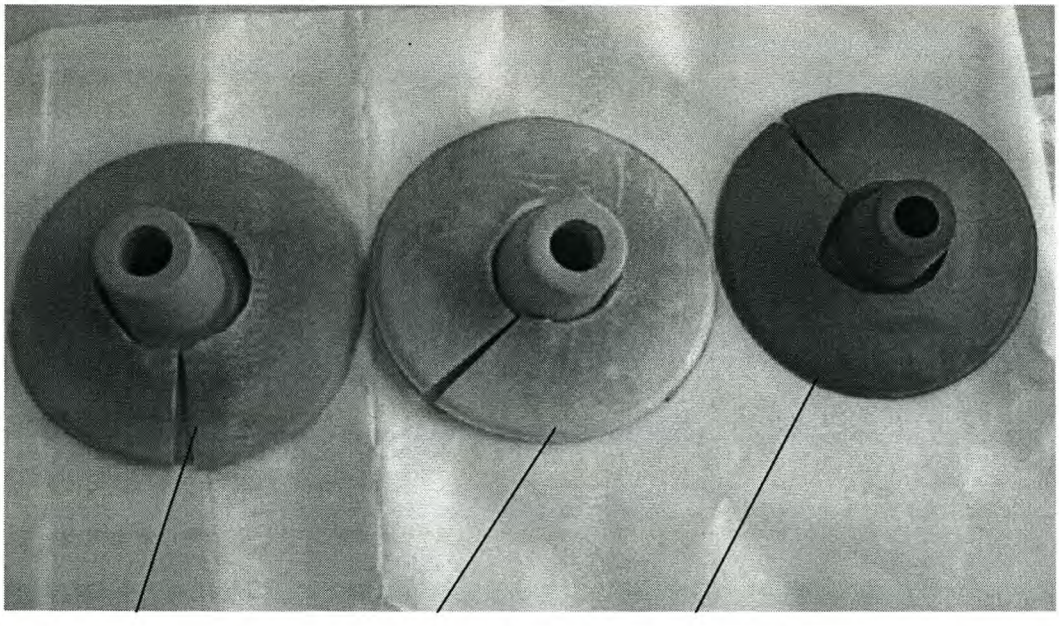

Blue *Light grey* *Dark grey*

Figure 3.3: Three different KIPTS aged HTV insulators.

3.3 Instrumentation

Various analytical techniques and measurement were used for the analysis of the samples, as described in Sections 3.3.1-3.3.5.

3.3.1 Positron annihilation spectroscopy

Positron annihilation spectroscopy (PAS) is a unique technique and well recognized as a powerful nano-probe for micro structural analysis of polymeric materials [5, 6]. PAS is able to directly determine the free-volume properties in polymeric materials. Positrons (e^+) are the anti-particles of electrons (e^-). Typically they are produced in a radioactive source such as Sodium-22 and Germanium-68. When they come in contact with electrons, they can form positronium (Ps), which is the bond state of an electron and positron. Positronium can be formed in two states: para-positronium (spins anti-aligned) and ortho-positronium. The positron and electron have parallel spin (spins aligned). The formation probability for these two states is 1:3. However, o-Ps has a longer lifetime in molecular substrates [7]. Positron techniques are based on the measurement of the annihilation radiation produced when positrons implanted into a polymer matrix and the electron in the polymer matrix meet and annihilate. The annihilation occurs since a positron is essentially the anti-matter of an electron. During annihilation both the positron and electron are destroyed and the masses of each converted to energy (photons).

As mentioned above, the basic principle of PAS lies in the fact that the electromagnetic interaction between electrons and positrons makes possible annihilation of the e^+- e^- pair, in which the total energy of the annihilation pair may be transferred to photons. These annihilation gamma photons carry information on the electronic environment in which the positron annihilates. In polymers the positronium atoms formed are localized in the free volume holes of the polymer. The annihilation characteristics of the positronium atoms contain information about the nature of the free volume holes. Due to the localization of the positronium in the open spaces, the positron annihilation techniques has proven to be the most sensitive technique for tracking changes that occur in the polymer structure. Positron annihilation lifetime spectroscopy can provide important information about defect size and concentration and on open volume defects in most solid materials [8].

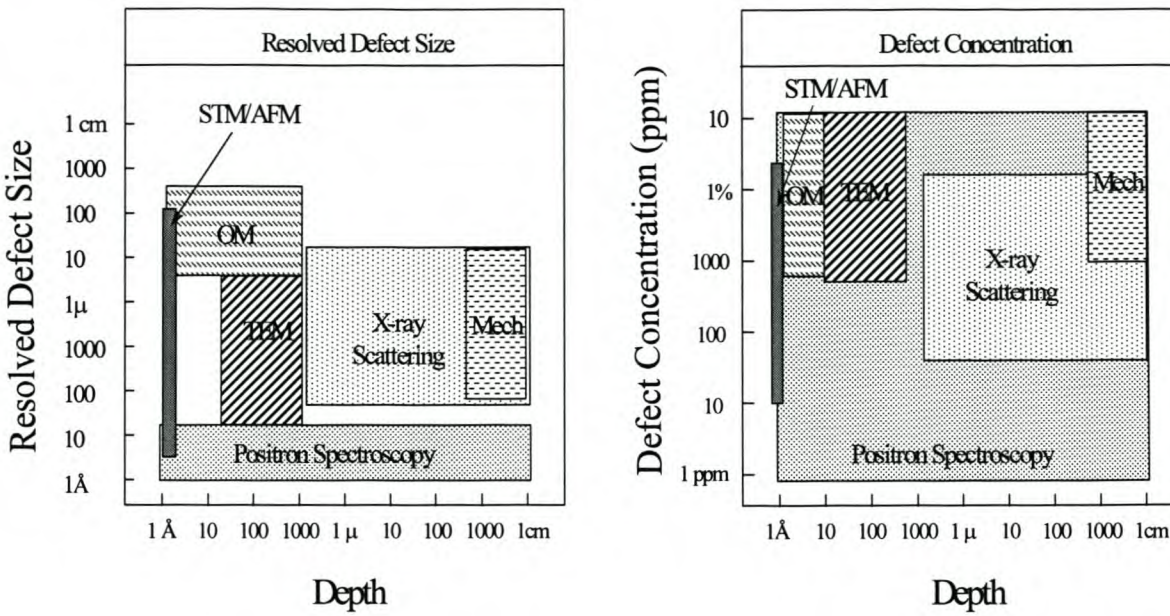

Figure 3.4: Schematic representation showing that PAS analysis has a special position in vacancy defect analysis over optical microscopy (OM), neutron scattering (ns), transmission electron microscopy (TEM), scanning tunnelling microscopy (STM) and atomic force microscopy (AFM), and X-ray scattering [8].

There are other methods available for the general detection of open volume defects. Some of the best-known are the microscopic techniques such as transmission electron microscopy (TEM), atomic force microscopy (AFM), scanning electron microscopy (SEM) and optical microscope (OM). As is shown in Figure 3.4, all have specific regions of high sensitivity and resolution. Positron annihilation lifetime spectroscopy, however, is effective and sensitive in providing size information at any sample depth for defect sizes below the effective resolution of other techniques mentioned above. Positron techniques are both highly sensitive and can resolve the size of atomic vacancies at any depth in a sample.

In this study the positron beam results are reported as the S parameter or defect parameter, and it is calculated from Doppler broadening energy spectra. The S parameter is defined as the ratio of the central area to the total area of the 511 keV annihilation peak after the background is properly subtracted. Figure 3.5 shows the Doppler broadening energy spectra and the definition of the S parameter. The energy parameters (E_1 and E_2) are chosen so that the value of the S parameter = 0.50 for pure silicon.

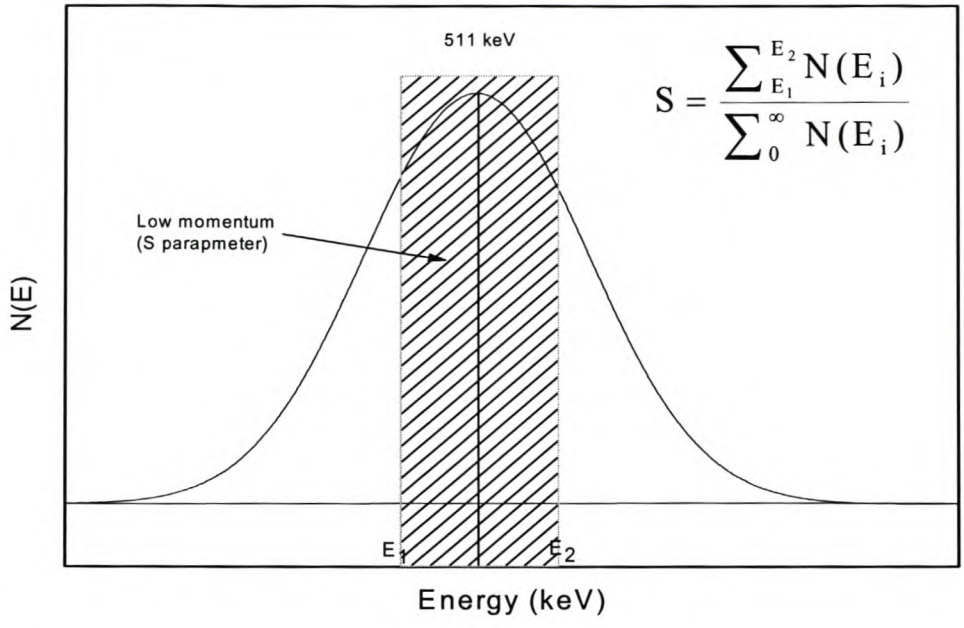

Figure 3.5: Doppler broadening energy distribution of annihilation radiation showing the definition of the S parameter.

In polymeric materials the S parameter represents the contribution of the low momentum part of the positron-electron annihilation radiation in sub-nanometre defects, such as free volume and holes [5]. The beam measurements were performed on the variable mono-energetic positron-beam at the University of Missouri, Kansas City, USA. A detailed description of the procedure can be found in Zhang *et. al.* [9].

When a positron with well-defined energy is accelerated from a vacuum into a polymer, it either reflects back to the surface or penetrates into the polymer. The fraction of positrons penetrating the polymer substrates increases rapidly as a function of positron energy. The mean implementation depth as a result of inelastic interactions with polymer molecules is expressed as [10]

$$Z(E_+) = \left(\frac{40 \times 10^{3}}{\rho}\right) E_+^{1.6} \qquad (3.2)$$

where Z is the thickness of the material in nanometres, ρ is the density of the PDMS material in kilograms per cubic meter, and E_+ is the incident energy in kilo electron volts.

The depth profiling information on the free volume properties of a polymer can therefore be obtained by controlling the implantation energy, varied from 0.1 keV to 30.0 keV, and can provide information of the free volume from the very near surface region (<1 μm from the surface) to the bulk ($\pm 9 \mu m$ from the surface).

3.3.2 Atomic Force Microscopy

In this study samples of four different formulations were analysed by AFM. The formulations used were: sample C (pure PDMS), sample E (PDMS with 15% silica), G (PDMS with 26% ATH) and I (PDMS with both 15% silica + 26% ATH).

3.3.2.1 Force-distance relationship

Contact mode is the most common method of operation of the AFM. As the name suggests, the tip and sample remain in close proximity with the sample as the scanning proceeds, so that the atomic force acting between the tip and sample are repulsive. The repulsive forces result in a vertical deflection of the cantilever away from the surface [11].

Figure 3.5 shows a schematic diagram of a typical force-distance curve for AFM. Besides the investigation of the topographic image of surfaces, the AFM can be used to probe physical properties locally, at one point on a sample surface. The most common probing method is to record a force-distance curve between points A, B and C, as shown in Figure 3.5. AFM can generally measure the vertical deflection of the cantilever with pico-meter resolution. Therefore, the deflection signal obtained by the distortion of the laser beam is plotted as a function of the vertical distance as the probe is lowered onto the surface and retracted again.

The cantilever is lowered from a certain height above the surface until it touches the surface (A to B). In this region no force is acting on the probe and the cantilever is not distorted. At B the probe jumps into contact with the sample causing the cantilever to bend downwards. The tip comes into contact with the sample and the cantilever is deflected upwards (B to C), reflecting repulsive tip-sample forces. The gradient of this part (B to C) depends directly on the hardness of the sample and is larger for harder sample surfaces.

As the probe is retracted from the sample, it tends to stay in contact (stuck) with the surface, because of certain adhesive force acting between the sample and the probe (C to D). Therefore, a pull-off force is needed for the disengagement of the tip and the sample at D, where the cantilever finally comes loose and is no longer distorted. This pull-off force is used as a measure of adhesion between the probe and the sample. The distance from point D to the base line (section E) is a measure for the adhesive force acting between the probe and the sample. This force can be calculated by multiplying the deflection (E) with the spring constant of the cantilever.

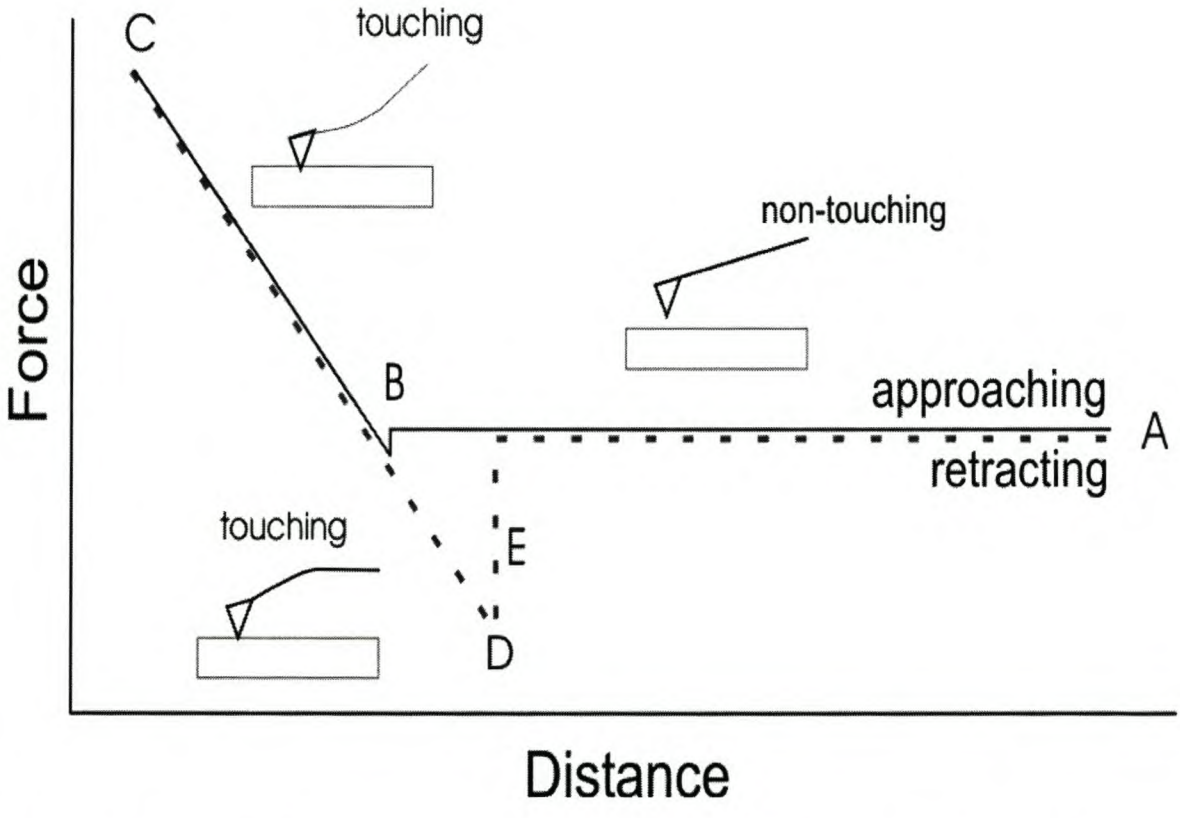

Figure 3.6: Schematic force-distance relationship of the cantilever deflection and the vertical distance in AFM.

The AFM measurements were performed on a Multimode scanning probe microscope from Veeco at several points on the PDMS sample. The force distance curves were recorded with a hydrophilic Si_3N_4 contact probe with a spring constant of k=0.2 N/m of Nanosensors. All measurements were carried out under ambient conditions. The adhesive forces acting between the hydrophilic probe and a hydrophilic surface are stronger than between the probe and a hydrophobic surface. Therefore, this method

can be utilized to measure the degree of hydrophillicity of the sample surface.

3.3.3 Scanning electron microscopy

The surface structures of the different samples of PDMS materials (virgin, and after exposure to corona discharge) were examined by scanning electron microscopy (SEM). The analyses were done using a fully analytical LEO S440 Scanning Electron Microscope. The elemental analyses were done using a Fisons Kevex Detector with Quantex Quasar Pro software. All the sample surfaces used for EDAX analysis were coated with a thin carbon layer before examination to improve the conductivity. The samples used for images were sputter coated with gold/palladium. The SEM and EDAX analyses were done at the University of Cape Town's Microscopic unit.

3.3.4 Fourier transform infrared spectroscopy

This method gives a characteristic transmittance, which can be used to show different bonds and chemical groups present in a material. FTIR spectroscopy detects the molecular vibrations of a molecule. The technique provides important information about the chemical nature of the surface of a material. In the past, FTIR was used to analyse non ceramic insulators to identify the degree of degradation of the polymer at the surface due to ageing [12]

Basically there are two types of surface specific FTIR: attenuated total reflection (ATR) and photo acoustic spectroscopy (Pas).

ATR is a surface-sensitive technique, commonly utilized to determine surface information on polymeric samples. The ATR instrumentation used in this study was a spectral-Tech with a horizontal zinc selenide mirror, and the beam angle was 45° at 10 bounces. The apodization was strong, with a mirror velocity of 0.2 m/s. The resolution was 4 cm^{-1}, with 1 cm^{-1} interval for 16 scans.

Pas is another simple FTIR analytical technique that does not require special sample preparation. The technique is easier to use than ATR, which requires good contact between the crystal and polymer surface. The samples to be analyzed were placed in an MTEC 300 chamber and flushed with ultra high-purity helium. Spectra were recorded on a Perkin Elmer Paragon 1000 FTIR.

3.3.5 Static contact angle measurements

The hydrophobicity of different samples aged for different periods of time by corona discharge and UV-C radiation were quantified by using the static contact angle measurement (using a magnifying glass and capturing images with a digital camera). The analyses were done at room temperature, and the NCI material to be measured was mounted on a horizontal smooth surface. A drop of distilled water (1 μl volume) was placed onto the surface by means of a 1 μl syringe. An image of the drop on the surface was then captured using a magnifying lense and a digital camera. This image was taken within 20-30 seconds of putting the drop on the surface. This contact angle was determined by analysing the dimensions of the drop from the digital image and using the formula in equation (2.2) to calculate the contact angle. An example of the digital image is shown in Figure 3.6 below.

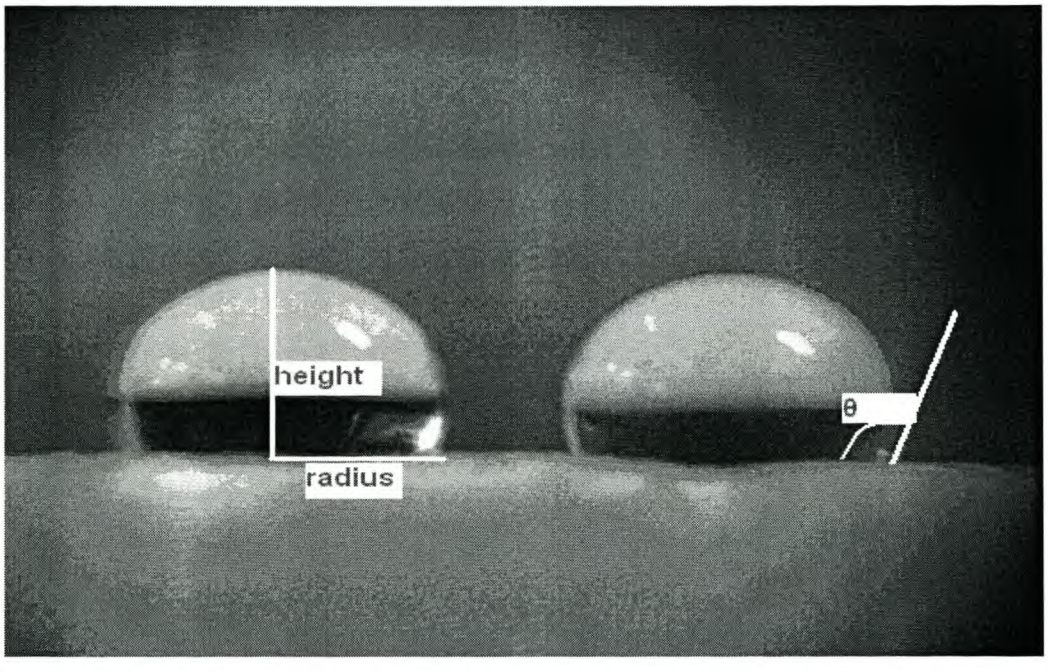

Figure 3.7: Digital image showing height and radius of SCA measurement.

To minimise possible human error in reading the dimensions, 10 droplets were measured and an average value taken. All contact angle measurements reported in this thesis are therefore the average of 8-10 measurements. Care was taken not to place the drops in the same positions on the sample as this may also influence the measurement.

3.4 References

1. H. Hillborg, S. Karlsson and U. W. Gedde, Polymer, Vol. 42, 8883-8889, 2001.
2. H. F. Mark, N. M. Bikales, C. G. Overberger and G. Menges, *Encyclopedia of Polymer Science and Engineering*, John Wiley & Sons, New York, Vol. 5, 539, 1986.
3. http://www.polyplastics.com/en/support/tech/treat/treat_2.html (28-01-2004).
4. V. M. Moreno, R. S. Gorur and A. Kroese, IEEE, Trans. Diel. Elect. Insul., Vol. 10, 80-95, 2003.
5. Y. C. Wu, Chia-Ming, Huang, Y. LI, R. Zhang, H. Chen, P. E. Mallon, J. Zhang, T. C. Sanderczki, Da-Ming. Zhu, Y. C. Jean, R. Suzuki and T. Ohdaira, J. Polym. Sci. Part B, Polym. Phys., Vol. 39, 2290-2301, 2001.
6. H. Cao, J. P. Yuan, R. Zhang, C. M. Huang, T. C. Sandreczki and Y. C. Jean, Macromolecules, Vol. 32, 5925-5933, 1999.
7. H. Cao, Y. He, R. Zhang, J. P. Yuan, T. C. Sandreczki, Y. C. Jean and B. Nielsen, J. Polym. Sci. Part B, Polym. Phys., Vol. 37, 1289-1305, 1999.
8. Y. C. Jean, P. E. Mallon, D. M. Schrader, *Principles and applications of positronium and positronium chemistry*, Eds World Scientific Publishing, Singapore, 2003.
9. R. Zhang, H. Cao, C. M. Huang, P. E. Mallon, T. C. Sandreczki, J. R. Richardson, Y. C. Jean, B. Nielsen, R. Suzuki and T. Ohdaira, J. Radiat. Phys. Chem., Vol. 58, 639-644, 2000.
10. H. Cao, R. Zhang, C. S. Sundar, J. P. Yuan, Y. He, T. C. Sandreczki and Y. C. Jean, Macromolecules, Vol. 31, 6627-6635, 1998.
11. S. S. Sheiko, *Imaging of polymers using scanning force microscopy: from superstructures to individual molecules*, Advances in Polymer Science, Vol., 151, Springer-Verlag, Berlin, Heidelberg, 2000.
12. N. Yoshimura, S. Kumagai and S. Nishimura, IEEE. Trans. Diel. Elect. Insul., Vol 6, 632- 649, 1999.

Chapter Four
Results and Discussion

4.1 Wettability and hydrophobicity recovery

The importance of surface water repellence for the performance of polymeric high voltage insulators has been known for a long time. This repellency suppresses electrical surface activity like dry-band arcing or corona discharge, which otherwise degrades the polymer surface.

Although PDMS materials lose their hydrophobicity due to corona discharge, they exhibit a fast recovery of hydrophobicity after corona treatment compared to other polymeric insulating materials [1-3]. This is mainly due to the diffusion of LMW oligomers from the bulk to the surface of the insulators. It is this property that makes PDMS compounds so important in the field of high voltage insulating materials, and has led to their increased application over the past few decades. It is essential, therefore, to evaluate the wettability and rate of hydrophobicity recovery of PDMS to improve our understanding of the material's behaviour. The surface wettability of a material is usually estimated by measuring the wetting angle of a water droplet resting on the surface.

4.1.1 Rate of hydrophobicity recovery

Figure 4.1 shows the images of a water droplet on a pure PDMS polymer sample (C) after 5 minutes of corona treatment. Immediately after corona treatment the static contact angle became completely flat, meaning that the material became completely hydrophilic. With time, the material became progressively hydrophobic and a complete recovery was recorded after 24 hours. After a full day, a discrete droplet was formed, unlike the drop after 10 min showed small increase from complete flat. Although the degree and rate of recovery differed from sample to sample, a similar trend to that observed in Figure 4.1 was observed for all samples.

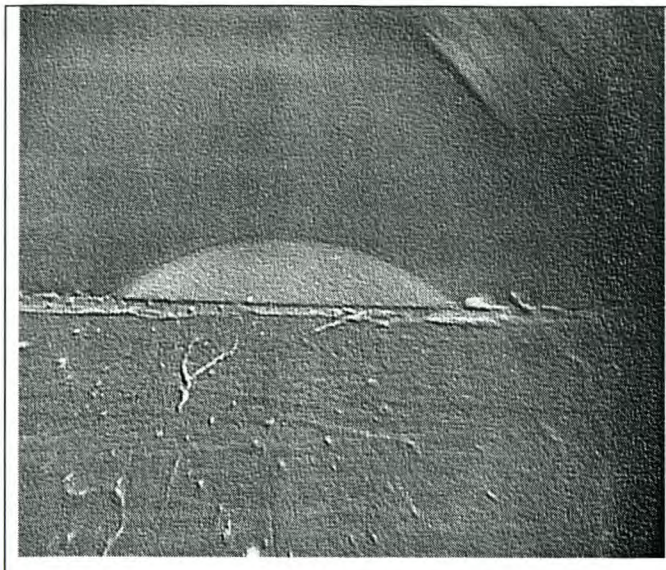

10 minutes after corona treatment, 39°

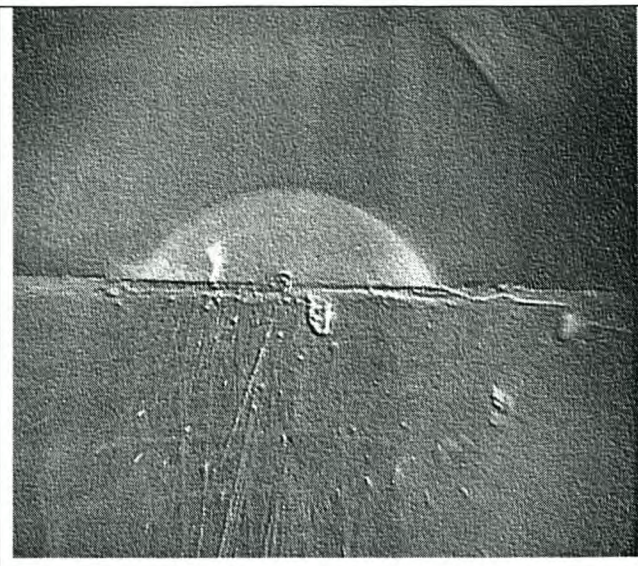

30 minutes after corona treatment, 60°

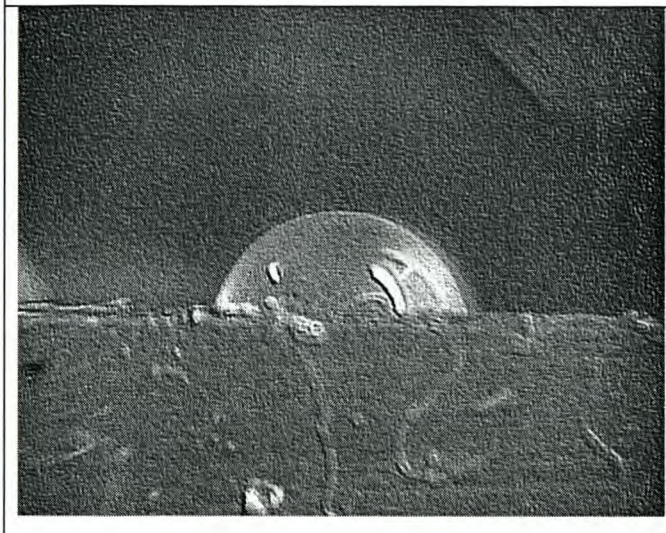

1 hour after corona treatment, 72°

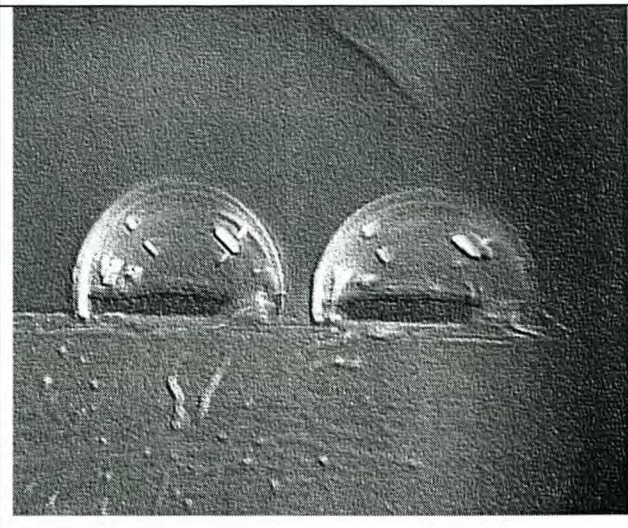

24 hours after corona treatment, 95°

Figure 4.1: SCA Images after 5 min corona treatment of sample C taken with a digital camera, showing hydrophobicity recovery with time.

4.1.2 Impact of filler on hydrophobicity recovery

Corona discharge strongly influences the loss and hydrophobicity recovery of PDMS materials. According to ASTM D2275 [4], during corona treatment there is generation of ozone gas and formation of atomic oxygen, both of which are strong oxidising agents. These initiate surface oxidation of the polymer, which leads to loss of hydrophobicity. To quantify the loss and hydrophobicity recovery, the static contact angles were measured. Each point in the graph represents an average of 8 to 10 measurements.

Figure 4.2 shows the results of the static contact angle measurements obtained for different formulations of samples after 30 min desktop corona treatment, as a function of recovery time.

Generally, all the PDMS samples, regardless of their formulation, led to a full loss of hydrophobicity after exposure to corona for a certain period of time as is indicated by the flatness of the water drop. The contact angle measurement at zero time (immediately after corona) was found to be completely flat after 30 minutes of desktop corona treatment, which signifies that the material became temporarily hydrophilic. When water was placed on the surface, there was complete formation of a film on the surface. However, the different types of formulations recovered slowly with time, although the degree and rate of recovery differed from sample to sample. When comparing the samples with additive (fillers) and the ones without any filler, those without fillers recovered faster than those with fillers.

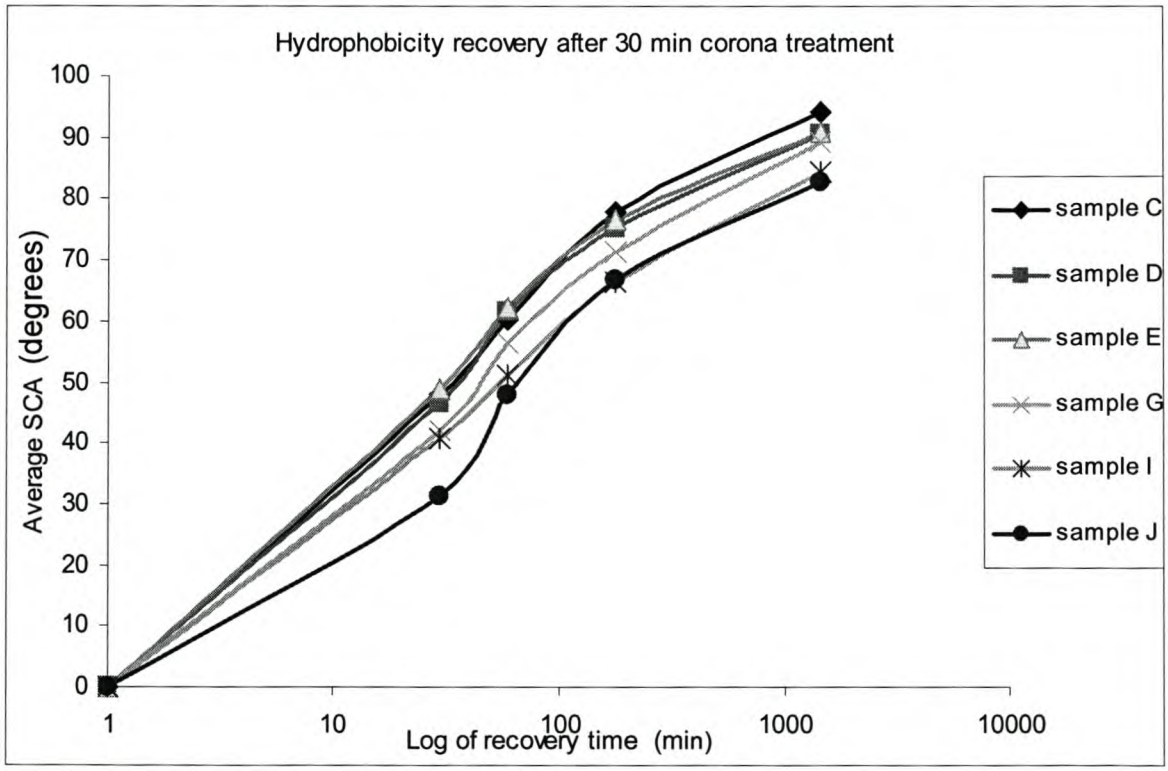

Figure 4.2: Rate of hydrophobicity recovery of different PDMS formulations: after 30 min desktop corona treatment of samples C, D, E, G, I and J. (Refer to Table 3.1 for the formulations)

As can be seen from Figure 4.2, those samples without ATH filler, i.e. C, D and E (as indicated in Table 3.1), which have the same degree of crosslinking density as samples

I, J, and G, recover faster than all the other samples. Samples C and D (pure PDMS) completely recovered after 24 hours, whereas all the other samples with different types and amounts of fillers recovered more slowly. Even after 24 hours recovery time they had not recovered fully.

Furthermore, the filler type and level also affects the hydrophobicity recovery. Samples I and J contained more than 40% filler (a combination of silica and ATH) and were observed to have a slower rate of recovery (as indicated in Figure 4.2). Sample G, PDMS with ATH filler, had a slower recovery rate than sample E, PDMS with silica. Therefore, one may conclude that the filler added to the different formulations could have a negative effect on the rate and degree of the hydrophobicity recovery. This could be due to the mechanical strength that a product containing filler has. Such materials are mechanically stronger than those without filler and can resist the de-polymerisation process which occurs during corona treatment, leading to the formation of less low molecular weight degradation products, which are responsible for the recovery.

Hillborg and Gedde [5] suggested that the formation of a silica-like inorganic layer retards the rate of hydrophobicity recovery by reducing the movement of the low molecular weight species from the bulk to the surface. The results shown in Figure 4.2 also reveal that the sample with filler, particularly ATH, recovered slowly. Therefore, there is a higher probability of silica-like and hydrophilic group formation in those samples with ATH filler, due to the presence of O-H groups in the filler.

Samples with different formulations have different recovery rates, depending on the formulations and method of preparation. Figure 4.3 presents the recovery rates of three different PDMS polymers as a function of recovery time after 30 min corona ageing. Although all three samples had zero contact angles when measured immediately after 30 minutes corona treatment, the sample with no filler (sample C) recovered faster, whereas samples M and I which had a similar composition but differed only in the way they were prepared, recovered slower than C. Both samples with filler did not recover fully, even after 24 hours recovery time.

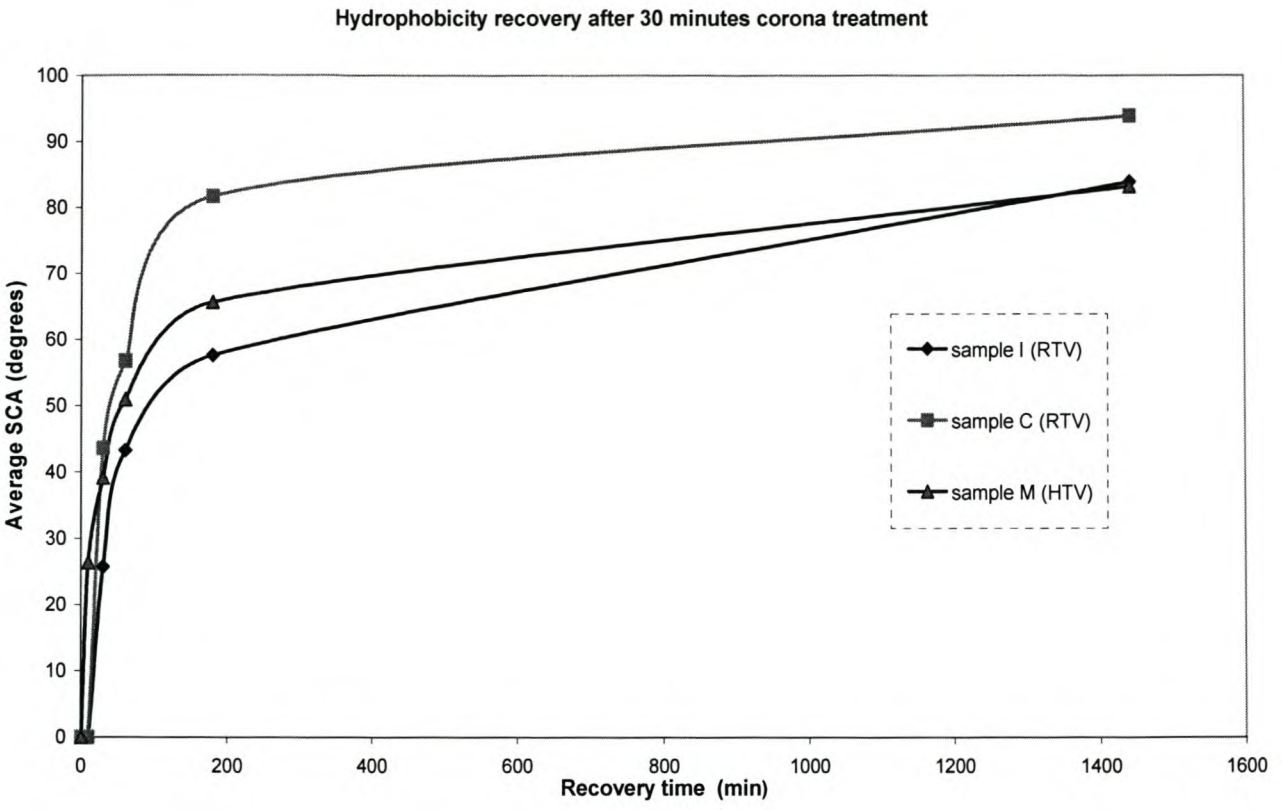

Figure 4.3: Graph comparing hydrophobicity recovery after 30 min corona of RTV and HTV PDMS samples.

Sample M, a commercial HTV sample, recovered slightly faster than Sample I, a RTV sample of similar crosslinking density. This result agrees with the conclusion given by Janssen et. al. [6]. HTV PDMS contains both linear and cyclic LMW oils whereas RTV PDMS, like sample I, contains only cyclic LMW oils. The linear LMW oils in the HTV PDMS are suggested to cause the difference in rate of recovery of hydrophobicity. It is suggested that linear LMW oils are more effective for the recovery of hydrophobicity than the cyclic oligomers. This is due to their special structures that make it easier for them to diffuse to the surface of the polymer.

4.1.3 Influence of low molecular weight oils addition on hydrophobicity recovery

Diffusion of low molecular weight siloxane from the bulk polymer to the surface is one of the suggested mechanisms of hydrophobicity recovery which is accepted by most researchers [6-10].

The rate of hydrophobicity recovery and level of the contact angle after complete recovery depends on the amount of low molar mass silicone oils that migrate from the

bulk to the surface of the material. These LMW species may originate as by-products of degradation or be present in the material as a result of the production process or incomplete curing.

Toth [11] has reported that removal of the LMW extractable species prior to the corona treatment reduced the rate of hydrophobicity recovery. Normally one can expect that a sample containing pre-existing LMW siloxane will recover faster if the low molecular weight siloxane oligomers are responsible for the rate of recovery. However, as seen in Figure 4.4 (a) and (b), the effect recorded in this study is not as pronounced. The figure shows that both samples D and C have rather similar recovery rates. Even though sample D is prepared by addition of extra LMW siloxane it has no effect on the speed of recovery. As mentioned earlier, the low molecular weight oligomer added to sample D was the Wacker AK35 oil, which has a molecular weight of about 2500 g/mole and corresponds to an oligomer of between 4-5 units long.

To investigate the effect of the removal of LMW species that could exist in the material, we performed solvent extraction with chloroform. Interestingly, the extracted sample C recovered more rapidly than the unextracted sample C and the one prepared by addition of extra LMW oligomers (sample D). This is contrary to the expected result. One possible explanation for this result could be that the extracted samples were deformed and damaged during the extraction process. During extraction, the sample was swollen by chloroform, after which it became full of cracks due to evaporation of solvent when exposed to air. It is expected that the recovery rate, due to the cracked surface, would be faster than the case of specimens lacking surface cracks. This is because the diffusion of LMW PDMS oils can easily occur by diffusing from the bulk to the surface through these cracks.

A report by Hillborg *et. al.* [5] reveals that the hydrophobicity recovery of untouched samples is slower than the recovery of mechanically deformed samples. The reason given was that in the mechanically deformed samples cracks are formed on the thin silica-like layer and mobility of the LMW is increased through these cracks.

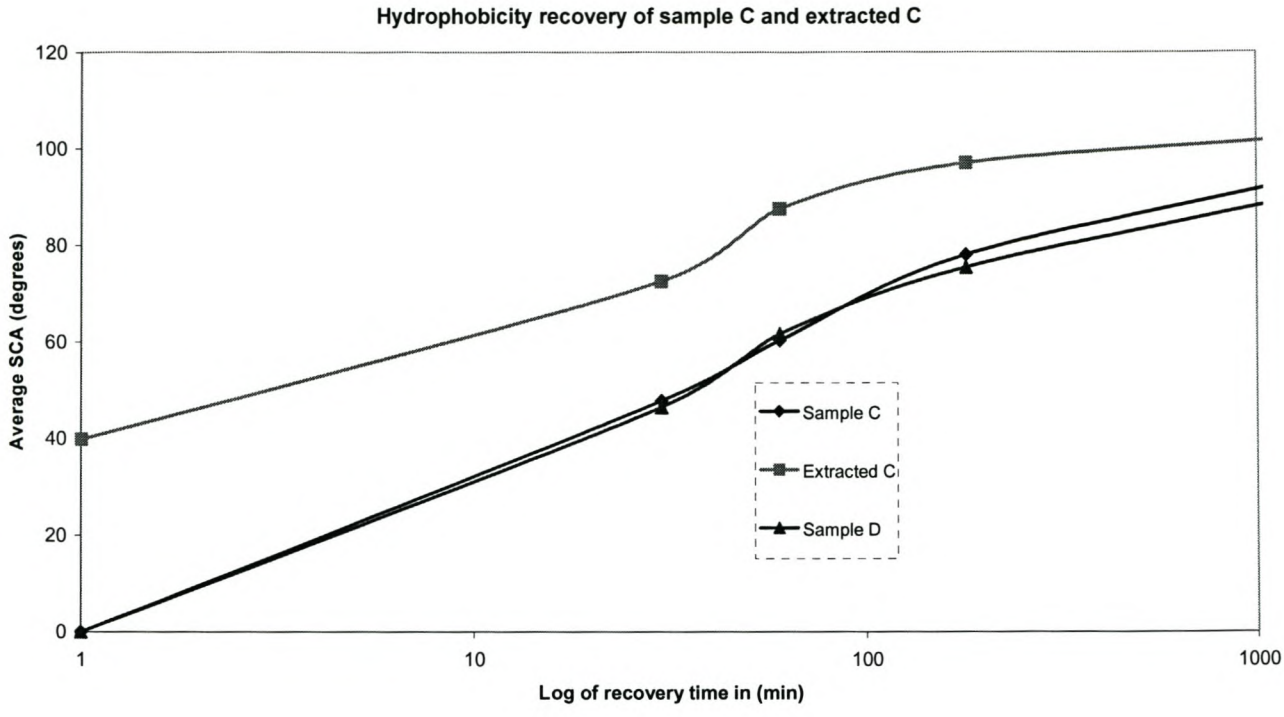

a)

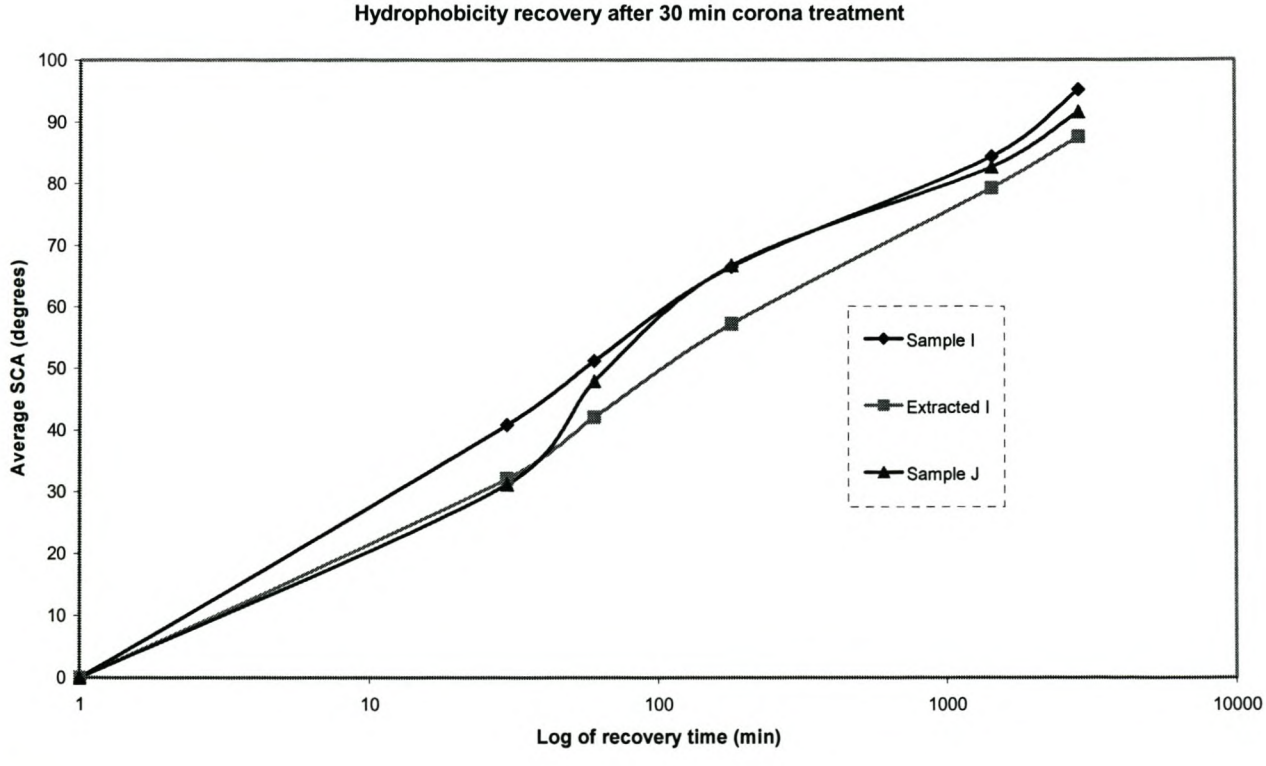

b)

Figure 4.4: Recovery of hydrophobicity of a) PDMS samples C, D and extracted C and, b) samples I, J and extracted I.

Similar result were obtained for samples J and I. Sample J, prepared with the addition of extra LMW oils, recovered more slowly than the samples without added LMW species, especially during the first hour. The extracted sample I recovered more slowly than the unextracted sample, as shown in Figure 4.4 b. This is contrary to the results obtained for the pure PDMS compounds (sample C) were the extracted sample recovered faster than the unextracted sample. This could be due to the better mechanical strength of sample I. In sample I, unlike sample C, there was no crack formation after extraction and deswelling, due to the added mechanical strength lent by the fillers.

Figure 4.5 shows the contact angle recovery after corona treatment for samples E (with SiO_2 filler) and F (the same as E, but with addition of LMW oils of PDMS). Initially sample F showed a slightly faster recovery, but after 30 min E recovered at a faster rate.

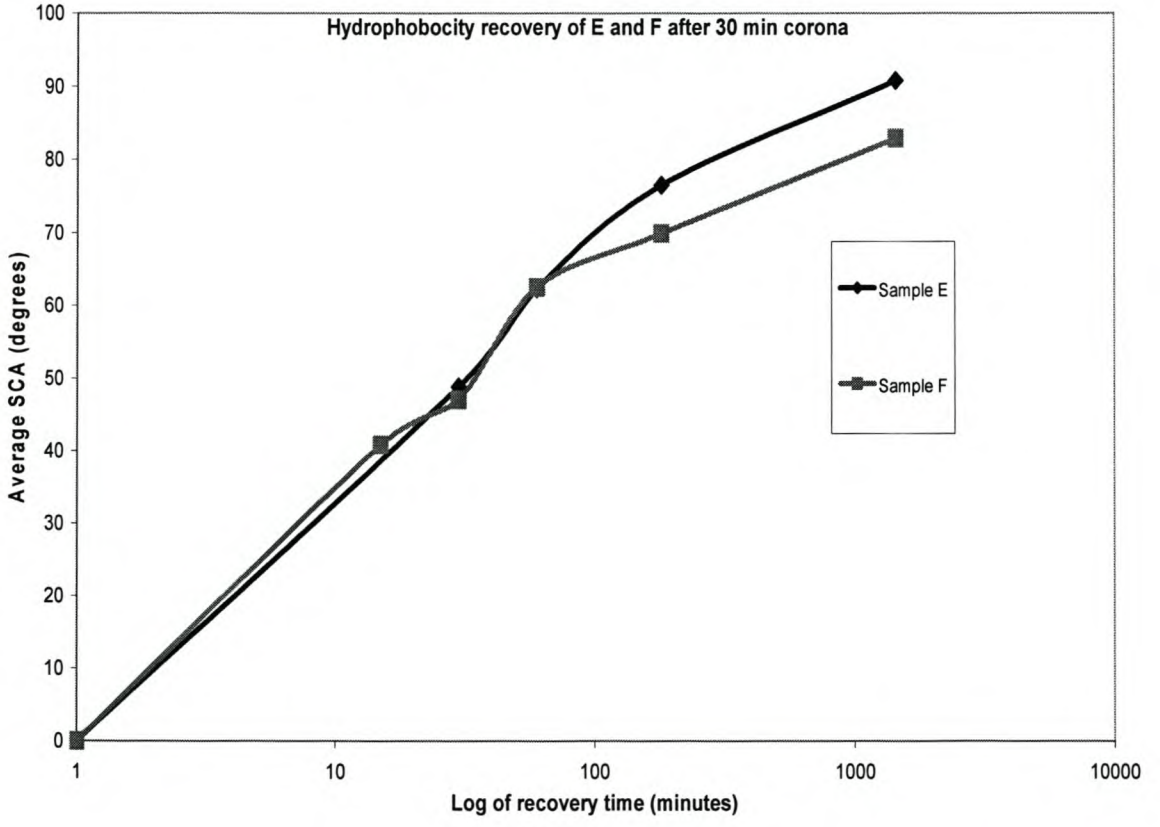

Figure 4.5: Hydrophobicity recovery of samples E and F (extra LMW oils added) after corona treatment.

These results agree with previous findings [5] that the recovery of hydrophobicity by diffusion of LMW species from the bulk to the surface is governed predominantly by the

formation of low molecular weight species due to de-polymerisation in the process of the corona discharge (*in situ*) formation and not by the pre-existing low molecular weight species in the matrix.

4.1.4 Effect of duration of exposure to corona

Figure 4.6 a and b shows the loss and rate of hydrophobicity recovery after different periods of treatment time with the desktop corona discharger for samples C and I. In all cases hydrophobicity loss is observed even after a very short period of corona treatment time (5 min).

Samples C and I treated for 10 minutes recovered faster than the others. Samples treated for a longer time (30 minutes corona treated) took a longer time to recover. Both samples treated for 30 minutes recorded zero contact angles even after 10 minutes. These results agree with the findings of Yoshimura *et.al.* [12], who reported that corona treatment of a weak intensity and for a short period of time activates LMW chains while treatment for long time and strong intensity suppresses them, especially in the cases of materials prepared with higher levels of ATH. The five minutes corona treatment may not be long enough to generate adequate LMW PDMS oils for the fast recovery.

The longer recovery time for the 30 min corona treated sample is most probably due to the formation of a SiOx degradation layer that restricts diffusion of LMW short chains to the surface. This is confirmed by positron beam results, were the 30 min corona treated sample shows a significant surface layer (at least 40-60 nm), as will be discussed in the section describing the positron results (4.2).

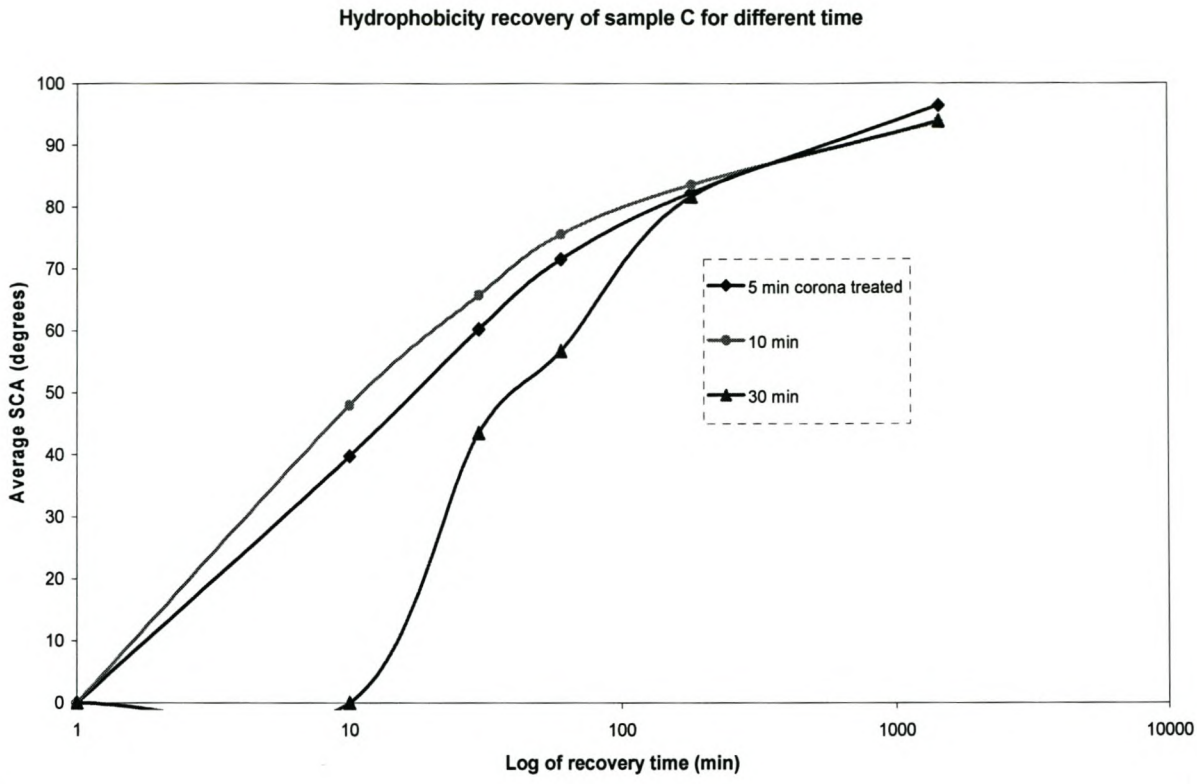

a)

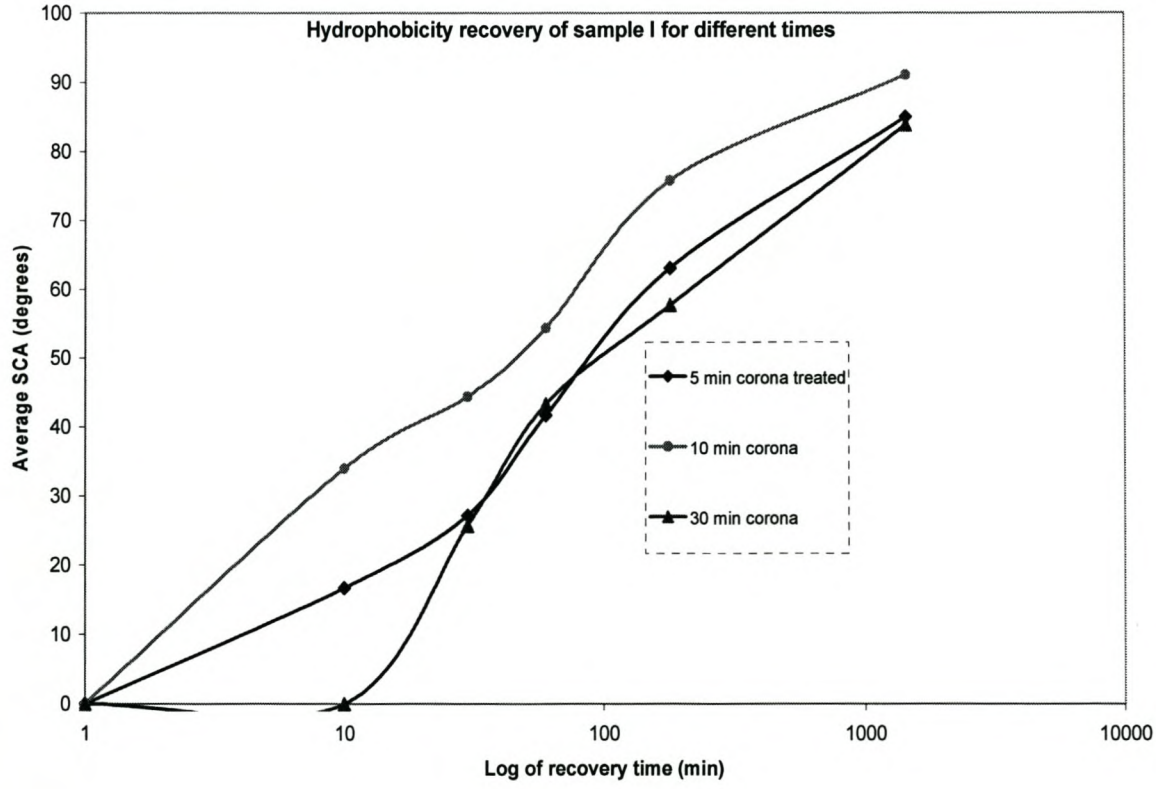

b)

Figure 4.6: Loss and recovery of hydrophobicity exposed to desktop corona discharge samples of a) C, b) I.

4.1.5 Impact of UV-radiation

Some researchers [13] have shown that UV radiation of various silicone rubber grades has a negligible impact on the material, due to the bonding strength between molecules within the PDMS materials. On the other hand, other researchers have suggested that UV radiation plays a role in the gradual reduction of the hydrophobicity [12]. Elastomeric materials, such as EPDM, show micro cracks after a certain period of time of outdoor exposure, mainly due to UV-radiation, as suggested by Gubanski [14]. The micro cracks therefore lead to a spreading of moisture and the EPDM insulators became hydrophilic.

Corona discharge produces UV radiation. It is well known that PDMS is highly resistant to UV-A (340 nm) and UV-B (313 nm) radiation due to strong bonds between oxygen and silicone atoms, it is therefore highly resistant to UV-radiation from natural sunlight. Shorter wavelength UV-C (254 nm) radiation is, however, a possible component of corona-produced UV light. The aim of this study was to investigate whether this short wavelength UV-C has a significant influence on the PDMS material.

Figure 4.7 shows the SCA as a function of recovery time for PDMS samples after 100, 200, 300 and 500 hours of UV-C radiation.

These results confirm that there is only a very small reduction of the hydrophobicity with longer exposure time to UV-C. There is a slight difference between the 100 hours UV-C lamp exposed sample and the 500 hours exposed sample. It was observed that the hydrophobicity measurement of the HTV sample after 500 hours was reduced to 85° from 102°.

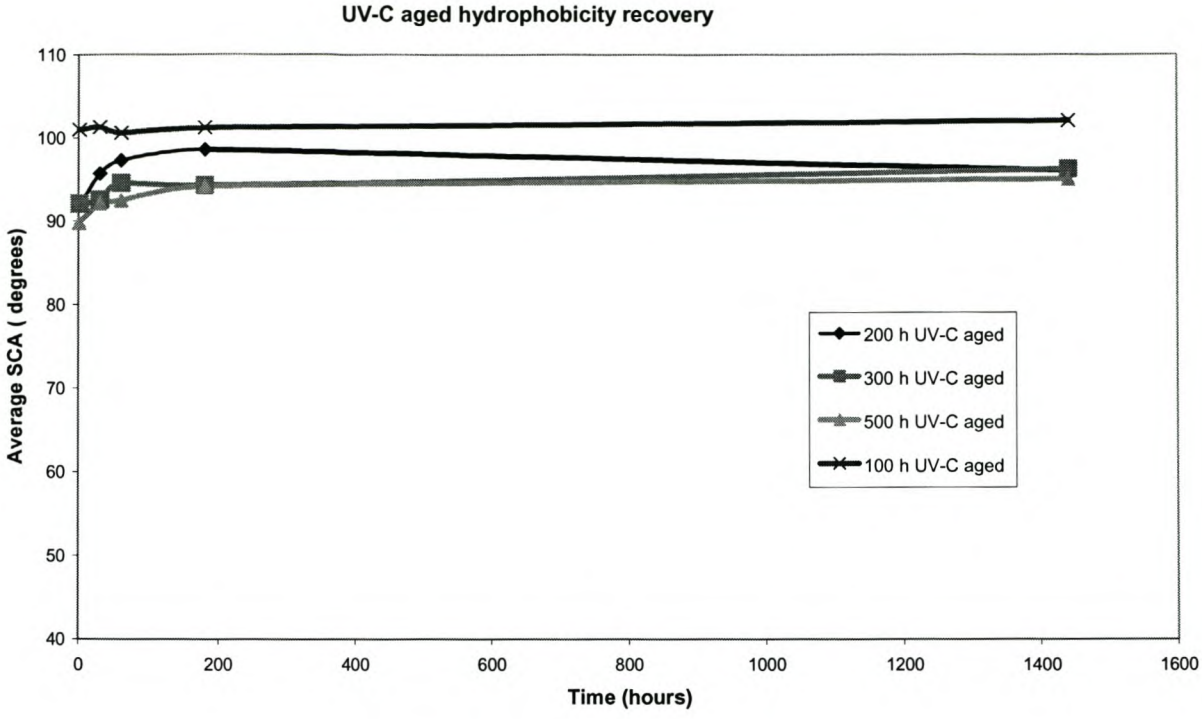

Figure 4.7: Loss and recovery of hydrophobicity of sample M (HTV) UV-C aged as determined by SCA measurement.

Results of HTV samples, which confirm little change after ageing with UV-B radiation, as studied by positron annihilation spectroscopy, can also be seen in Figure 4.8 below. After 240 hours UV-B exposure there is only slight change in the S parameter.

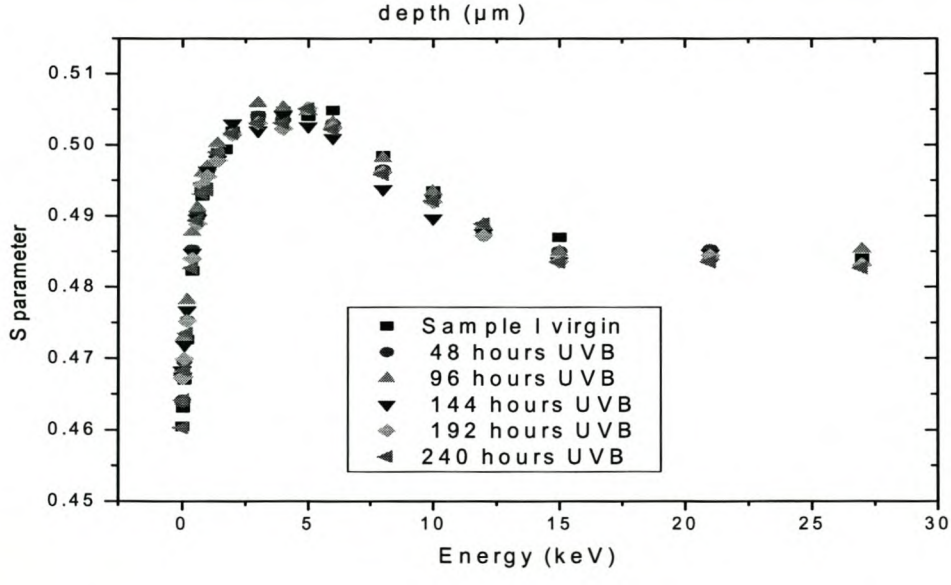

Figure 4.8: PDMS sample UV-B aged for up to 240 hours, as studied by PAS.

4.1.6 Comparison of two types of corona ageing

As mentioned in chapter three, two types of corona were used: the desktop type ageing and the French cell type corona. Figure 4.9 a and b shows the static contact angle measured for samples treated for different periods of time with the French cell type corona. Most of the samples treated by the desktop corona recorded a completely flat (zero) angle (indicating a hydrophilic surface) during the contact angle measurement even after a very short treatment time, unlike the samples treated using the French cell were the contact angle is only reduced to about 70° even after 60 min of treatment. In the case of the French cell treatment the contact angle only reached 0° after 6 hours of treatment time. This might be associated with the higher frequency of the desktop corona treatment. Since the corona discharge is directly on the surface of the sample, there is ion bombardment, whereas in the French cell corona type the treatment is done under a glass cover, which makes it milder. Ion bombardment is known to play a large role in the degradation of the PDMS material [15-16]. Therefore, this could be the reason that samples treated by desktop corona result in complete loss of hydrophobicity, even after a relatively short period of time. The French cell corona type needs a longer treatment time to achieve such a large change. The difference between the desktop and French cell type corona is basically that the desktop corona is more aggressive than the French cell corona type.

Figure 4.9 (a and b) shows that the French cell type corona needs a longer treatment time before an effect on the contact angle can be measured. As indicated earlier, the desktop corona led to a zero contact angle even after only five minutes of treatment, but in the French cell type it did not show appreciable change even after an hour (as is seen in Figure 4.9 a). In Figure 4.9 b the contact angle is measured as zero after 6 hours corona treatment. This comparison will be also discussed in section 4.2.2, where the positron results are discussed.

Figure 4.9 b shows that the sample treated with desktop corona recovers more slowly than both the 6 and 10 hours French cell type corona treated samples. This indicates that the desktop corona has a greater influence on the loss of hydrophobicity than the French corona type does. This slower recovery is also most probably due to the formation of a thicker SiOx layer after desk top corona treatment, as will be conformed by the positron results described in section 4.2.2.

a)

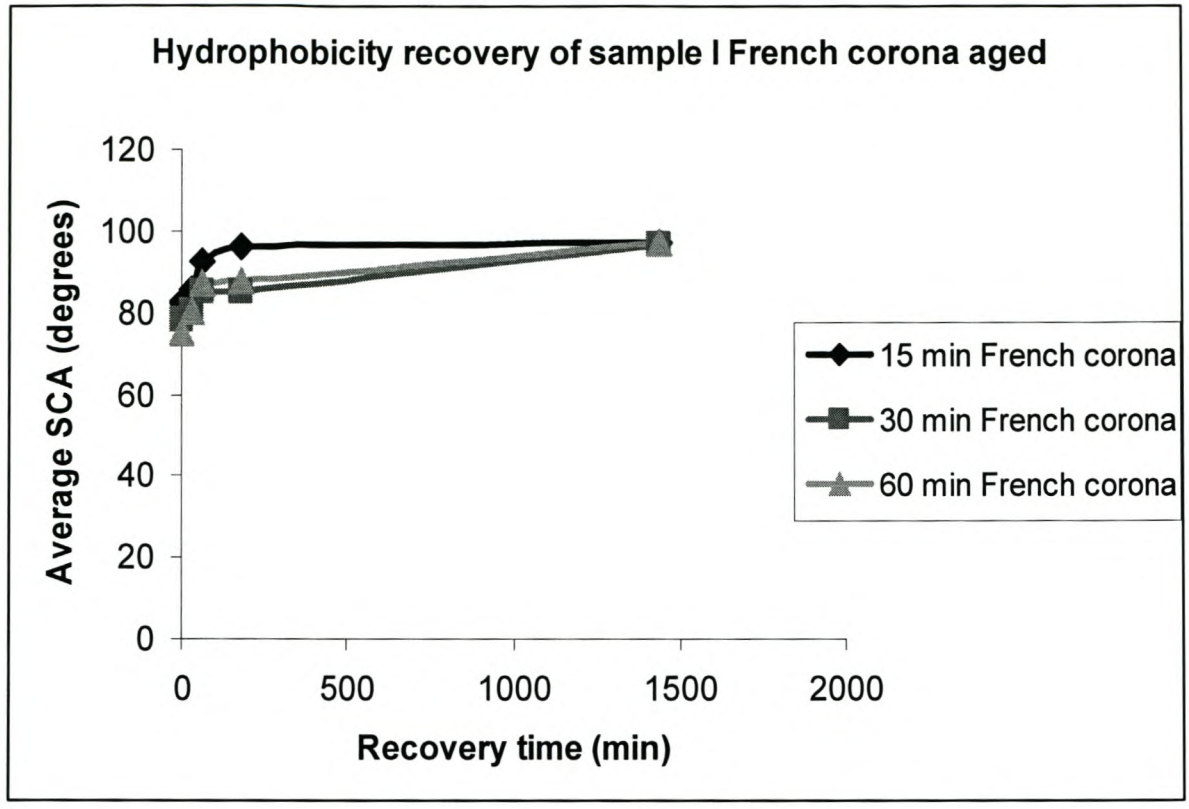

b)

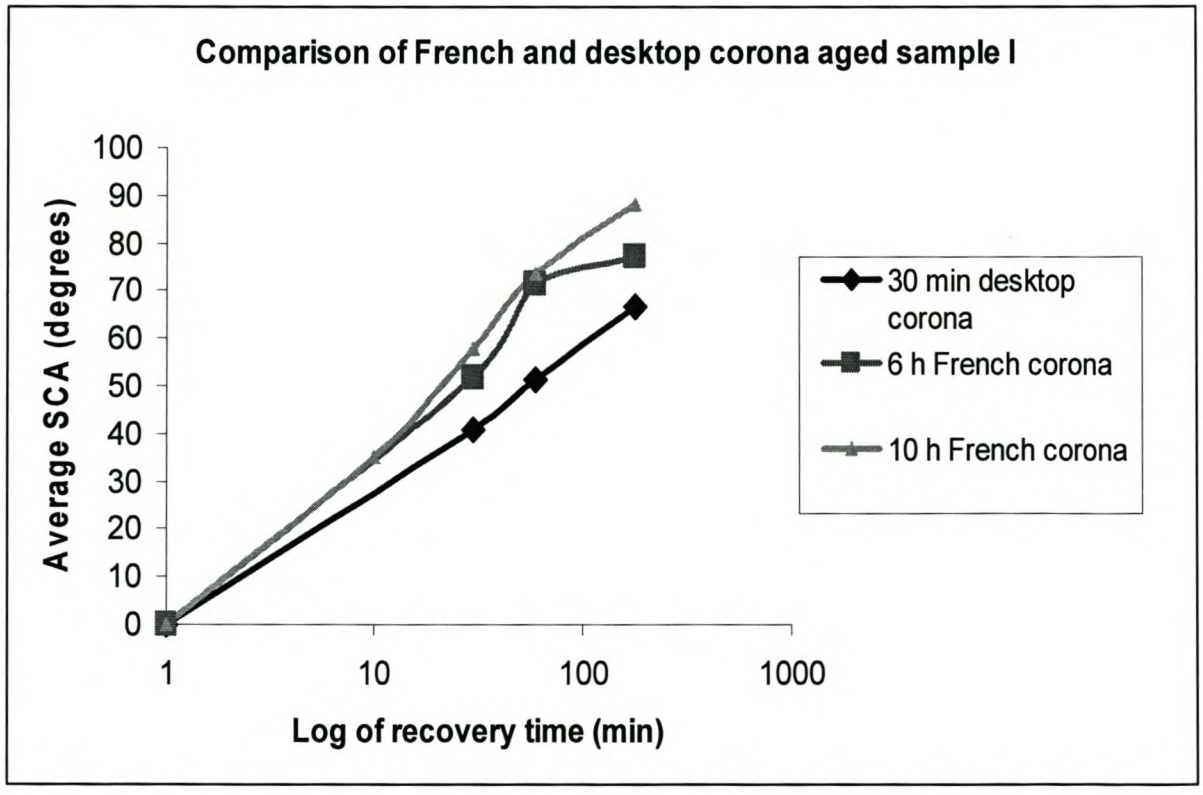

Figure 4.9: Hydrophobicity recovery of sample I after corona treatment for (a) short (b) long corona treated with French type and 30 min desktop corona

4.2 Positron annihilation spectroscopy analysis

Positron annihilation spectroscopy is a special non-destructive evaluation technique for material characterization [17-18]. It provides useful information about defect properties of the material under consideration. In this study the positron results will be presented in terms of the S parameter or defect parameter. In polymer materials, a larger S parameter indicates a larger free volume (defect parameter) [19]. The S parameter is the ratio of the central part of the 511 keV annihilation peak to the total peak area. This technique is useful for investigating micro structural change at the molecular level at the early stage of material degradation. The technique has been shown to be highly effective for tracking material changes in polymeric coatings as a function of various artificial and natural weathering [19].

4.2.1 Time dependency study of PDMS samples

Corona treatment has a dramatic effect on the S parameter profiles of PDMS samples. In our recent publication [20], we presented results that show a systematic change in the S parameter depth profile for pure PDMS compounds as a function of the corona treatment time. Figure 4.10 shows the variation in the S parameter as a function of the positron incident energy and mean depth of penetration for pure PDMS compounds for different periods of corona treatment. Similar to most polymers [18, 21], the S parameter near the surface for the virgin PDMS polymer (which is less than 1 keV incident positron energy) is small. This is due to back-scattering and back-diffusion of the positron and positronium (Ps) from and near the polymer surface. The back-scattering positron component is an inevitable problem in slow-beam positron spectroscopy and a considerable fraction of back-diffused positrons at the low implantation energy < 1 keV reduce the fraction of positrons and Ps that annihilate inside the material under investigation [17]. The energy at which the S-parameter reaches a maximum indicates the diffusion length of the positron and Ps.

In polymeric samples, the S parameter is used as a qualitative measurement of the free volume holes. The decrease of the S parameter is associated with the loss of free volume in polymer materials [22]. The data in Figure 4.10 show that the effect of the exposure of the PDMS polymer (sample C) to corona reduces the free volume of the sample near the surface, as is indicated by the decrease of S parameter, although a chemical effect is most probably also present.

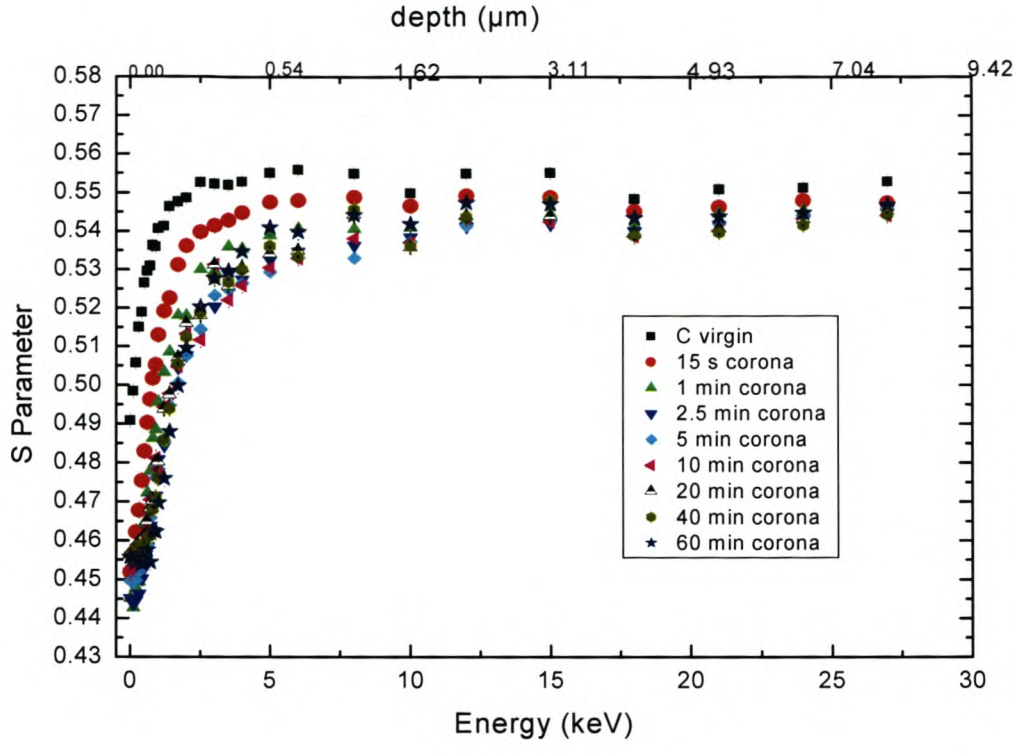

a)

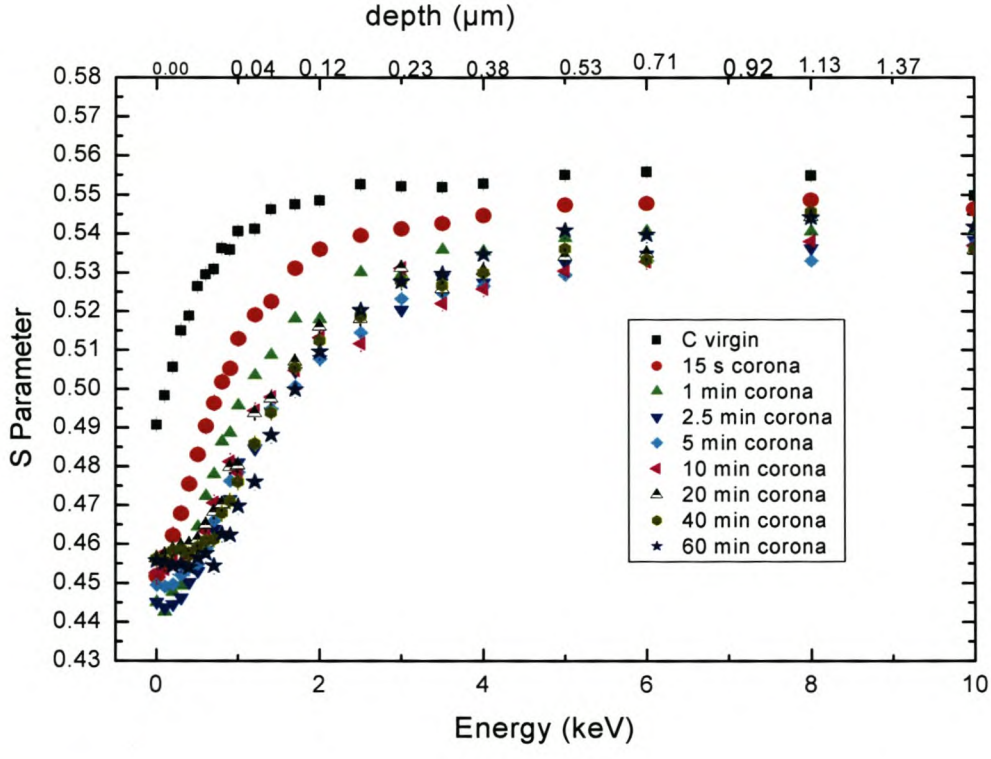

b)

Figure 4.10: a) S parameter profiles of sample C as a function of corona treatment time, and b) an enlarged profile (0-10 keV implantation energy).

Corona treatment of the pure PDMS polymer (without filler) surface results in a significant change in the S parameter of the sample. Even after a very short period of time (15 seconds), there is a large drop in the S parameter near the surface of the polymer. This once again illustrates the extreme sensitivity of the PAS technique in material analysis; very small material changes can be detected. The decrease in the S parameter near the surface continues appreciably with increasing corona treatment time, until about 5 min. With further corona treatment, it is observed that there is an increase in the S parameter at the very near surface region. At this point there is also a "levelling off" of the S parameter profile even with further corona treatment. Therefore, at the early stage of degradation the S parameter is observed to show a dramatic decrease until 5 min corona treatment time. This is due to the start of polymer degradation and probably the start of crosslink formation, as well as breakdown of the polymer chain. It has already been shown by Zhang *et. al.* [23] that there is a direct relationship between the decreases in free volume (S parameter) and an increase of crosslink density for polyurethane coatings after ageing.

The increase in the S parameter with further corona treatment time, as shown in Figure 4.10, might be due to extreme damage of the polymer, to the extent where it is no longer considered as a polymer and the formation of a silica-like layer at the surface has occurred.

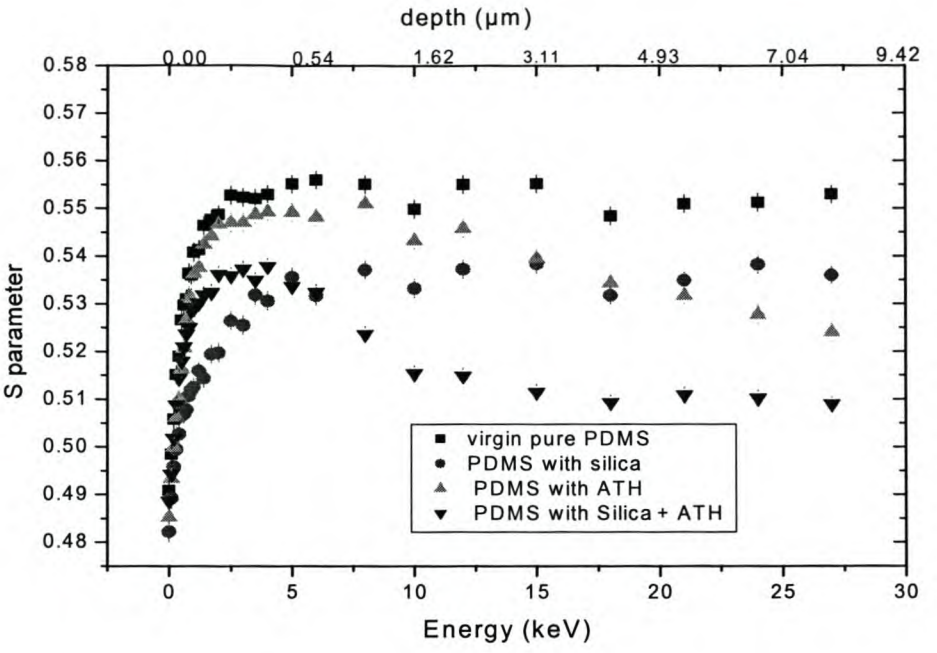

Figure 4.11: Depth profiles of different RTV PDMS compounds.

Figure 4.11 shows the S parameter profiles of RTV PDMS compounds of different formulations. In both the PDMS samples containing ATH the S parameter increases from the surface, it reaches a maximum and then decreases into the bulk. This is ascribed to the effect of the ATH filler. It indicates that the RTV compound consists of a polymer "skin", an intermediate layer (where the filler starts to affect the S parameter) and the bulk. The ATH particle size was determined to be between 1 and 2 μm. The decrease in the S parameter corresponds well with this value in that the decrease is observed between 0.5 and 1 μm from the surface. The S parameter near the surface is lower for the compounds that contain silica. The very near surface profile of the sample containing both ATH and silica is very similar to the profile of the compound contain silica. This indicates that in the former compound the surface layer of the polymer does contain silica. A similar result was found by Reynders *et. al.* [24] using XPS for analysing PDMS compounds. They also concluded that the surface of PDMS compounds contain a polymer-rich layer of about 20 nm thickness before the effect of the ATH filler became dominant. Results obtained in this study indicate that the compound studied has a polymer-rich layer of about 0.5-1 μm near the surface, indicated by the maximum in the S parameter curve. A similar S parameter profile has been reported by Cao *et. al.* [25] for commercial polymer coatings containing pigments of TiO_2 filler.

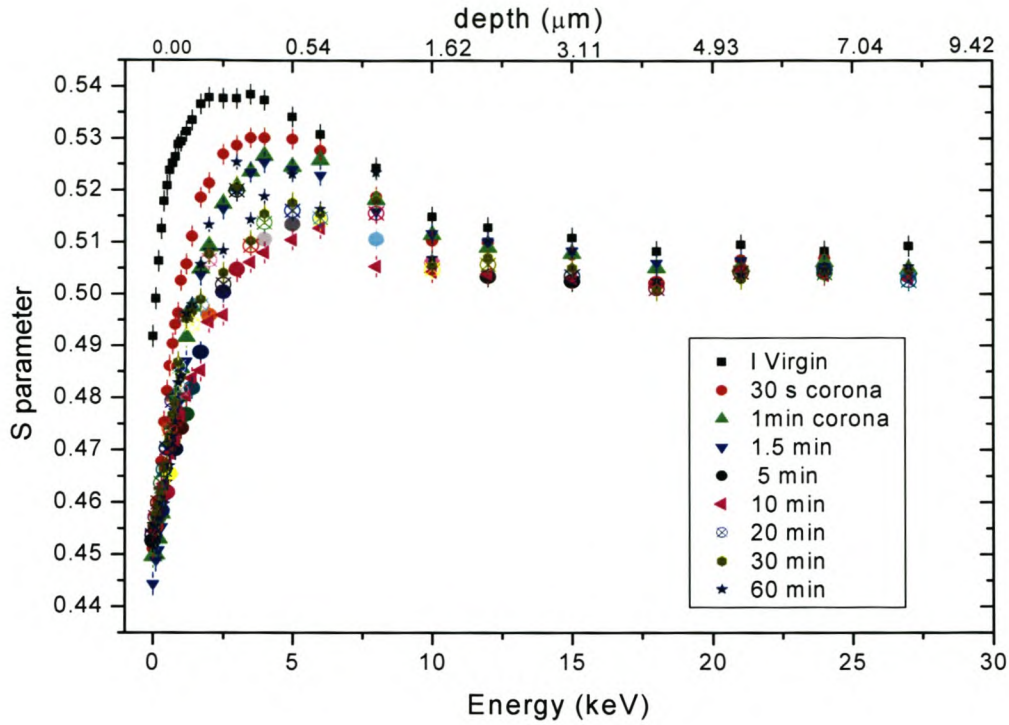

a)

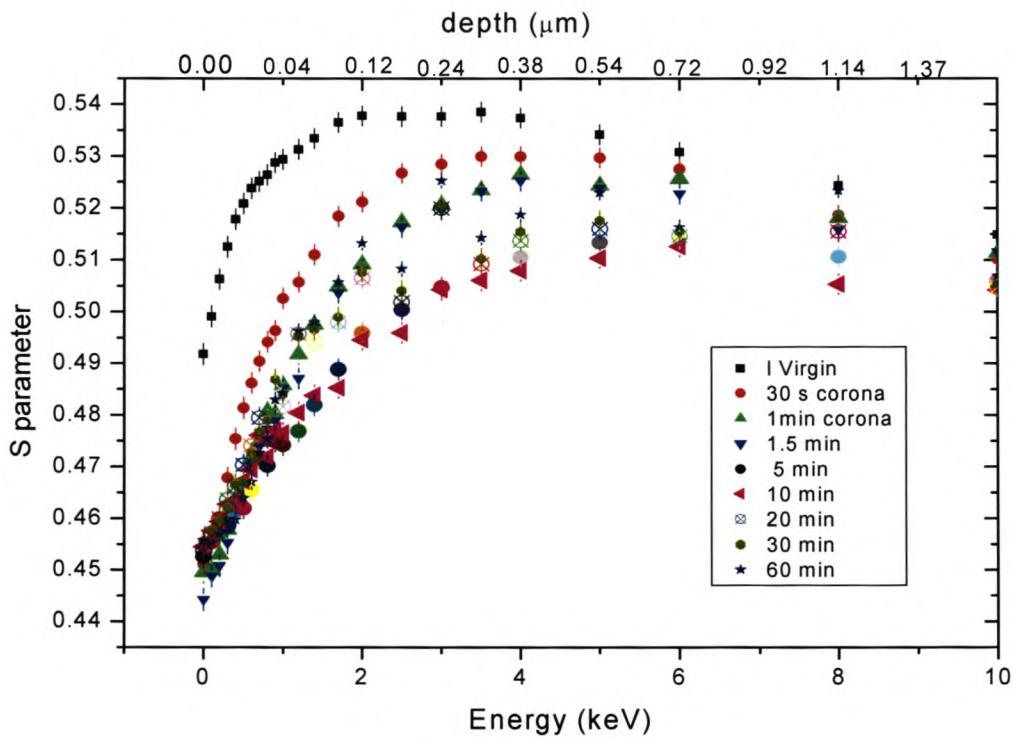

b)

Figure 4.12: a) S parameter profiles of sample I as a function of corona treatment time, b) an enlarged section of Figure a.

Figure 4.12 shows the S parameter as a function of positron incident energy of the virgin sample I (15% silica and 26% ATH) and different corona treatment time of the same sample. The S parameter of this ATH and silica-filled PDMS compound reaches a maximum and then decreases at higher positron implantation energy. This is indicative of a polymer-rich surface layer, as discussed above. This peak maximum is absent in the pure PDMS compounds, as well as in only silica-filled PDMS samples, like sample E.

In a similar fashion to the pure PDMS compounds, sample I (which is a typical commercial formulation) shows a significant change in the S parameter after different corona treatment times. There is a considerable decrease in the S parameter with an increase in corona exposure time up to 5 minutes corona, as shown in Figure 4.12, after which there is an increase in the S parameter with further exposure to corona discharge very near the surface. The initial bump in the curve, as shown in Figure 4.12 a, ascribed to the polymer layer at the surface in the virgin sample, is no longer observed after corona treatment, indicating that the corona treatment of the sample destroyed the polymer "skin" completely.

Figures 4.13 and 4.14 show similar S parameter profiles as a function of corona treatment time for samples E and G, respectively. Comparing Figures 4.13 and 4.14, which represent PDMS containing silica and ATH filler respectively, Figure 4.13 shows that sample E with silica filler does not show a maximum peak near the surface of the virgin material. There is a decrease in S parameter after corona treatment. On the other hand, Figure 4.14, which is that of sample G with ATH filler, shows a maximum peak near the surface and then a dramatic decrease in the S parameter after corona treatment, similar to what was observed for sample I (commercial RTV formulation). As mentioned above, the initial bump in the profile attributed to the polymer skin is seen to disappear on corona treatment.

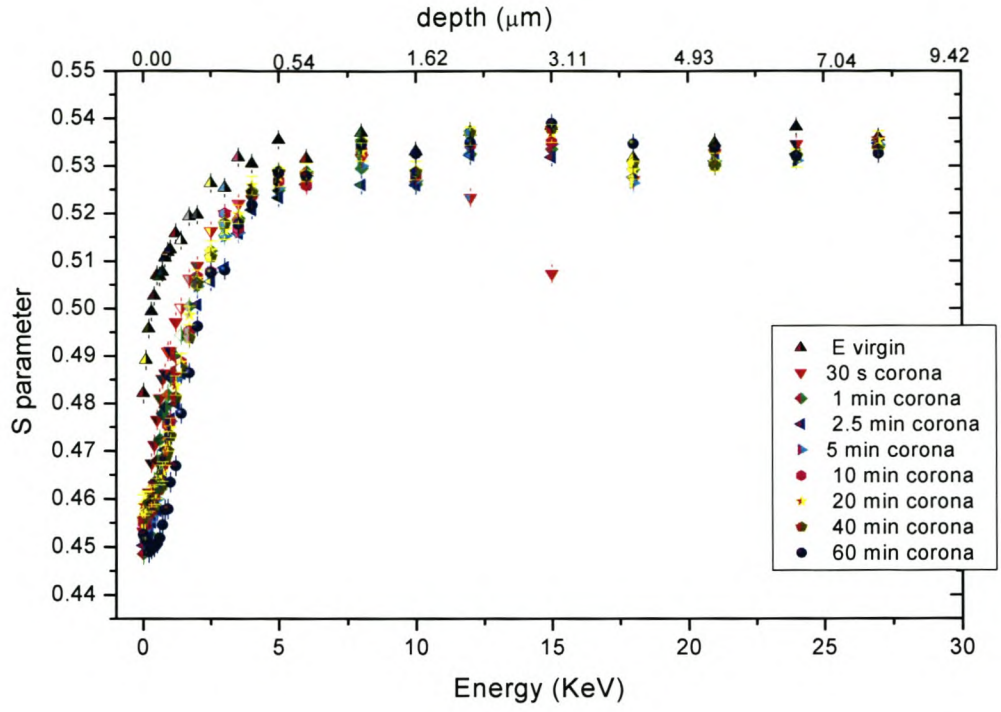

a)

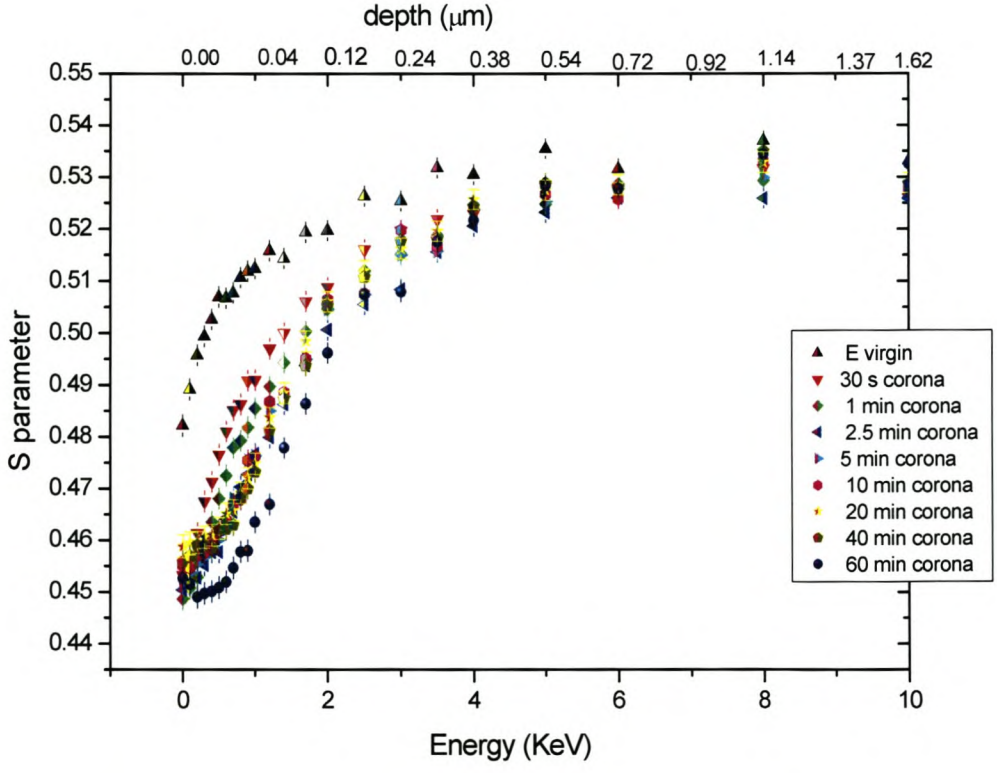

b)

Figure 4.13: a) S parameter profiles of sample E as a function of corona treatment time and b) an enlarged figure a.

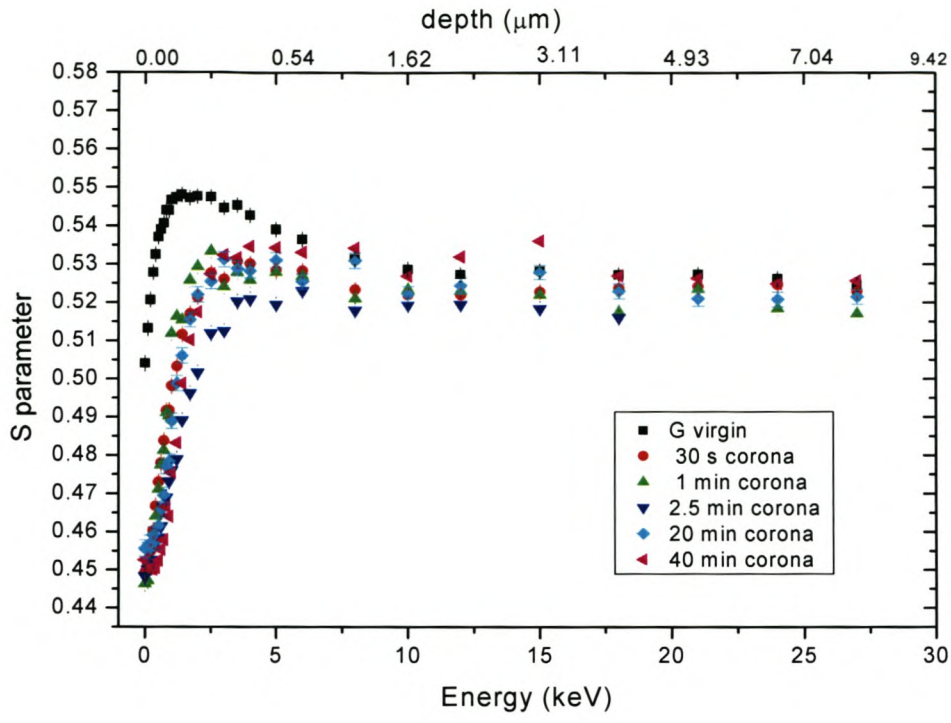

a)

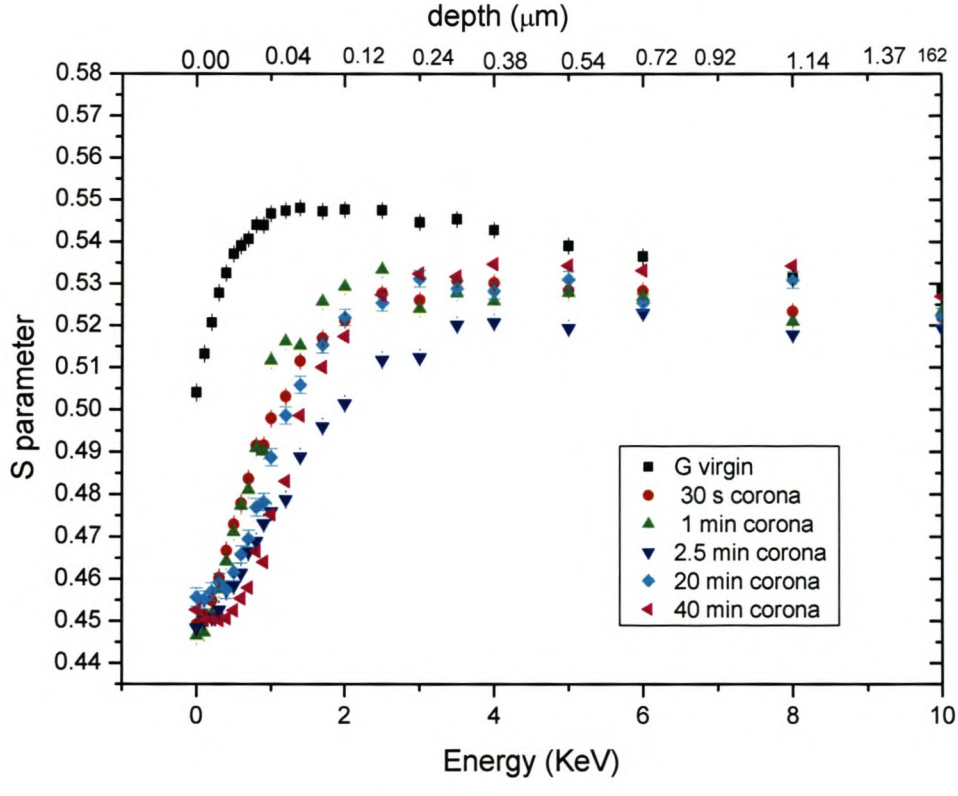

b)

Figure 4.14: a) S parameter profiles of G as a function of corona treatment time and b) an enlarged figure a.

It has been suggested that an inorganic silica-like surface layer of about 10-100 nm thicknesses forms on the polymer surface during exposure of PDMS compounds to corona [26-27]. The results of this study provide additional supporting evidence for the formation of the thin silica-like layer after corona treatment. It is proposed that the observed change in the S parameter as a function of corona treatment time can be explained in terms of the formation of the silica-like layer.

As can be seen from Figures 4.11 to 4.14, at very short treatment times (early stage of degradation) the initial decrease in the S parameter is due to the initial stage of the degradation of the polymer. This initial breakdown may lead to crosslinking and breakdown of the PDMS polymer chain. The increase in the crosslink density is due to the formation of new bonds between the polymer chains. This increase in crosslink density and bond formation is therefore responsible for the decrease in the S parameter. The S parameter decrease after corona treatment can be also interpreted by the overall decrease of free-volume holes. Therefore, the decrease in free-volume holes can be due to the intermolecular crosslinking, which causes a shorter Si-O bond length due to the SiO_x network formed. The decrease in the S parameter may also, at least partially, be due to a chemical effect. During corona treatment there is oxygen enrichment at the surface of the polymer, as determined by EDAX results (see section 4.4.4).

Hillborg [28] suggested that the free volume and mobility of the PDMS exposed to corona decreased considerably due to the formation of silica-like layer in the denser top layer where the silicone atoms bonded to more than two oxygen atoms due to the intermolecular crosslinking and shorter bond lengths. This can be associated with the large drop of the S parameter at the surface.

The results of this study also show that after about 5 minutes corona exposure time there is an increase in the S parameter and levelling off of the S parameter very near the surface. This is most probably due to the PDMS polymer degradation occurring to such an extent that it no longer be considered as a polymer near the surface and the silica-like layer has started to form. After 60 min corona treatment, it is estimated that a silica-like layer of about 40-60 nm has formed at the surface, as indicated by the level or flat portion of the S parameter profiles at the surface.

The change in S parameter with respect to time of exposure to corona can be best expressed by plotting the change in S parameter (- S_O) as a function of treatment time

$$-\Delta S = S_t - S_O \tag{4.1}$$

where S_t is the S parameter after corona treatment time t, and S_O is the S parameter of the virgin sample for each positron implantation depth.

Figure 4.15 shows the magnitude of the change in the S parameter ($-\Delta S$), calculated according to equation 4.1, versus corona treatment time for samples C, I, E and G. (The trend lines drawn in the figures are meant only as a guide).

Values for $-\Delta S$ versus time of selected depths are shown in Figure 4.15 and, as expected, the main effect of the corona treatment is limited to the very near surface region. It can be seen from the figure that there is an initial increase in the change of the S parameter near the surface during early ageing, followed by a decrease with increasing exposure time. Alternately, there is an initial decrease in the S parameter, after which it increases as a function of treatment time. This phenomenon is seen in all the samples, where the initial increase in the change of S parameter is followed by a decrease with increased exposure time. The change in S parameter is seen to be very limited beyond the 1.62 μm thickness.

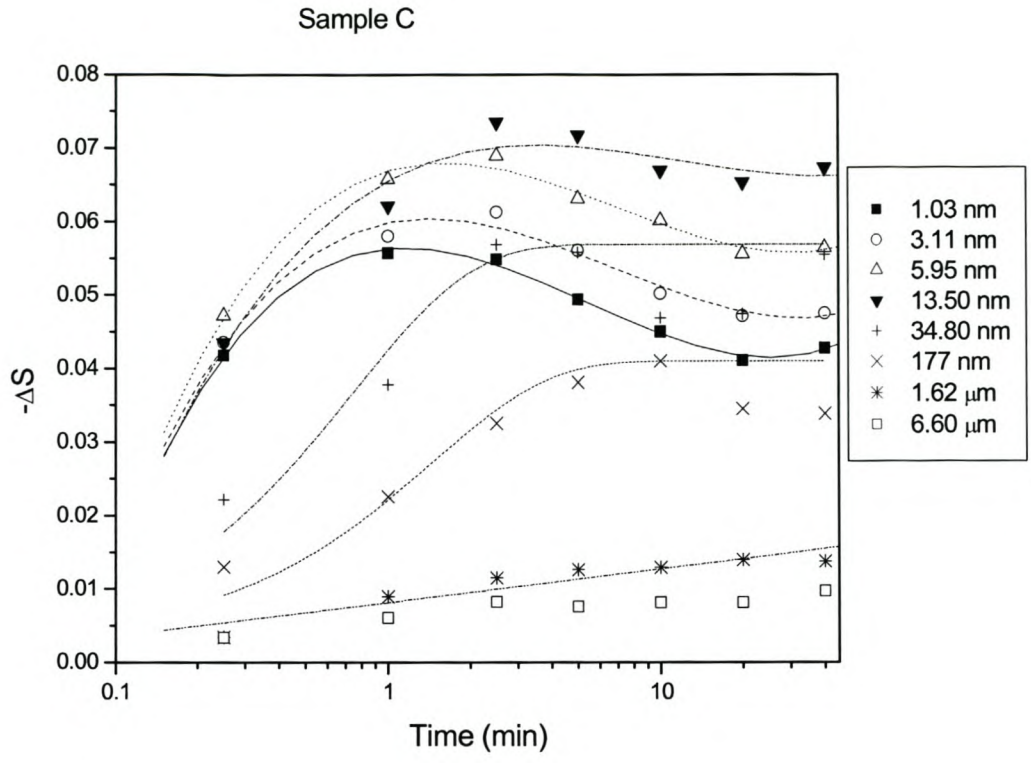

a)

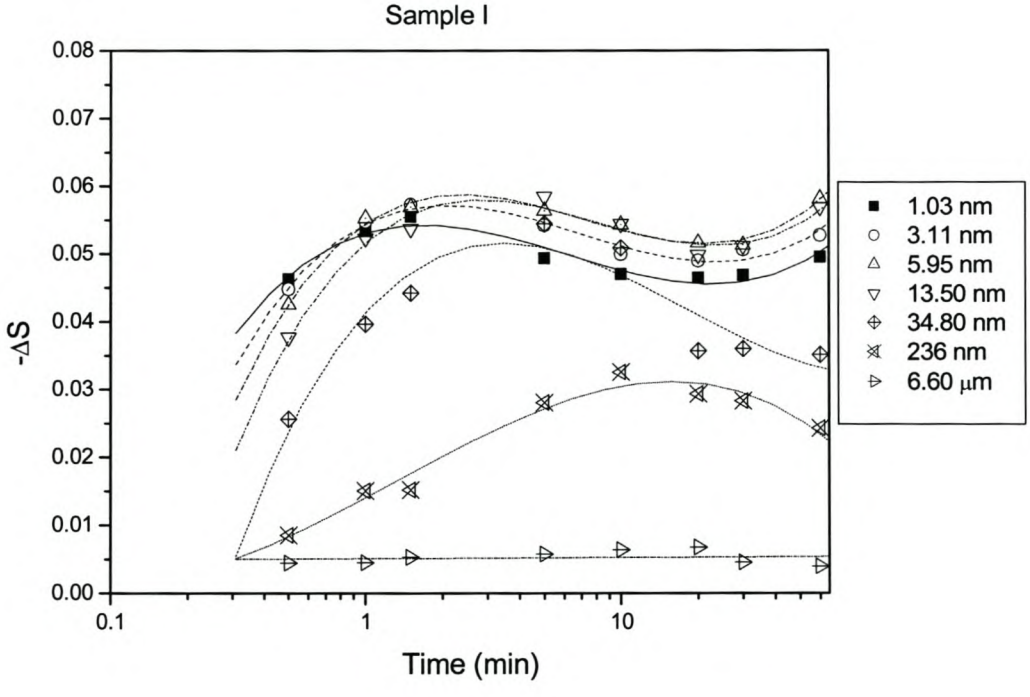

b)

Figure 4.15: Change in the S parameter as a function of corona treatment time for various depths from the surface of the polymer samples a) C, b) I, c) E and d) G. (Trend lines in the figure are drawn only as a guide) (Continued on next page)

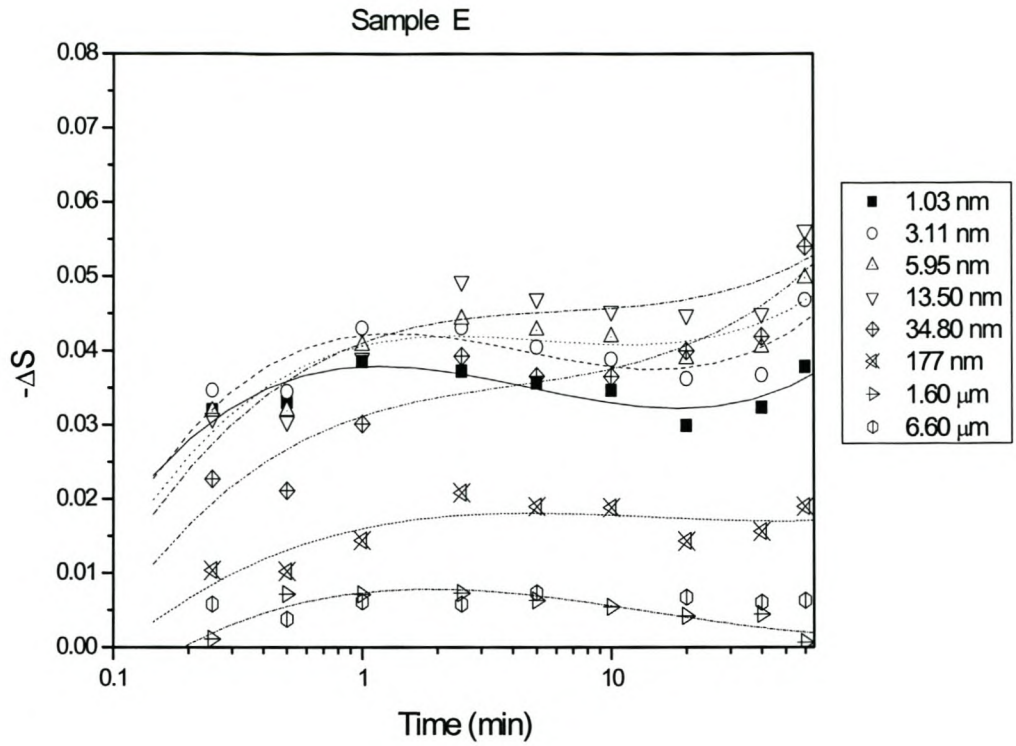

c)

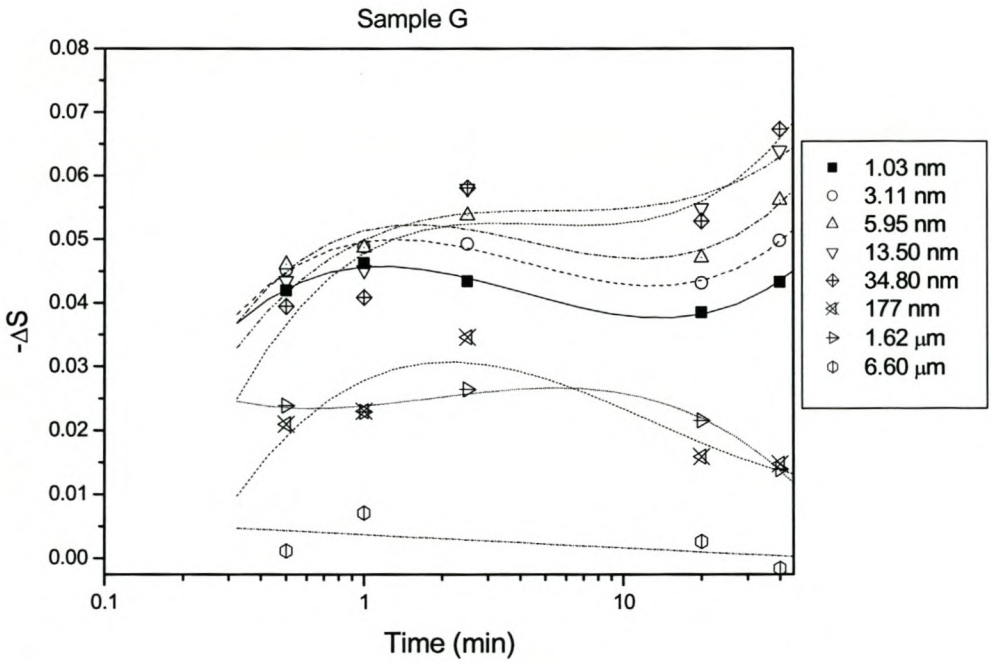

d)

Figure 4.15: Change in the S parameter as a function of corona treatment time for various depths from the surface (Continued from the pervious page)

Figure 4.16 shows the 3-D plot of sample C, showing that the effect of corona treatment is mainly at the surface of the material. The positron beam data in this study contain information on the material changes as a function of both the time of corona treatment as well as depth profiling information. To illustrate the advantages of the positron beam technique in simultaneously determining this information, Figure 4.16 shows a three-dimensional plot of these variables. This plot clearly shows that the main effect of the corona treatment is limited to the very near surface region. The increase and subsequent decrease in the S parameter as a function of treatment time is also illustrated in this type of plot. (It should be noted that the depth scale is not linear in this plot).

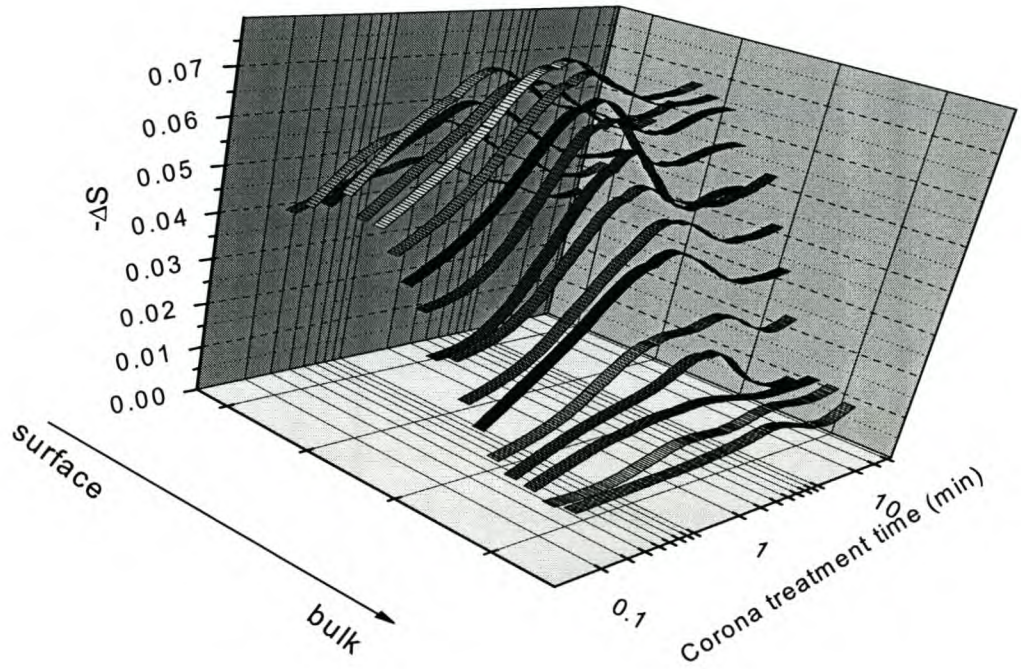

Figure 4.16: The 3-D plot of sample C showing the effects of corona treatment time and depth from the surface on the change in the S parameter ($-\Delta S$).

Figure 4.17 shows the treatment time need to reach the $-\Delta S$ peak maxima in Figure 4.15 a-d as a function of increasing depth of silica-like layer from the surface. Figure 4.17 shows that the peak maxima of $-\Delta S$ versus treatment time curves occur at progressively longer treatment times at greater depths from the surface. All the samples that were measured showed similar trends. The figure clearly indicates that with an increase in corona treatment time, there is an increase of depth, which represents the thickness of the inorganic silica-like layer formed by oxidation the polymer. Looking at

sample C (sample exposure to corona for one min) for example, it is estimated that a silica-like layer of about 0.5 nm thickness is formed, whereas treating the same sample for seven min results in formation of a layer of about 22.5 nm thickness. This thickness can be achieved at shorter treatment time (around 3.5 min) for sample I and a longer treatment time (10.5 min) for sample E. This could probably be due to the ATH filler effect that facilitates the formation of a silica-like layer in samples that contains ATH filler.

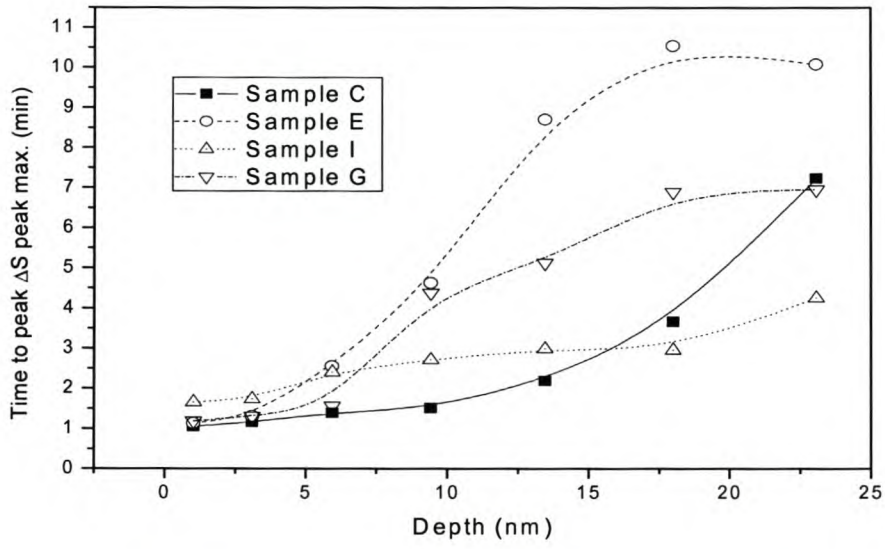

Figure 4.17: Time to peak maximum vs depth silica-like formation (trend line is only meant as a guide).

4.2.2 Positron annihilation lifetime analysis of corona treated pure PDMS sample

Figure 4.18 shows the variation in the otho-positronium lifetime (τ_3) and o-Ps intensity (I_3) as a function of the positron implantation energy for the virgin pure PDMS compound and for the sample at 30 min of corona treatment. It is seen that τ_3 is large near the surface and decreases towards the bulk. A similar result was reported for other polymers [19]. The I_3 value is low near the surface and increases with increasing implantation energy (bulk). τ_3 is a measure of the mean radius of the free volume holes and I_3 is proportional to the number or concentration of free-volume holes. Comparing the virgin sample and the 30 min corona treated sample, the later shows an increase in the τ_3 value and a large decrease in the I_3 value near the surface. This indicates that

the there is a decrease of free-volume and mobility in the aged samples near the surface. This is supporting evidence for the formation of the silica-like degradation layer.

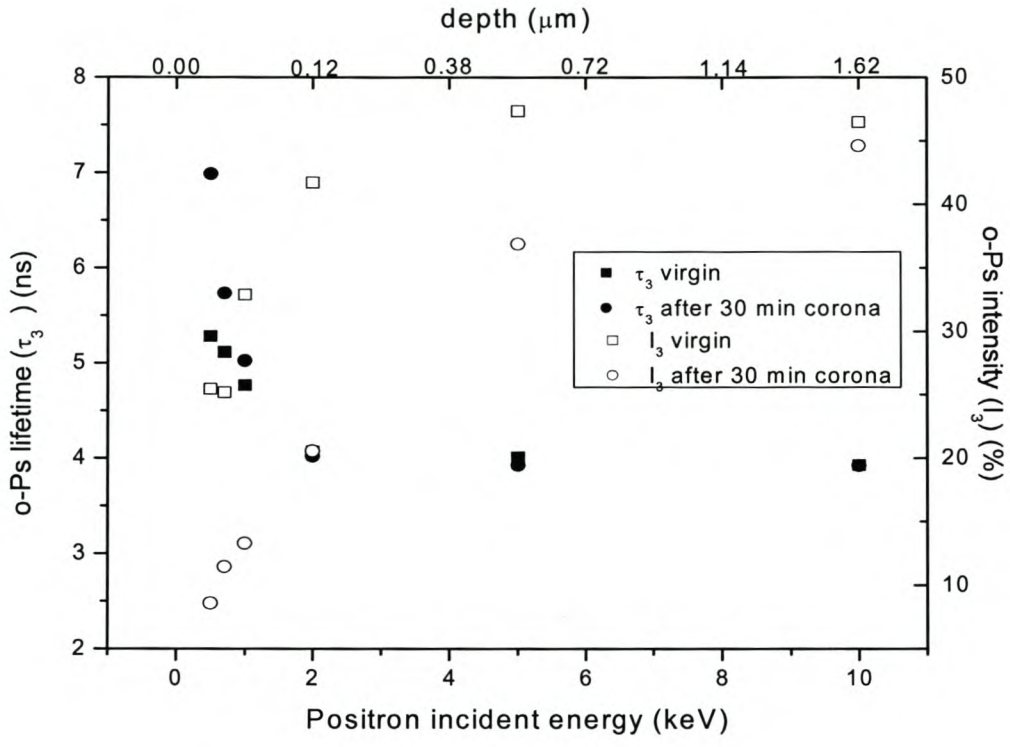

Figure 4.18: o-Ps lifetime (τ_3) and intensity (I_3) for virgin pure PDMS and 30 min corona treated PDMS, as a function of positron incident energy.

The PAL results as a function of positron incident energy (from 0.5 to 10 KeV) of pure PDMS (sample C) of the virgin and 30 min corona aged, are shown in Figure 4.19. There is a decrease in the fraction of o-Ps (ortho-positronium) near the surface (0.5 KeV) after the corona treatment, whereas there is no significant change in the bulk of the polymer. The bulk polymer did not show noticeable change after 30 min corona treatment, unlike in the near surface region. This can be clearly seen from Figure 4.19 c and d.

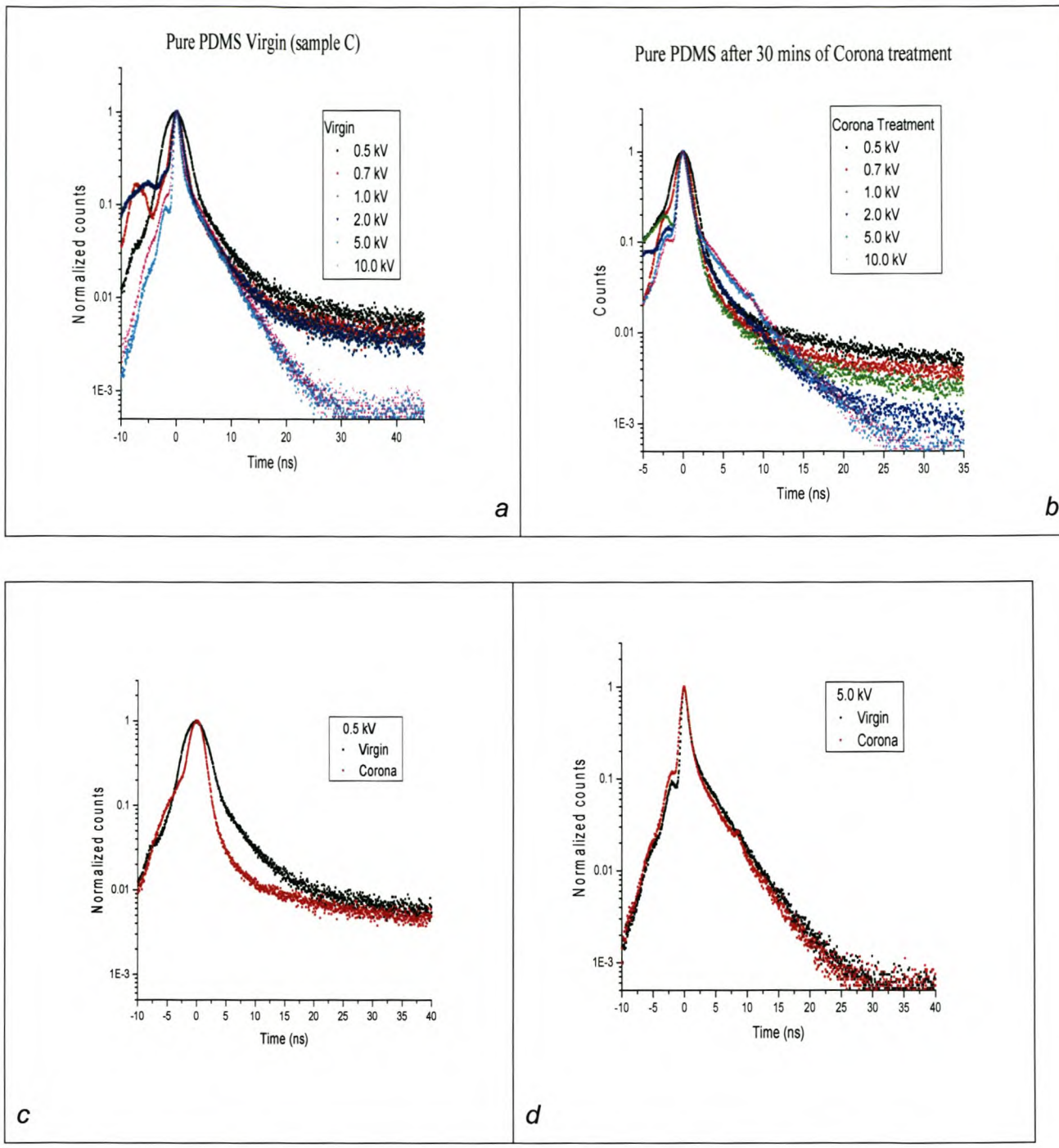

Figure 4.19: Positron lifetime spectra of sample C at different positron implementation energies: a) virgin b) 30 min corona treated c) virgin and 30 min corona treated near surface (0.5 keV) and d) virgin and 30 min corona treated of bulk (5 keV).

4.2.3 Comparison of different corona treatments

As seen from the contact angle measurement (section 4.1.6), the French type corona is very mild when compared to desktop corona type treatment. The S parameters profiles for the French cell-treated samples show a relatively small drop in the S parameter near the surface when compared to the desktop treated samples (see Figure 4.20 a and b).

As a comparison, the 1 min desktop treated sample is included in the figures. Although the change is relatively small, the results show that there is a permanent material change in the sample after corona treatment with the French cell.

Figure 4.20 shows the comparison of both samples C and I after different corona treatment times with French cell corona and desktop corona types. Both samples show a smaller change in the S parameter between the virgin sample and the two hours French cell type corona when compared to the desktop corona treated samples. For the desktop corona treated sample even, the 1 minute treatment time is much more severe than the two hours French type corona treated with regard to the S parameter decrease.

As mentioned, the desktop corona is highly aggressive because the treatment is directly on the sample. The ion bombardment is directed at the surface, unlike the French cell corona which is covered by glass. The desktop corona also has a very high frequency compared to the French cell corona.

The French cell type corona test exposure to the high voltage was done at the University of Stellenbosch one week before the positron tests were done at the University of Missouri, Kansas City. Therefore, any possible material relaxation would have occurred in the week prior to the measurement (as seen in Figure 4.9, where the contact angle recovers after 1500 min). The positron results confirm, however, that even though recovery has occurred, there are permanent, non-reversible changes in the material, as indicated by the decrease in the S parameter.

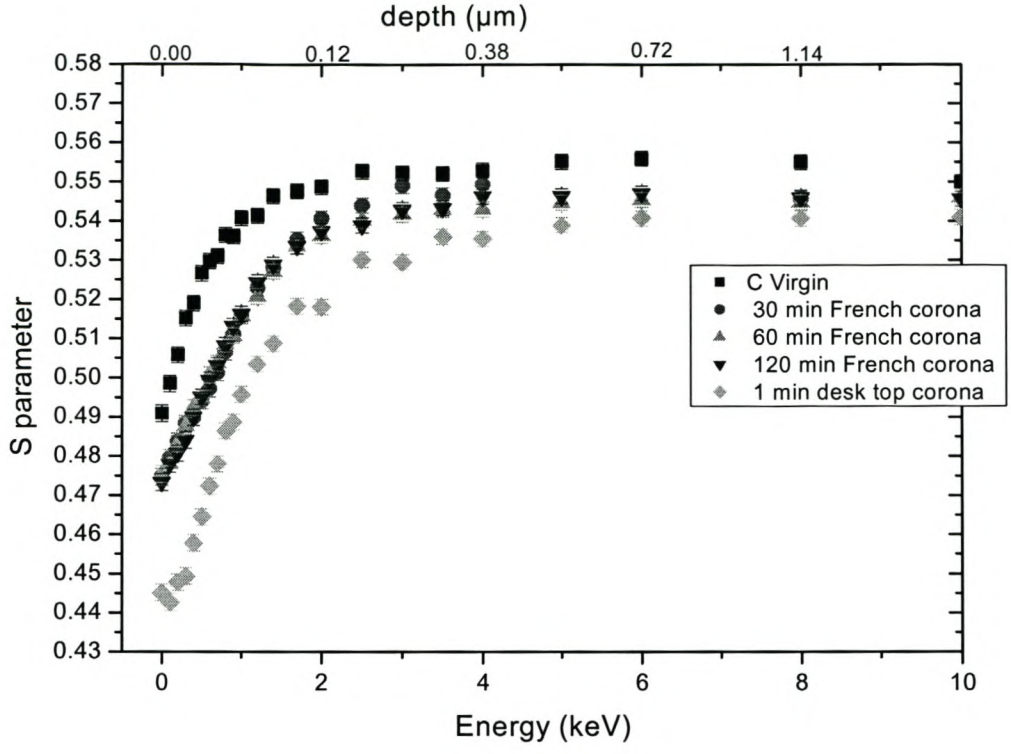

a)

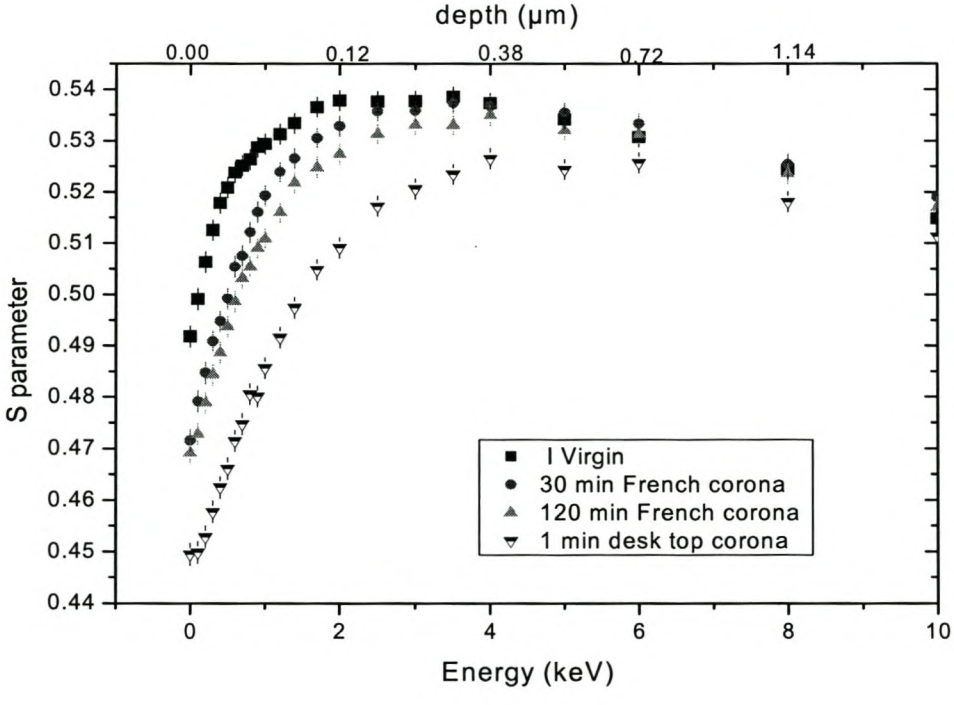

b)

Figure 4.20: Comparison of different types of corona treatment of a) sample C and b) sample I.

4.2.4 Comparison of commercial HTV samples of PDMS

Figure 4.21 shows the S parameter profiles of the commercial HTV samples designated as blue, light grey and dark grey, and sample I. These HTV samples were cut from the sheds of commercial insulators. All the virgin commercial samples (HTV) have similar S parameter profiles. They have a sharp maximum peak, and show a dramatic decrease in the S parameter with higher implantation energy. These profiles are similar to those of the RTV compounds that contain ATH filler. The rapid drop in S parameter of HTV samples at a relatively low depth indicates that the commercial HTV samples have a much thinner "polymer-rich" surface layer compared to the RTV sample I.

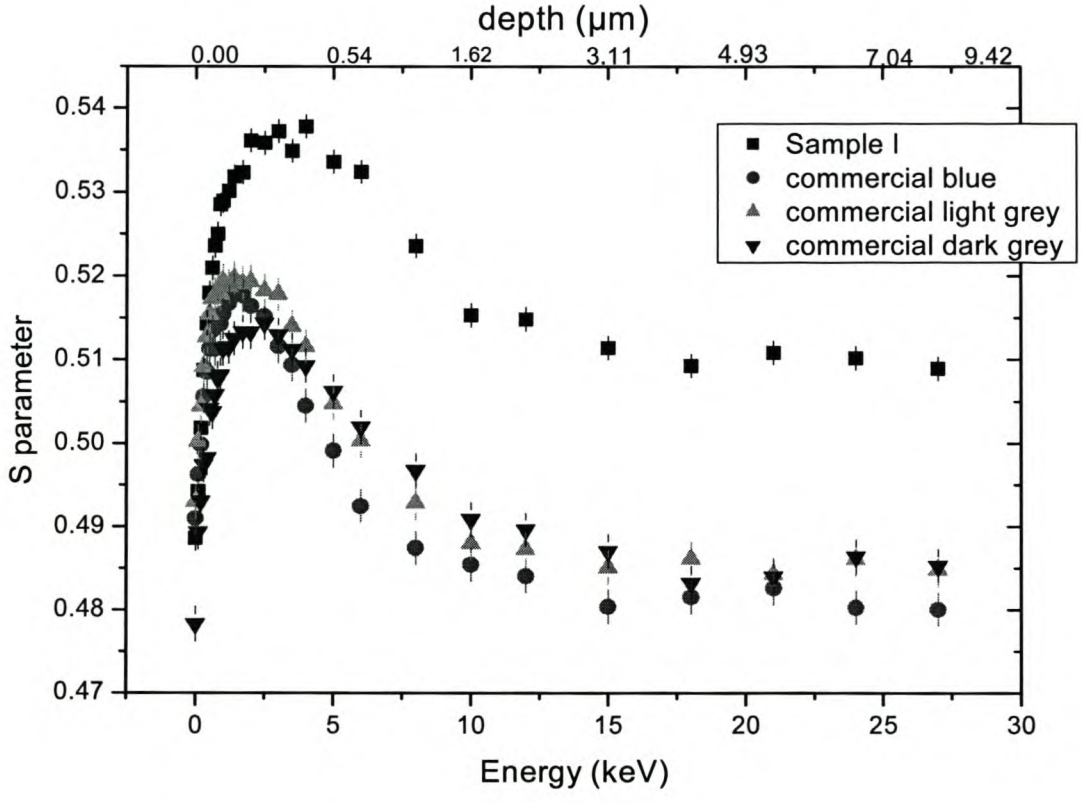

Figure 4.21: S parameter profiles as a function of positron implantation energy for three virgin commercial samples and sample. I

Figure 4.22 shows the S parameter profiles of the commercial blue sample after 30 min corona treatment and after 24 hours relaxation time. This is very little difference between the two curves.

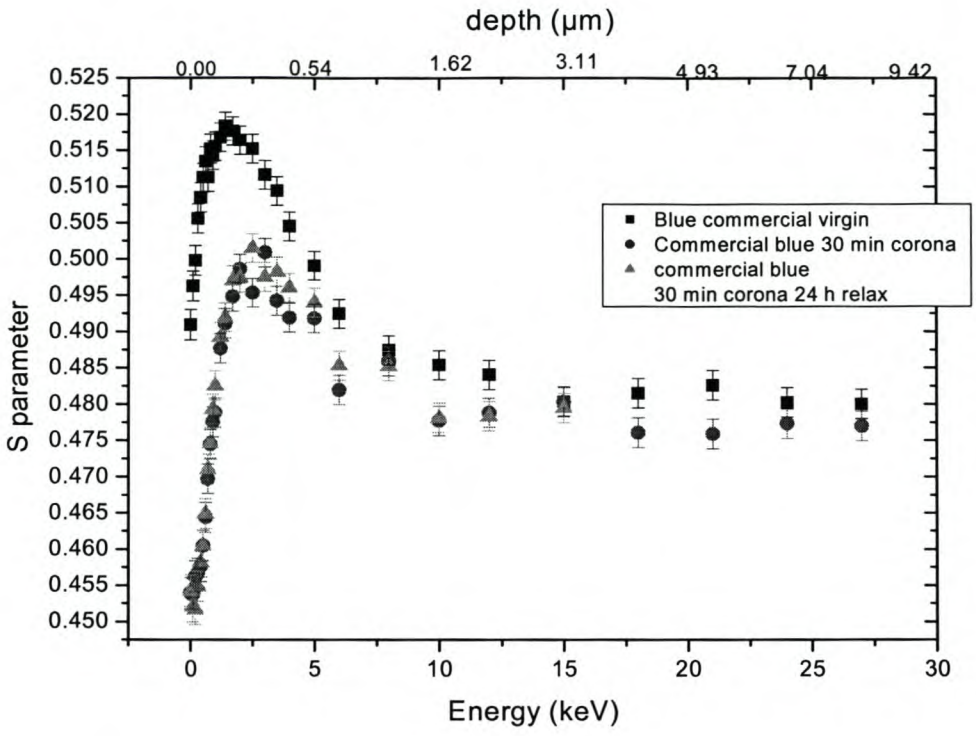

Figure 4.22: S parameter profiles as a function of positron implantation energy of blue commercial sample after 30 min corona and 24 hours relaxation time.

Similarly, Figure 4.23 shows the comparison of the 30 min corona treatment of the commercial dark grey PDMS. It shows a large drop of the S parameter after corona treatment, with very little change with the 30 min corona exposed sample after 24 hours relaxation time near the surfaces.

Once again, there is a large decrease in the S parameter near the surface (low implantation energy) after corona treatment of the commercial HTV compounds. In addition to this, a levelling off the S-parameter is observed in the very near surface region. This is again consistent with the formation of a silica-like layer on the surface after corona treatment.

In the case of the HTV sample, the "leveling off" of the S parameter at the surface occurs to a much lower depth compared to the RTV samples. This can be interpreted as there being a much "thinner" SiO_X layer after corona treatment. This is most probably due to the thinner polymer rich layer in the HTV samples, thus limiting the extent of the depth of polymer degradation. (The estimated silica-like layer of HTV of dark grey sample after 30 min corona is about 15-20 nm).

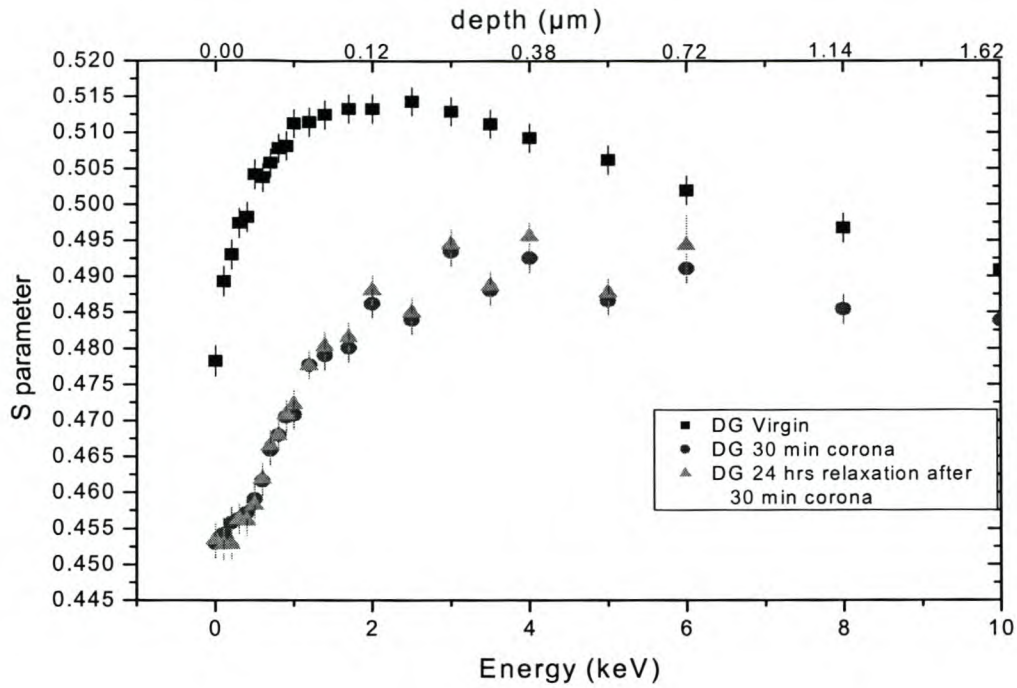

Figure 4.23: S parameter profiles as a function of positron implantation energy of polluted dark grey commercial sample after 30 min corona (DG represents dark grey).

4.2.5 Naturally aged in-service commercial insulators

The naturally aged samples were the commercially formulated insulators that had been aged at the Koeberg insulator pollution test site. Their specifications are given as blue, light grey and dark grey insulators, as mentioned in the previous section. The degradation of the naturally aged materials is influenced by environmental factors such as moisture, light, oxygen, salt, acid, temperature and electrical discharge [17]. This study is carried out to investigate the cleaning effect of the naturally aged samples after one year at the Koeberg test site. Since these samples had been exposed to the natural environment they contained a large amount of pollutants on the surface. Here it is important to bear in mind that, when using surface specific technique to evaluate the ageing of in-service aged materials, the presence of contaminants can interfere with the analyses.

Since the positron beam technique is extremely sensitive to these pollutants it is necessary to develop a method to remove the pollutants before a comparison between the natural and laboratory aged samples can be done by this technique.

Figure 4.24 shows the optical micrographs of the surface of the insulators before and after cleaning, as seen under light microscope.

Low mag before cleaning

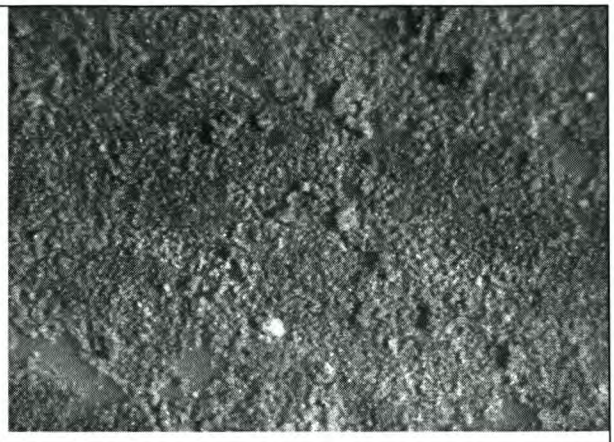

High mag before cleaning

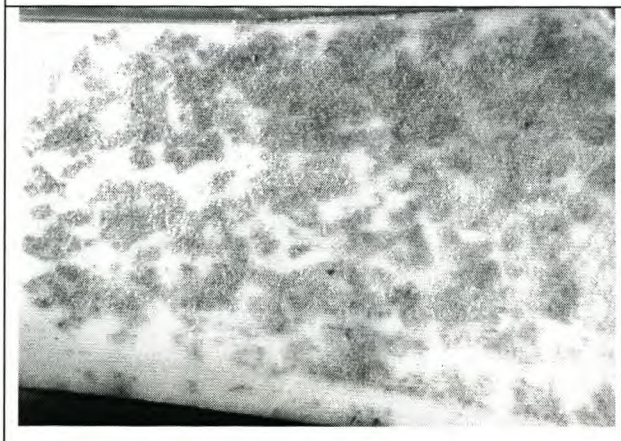

Low Mag US chloroform cleaning

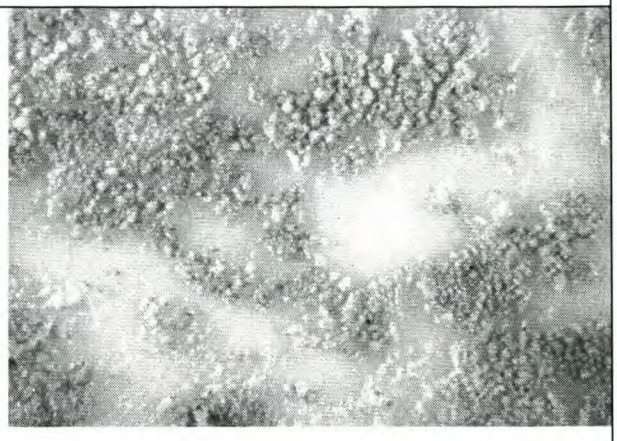

High Mag US chloroform cleaning

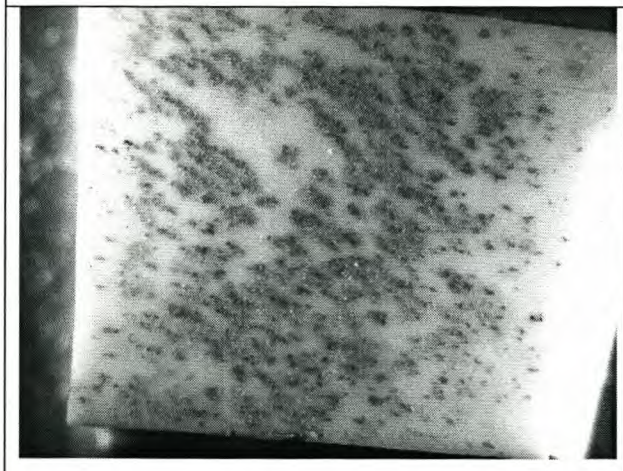

Low mag heat + US chloroform cleaned

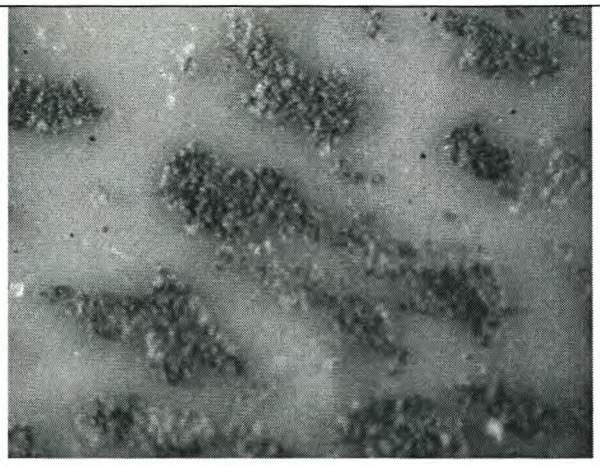

High mag heat + US chloroform cleaned

Figure 4.24: Pictures of the light grey sample aged at Koeberg for one year as seen under a light optical microscope before and after cleaning (mag refers to magnification).

The layers of pollutants which may interfere with the analyses can be clearly seen from the pictures. Before cleaning, the pollutant completely covers the surface of the polymer while, after cleaning, the polymer surface is exposed. A number of different cleaning methods were investigated and the optical micrographs of the results of two cleaning methods are shown. The results show that the cleaning method involving the use of an ultrasonic bath (US) after heating yielded the best removal of the pollutants although some pollutants can still be observed. The cleaning method which includes use of an ultrasonic bath (US) after heating is seems best. (See Figure 4.24).

Figure 4.25 shows the S parameter profile for the commercial blue sample before and after cleaning. The 30 min corona aged sample is included for comparison. The uncleaned commercial blue sample has a lower S parameter, especially at lower implantation energy, and there is no peak maximum as is observed for the virgin sample. The effect of the pollution layer is clearly evident.

Figure 4.25 b shows the effect of cleaning of the polluted blue sample. The S parameter of the polluted sample is far below that of the virgin sample and the samples cleaned with ultrasonic bath after heating to $200\,^{0}C$ are observed to have a slightly higher S parameter than the polluted sample. The top and bottom cleaned surfaces of the polluted blue sample have almost the same S parameters near the surface. It is further noted that even after cleaning the sample, the S parameter is relatively low at the surface. The cleaned samples have a similar S parameter profile to that of the laboratory treated corona sample. This may indicate that the naturally aged samples have undergone similar material changes as occurred during laboratory ageing.

Unfortunately it is extremely difficult to know if the decrease in S parameter is in fact due to the material degradation or due to the inadequate removal of the pollution layer. In these samples there is also the possibility of removal of the material degradation product (eg. the silica-like layer) during the cleaning process. Nevertheless permanent and significant material changes in these naturally aged insulator materials are observed by the positron beam technique.

The effects and types of surface cleaning of the naturally aged sample will have to be further investigated before a meaningful comparison between the naturally and laboratory aged samples can be made.

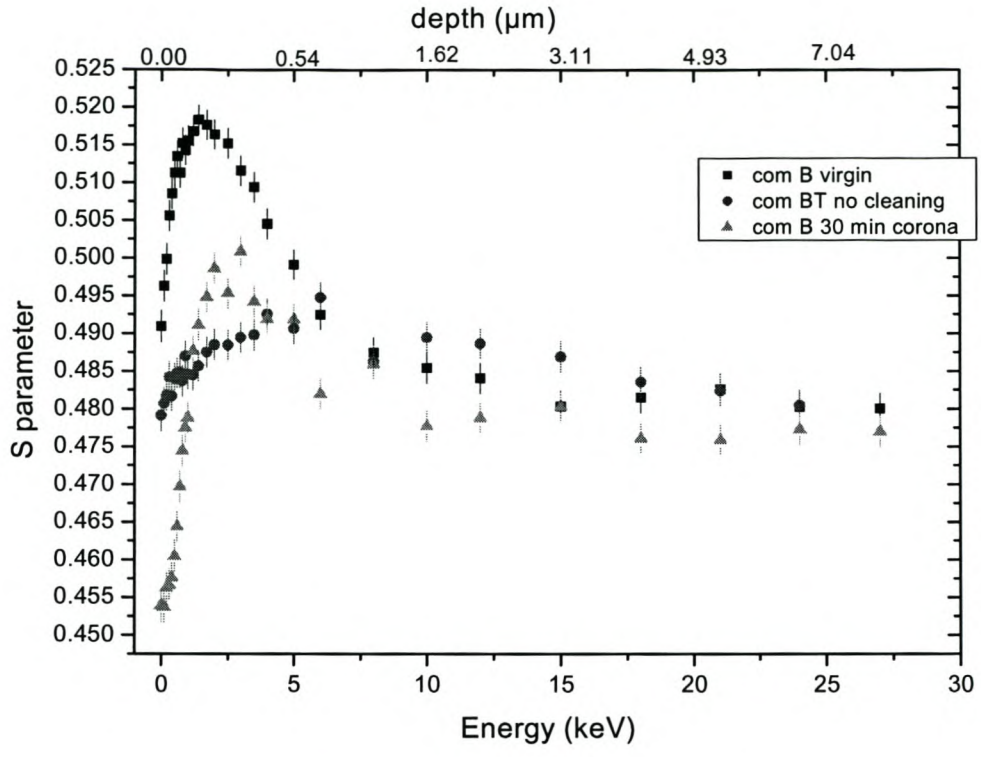

a)

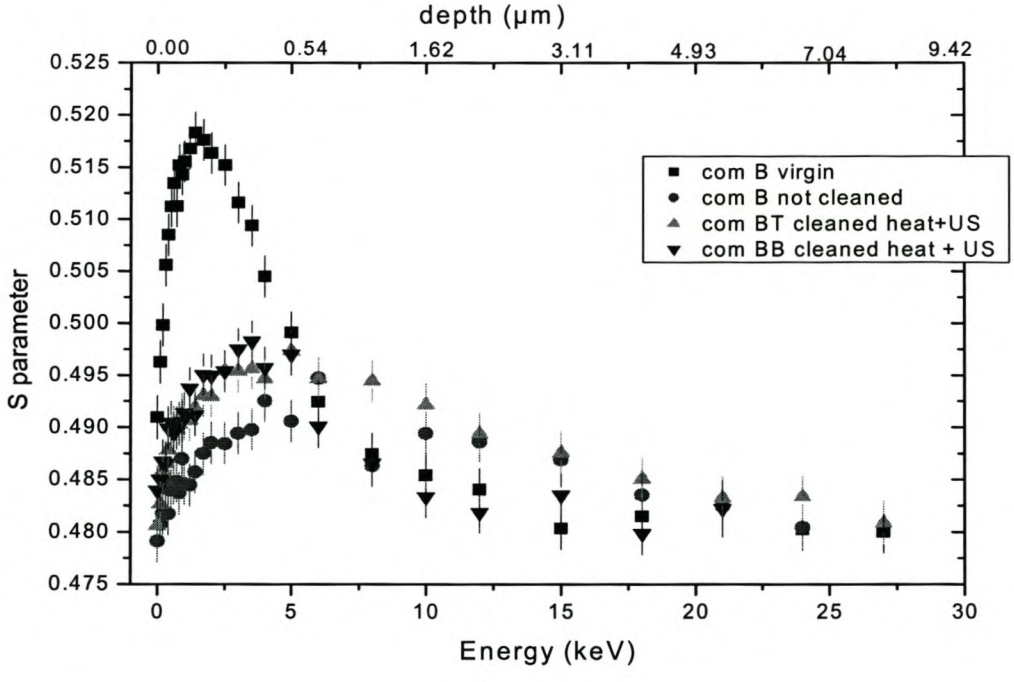

b)

Figure 4.25: S parameter profile as a function of implantation energy of a) polluted blue commercial sample and 30 min corona treated and b) cleaned naturally aged samples (Com B is commercial blue, BT is blue top and BB is blue bottom)

4.3 Analysis by atomic force microscopy

4.3.1 Surface hardness and hydrophobicity

The surface hardness and the hydrophilicity of PDMS samples as measured by AFM force-distance curves show significant changes after corona treatment. Both the properties of hardness and surface hydrophilicity can be monitored simultaneously by means of force-distance measurements.

Figure 4.26 shows force-distance curves of pure PDMS after 5 minutes corona treatment. For better readability, only the curves recorded at 24, 30, 55 and 95 minutes after corona treatment are displayed. The decreasing area (indication of adhesive force) between the approaching and the retracting curve in Figure 4.26 shows that the sample changes from a quite hydrophilic state, caused by the corona treatment, back into its original hydrophobic state with an increase in the resting time. The gap after 24 min recovery time is much larger than the gap after 95 min, which clearly shows that the hydrophilic surface (due to corona exposure) gradually changes to a hydrophobic surface with increasing time after treatment.

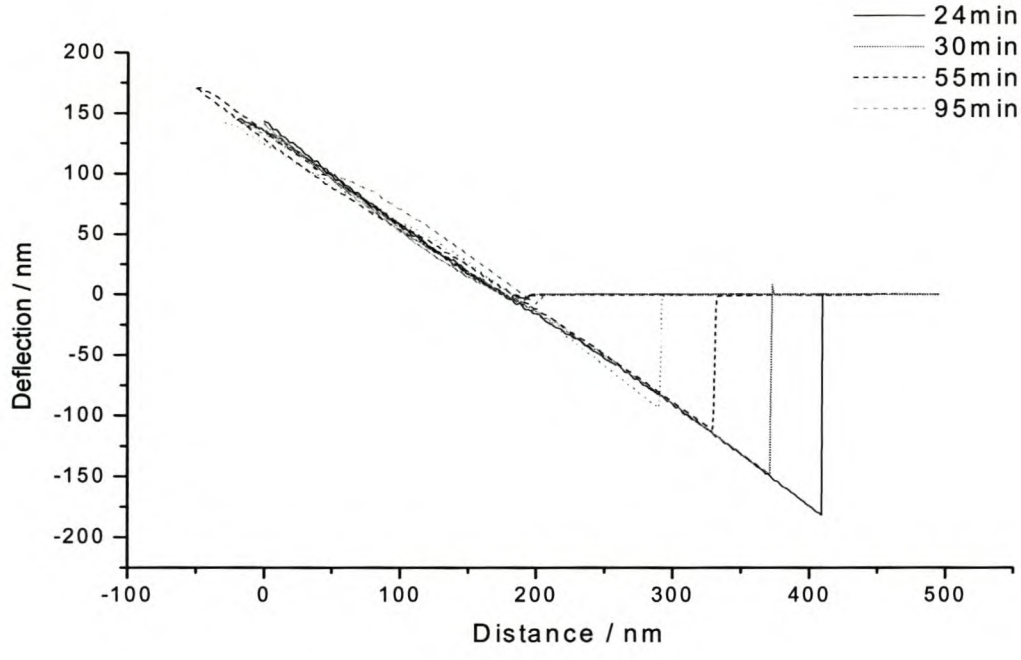

Figure 4.26: Force-distance curves of sample C at 24, 30, 55 and 95 minutes after a corona treatment for 5 min.

Figure 4.27 is an enlargement of the approaching curves in Figure 4.26, and displays the different gradients of the curves. These different gradients relate directly to the surface hardness of the sample. Here again, only four curves are plotted for simplicity. As mentioned in section 3.3.2.1, the larger the gradient is, the higher the hardness of the material. Figure 4.27 shows that at the shorter recovery time of 24 minutes the gradient is steeper than at the longer recovery time of 95 minutes which has a gentler slope. In other words, after a shorter recovery time (24 min) the surface is harder. The gradient as a function of recovery time is shown in Figure 4.27 b, and higher gradient is observed at shorter recovery time and decrease with increase resting time after corona treatment.

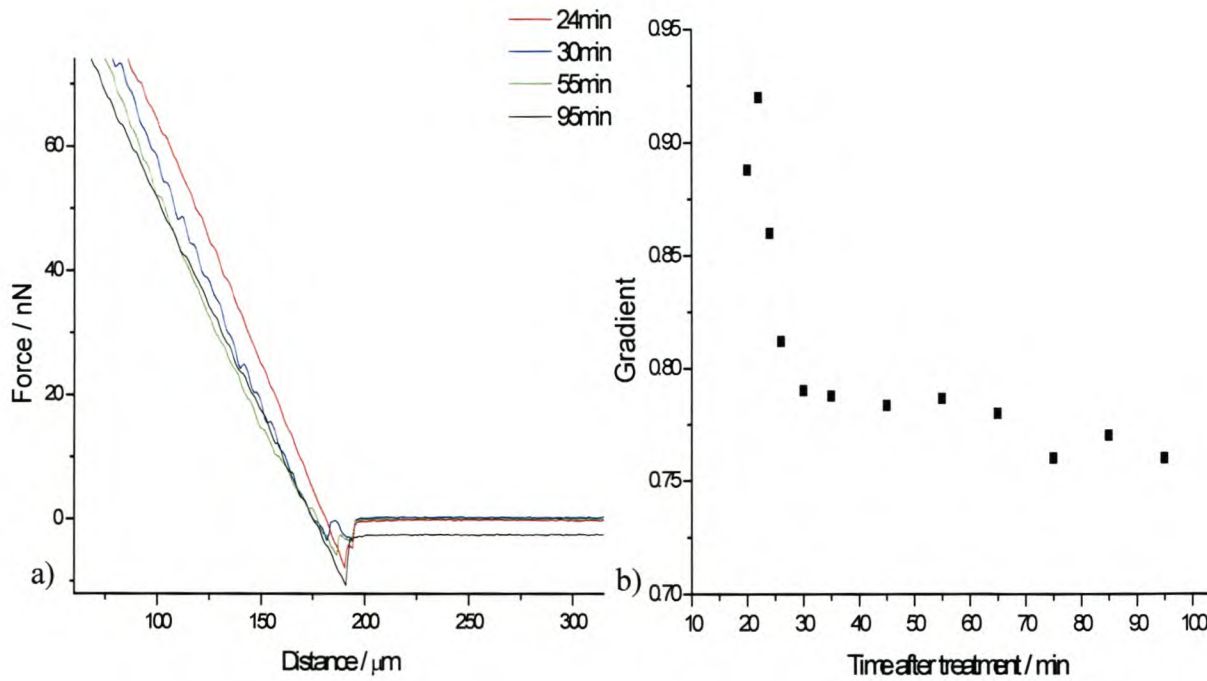

Figure 4.27: a) Magnified approaching curves from Figure 4.26 of sample C. b) Surface hardness (gradient) measured over a period of 100 minutes

Both figures a and b illustrate the hydrophobicity recovery of the sample with time. The corona treatment of PDMS induces a hardening of the surface coupled with a loss of the hydrophobicity. This could be due to the formation of the thin silica-like layer, observed in the positron data (section 4.2.1), which is responsible for the hardening of the surface. Both the hardness and hydrophilicity effects are diminished with time and the polymer recovers. This diminishing may be due to the diffusion of LMW from the bulk to

the surface, which subsequently covers the thin silica-like layer responsible for the loss of hydrophobicity. Though the thin silica-like layer formed during the corona discharge exist below the diffused LMW, the cantilever of AFM senses the physical properties like adhesion, stiffness, elasticity etc at the surface and depending on the elasticity also that of the underlying layers. In this case the changes on the recovery indicate that predominantly probing the properties of the surface layer.

Complete AFM analyses, as described above, were performed on samples C, E, I and G which have different formulations (see Table 3.1). In most cases the hydrophilicity and the surfaces hardness of the samples increased directly after corona treatment and recovered with time. These studies were done after 1, 5, 10 and 30 minutes of corona treatment for each different sample. Force-distance curves were recorded in well-defined time steps directly after treatment over a period of 100 minutes.

Figures 4.28 and 4.29 display the maximum values of the adhesive force and the surface hardness reached by the different polymers as a function of the time of the corona treatment.

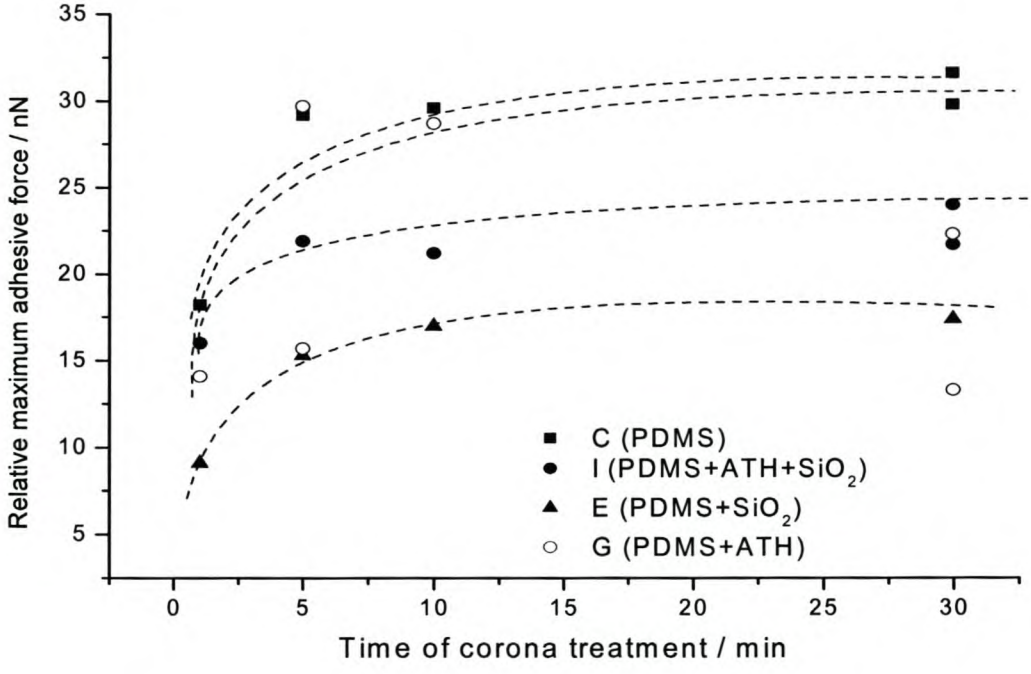

Figure 4.28: Maximum adhesive force (hydrophilicity) as a function of corona treatment time.

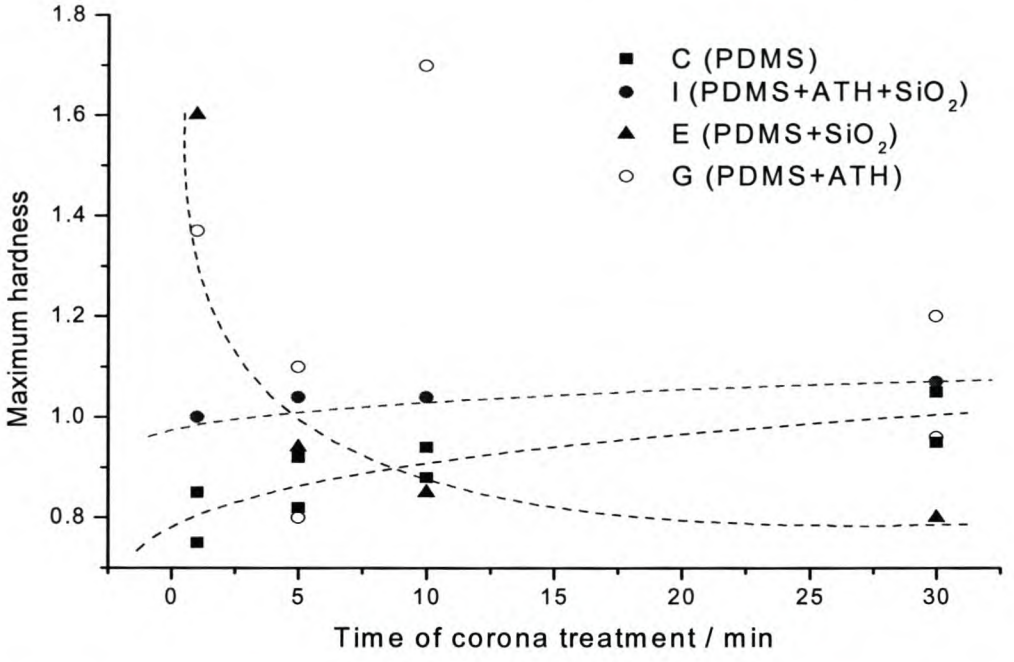

Figure 4.29: Maximum surface hardness as a function of corona treatment time.

For all samples (except G) the maximum adhesive force (hydrophilicity) follows a logarithmic curve with increasing treatment time and reaches a saturation value after which a longer corona treatment does not result in a higher hydrophilicity of the sample (see Figure 4.28). Only the curve of sample G, which consists of PDMS and ATH, a hard filler particle, does not follow this logarithmic curve. The values are scattered widely and are irreproducible. One possible explanation for the shape of this curve is that the AFM measures locally on one spot. Depending on the location of the tip the measured values could correspond to pure PDMS, which becomes more hydrophilic after corona treatment, or to the ATH, which is not affected by the corona treatment. Relatively sample C has the highest maximum adhesive force in all the treatment times than the other samples.

The same applies to the hardness measurements. The maximum surface hardness increases with increasing treatment time for sample C and I, as shown in Figure 4.29. As expected, comparing the hardness of samples C and I, sample I is harder than C due to the presence of filler in sample I. The hardness for sample G are inconsistent and are scattered, some following the pure PDMS curve and some values indicating a larger hardness. This could once again be explained by the fact that the ATH filler particles exposed to the surface after corona treatment and depending on the measurement location, the force distance curves yield the hardness of PDMS or of the

hard filler particles to be discussed later. Sample E (PDMS +SiO_2) shows an altogether different trend. The maximum hardness decreases exponentially with increasing treatment time as seen in Figure 4.29.

4.3.2 Speed of hydrophobicity recovery after different doses of corona treatment

Figure 4.30 shows the adhesive force determined from the AFM distance curve as a function of recovery time after 30 min corona treatment for sample C (pure RTV PDMS). The figure displays the adhesive force calculated from the "pull-off" force of the force-distance curves between the probe and the sample. It can clearly be seen that the adhesive force between the probe and the sample decreases with increasing of time after corona treatment. This is caused by the hydrophobicity recovery of the PDMS. The decrease in the adhesive force is much greater in the first 30 minutes, which implies that the hydrophobicity recovery in the few minutes after treatment is much faster. This result is consistent with the SCA measurements, which also indicate the faster recovery in the first 30 min after treatment.

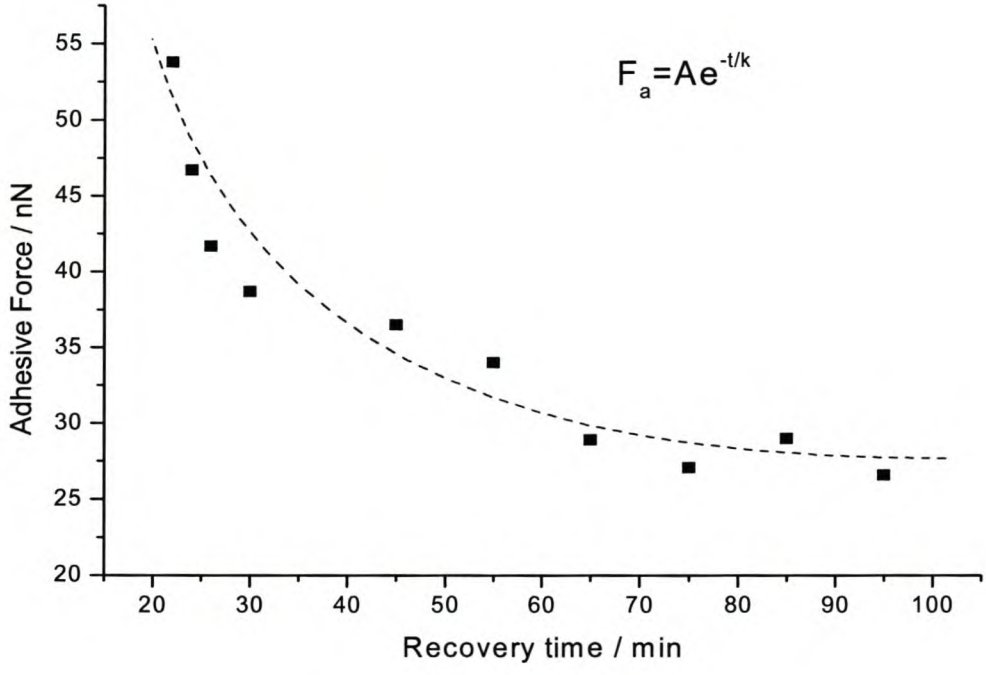

Figure 4.30: Decrease in adhesive force (increase hydrophobicity) of the pure PDMS compound with time after corona treatment.

The rate of hydrophobicity recovery in Figure 4.31 was determined from the slopes of

AFM force-distance curves constructed by fitting the points with an exponential decay:

$$F_a = Ae^{-t/k} \qquad (4.2)$$

where F_a is the adhesive force in nN, A is a constant, t is the recovery time (time after treatment when the measurement was done) and k is the rate of recovery (curvature). A larger value of k indicates a faster recovery of hydrophobicity.

Figure 4.31 shows the rate of hydrophobicity recovery (k) calculated by fitting the points with equation (4.2) to the adhesion recovery time curves for samples C, I, E and G as a function of different corona treatment times.

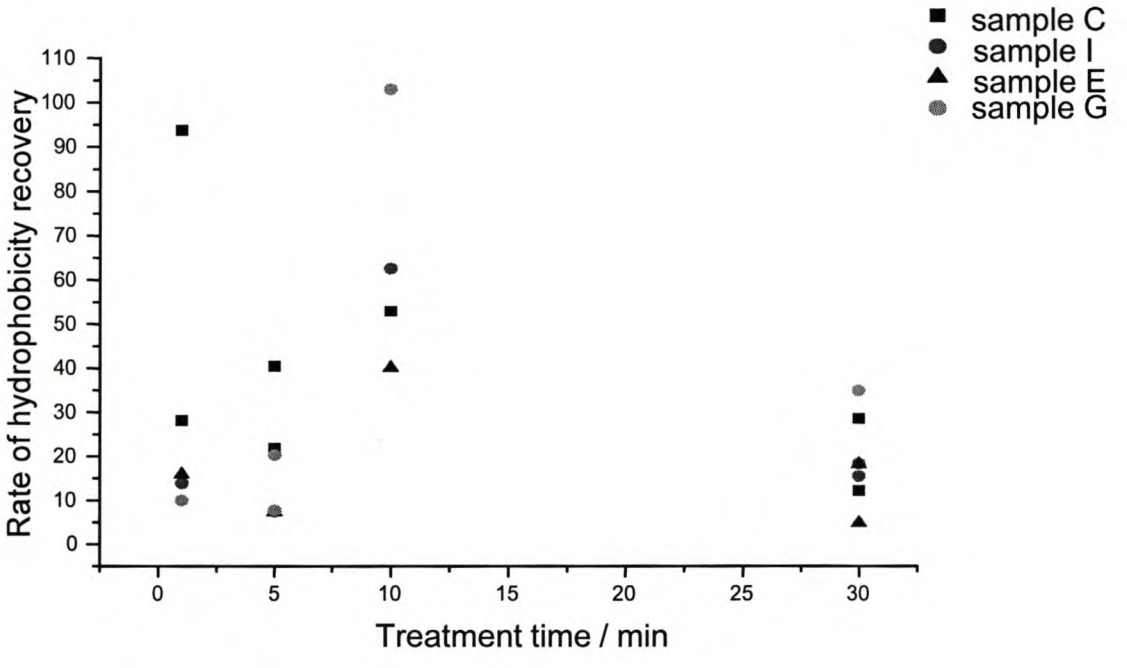

Figure 4.31: Hydrophobicity recoveries of different RTV samples with different formulations after different corona treatment times as determined by AFM.

As shown from the results of static contact angle measurement in Figure 4.6 a and b, the 10 min corona treated samples recover faster than the 5 min and 30 min samples do. Similar results can be observed from the AFM results in Figure 4.31, where the 10 min corona treated samples of all formulations showed a faster recovery than the 30 and 5 min corona treated samples did. As explained earlier (section 4.1.4) the low

intensity and shorter exposure time of 10 min activates the production of low molar mass PDMS oligomers which may migrate to the surface, unhindered by a very thick SiO_X layer (as is the case after 30 min), and increase the recovery rate.

To verify the fact that the surfaces of sample E and G are modified after corona treatment, phase images were recorded with the AFM. Atomic force microscope deflections also depend on the relative harness at the surface. In this mode it is possible to image material contrasts which cannot be seen otherwise. Figure 4.32 shows sample G, corona treated for 30 minutes. AFM images were taken at (a) 30 minutes and (b) 24 hours after treatment. It can be clearly seen that the hard filler particles (light areas) appear exposed at the surface of the soft PDMS matrix (darker areas) after corona treatment as shown in (a). However, in the image taken after 24 hours most of the lighter spots are not seen. This clearly indicates that the diffused LMW PDMS oils migrate from the bulk to the surface and cover the lighter spots, which represent of the filler. This image also supports the explanation where diffusion of low molecular weight silicone oils from the bulk to the surface is most probably responsible for the fast recovery of hydrophobicity in PDMS insulators.

The image also offers an explanation for the large scatter observed in the hardness and adhesion curves for sample G. Clearly different results would be obtained if the cantilever tip was resting on the harder exposed filler (light area) or softer darker areas.

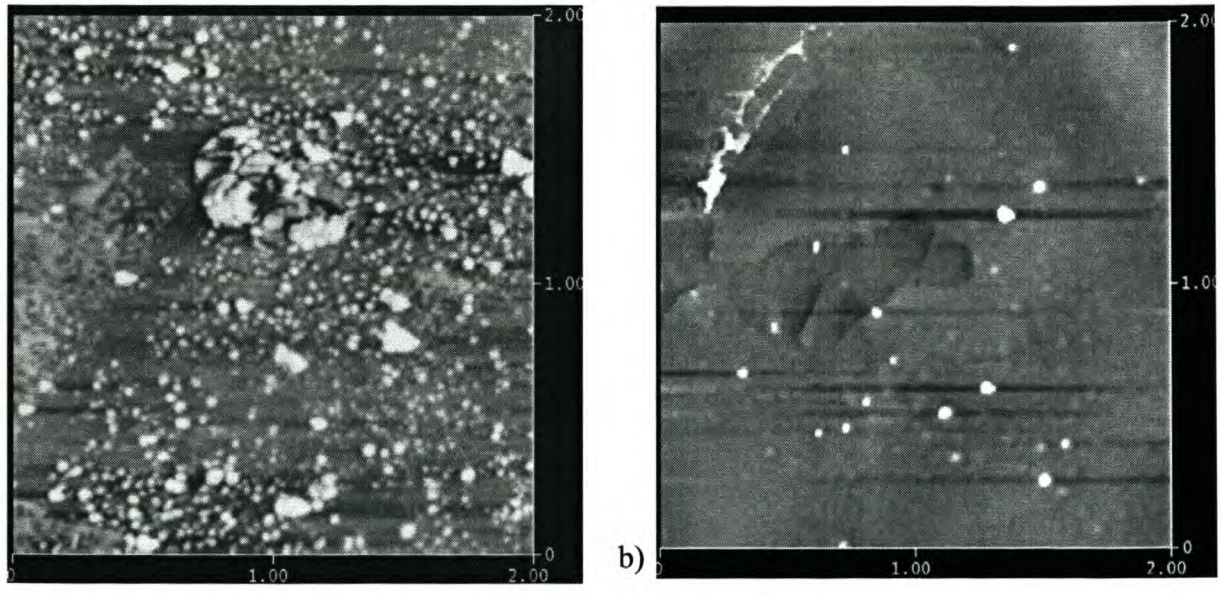

Figure 4.32: AFM image of Sample G, corona treated for 30 minutes: a) 30 minutes after treatment and b) 24 hours after treatment.

Figure 4.33 shows sample E, corona treated for 30 minutes. An AFM phase image recorded 30 minutes after treatment shows dark spots on the surface, representing a softer material.

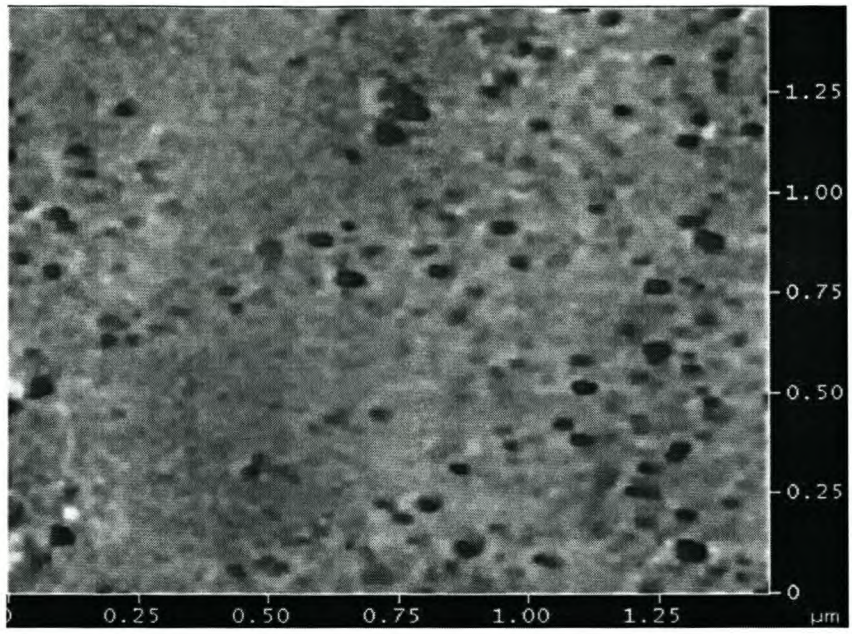

Figure 4.33: AFM image of sample E (PDMS + SiO_2) corona treated for 30 minutes, 30 minutes after treatment.

Figure 4.34 also shows sample I, after 30 min corona treatment.

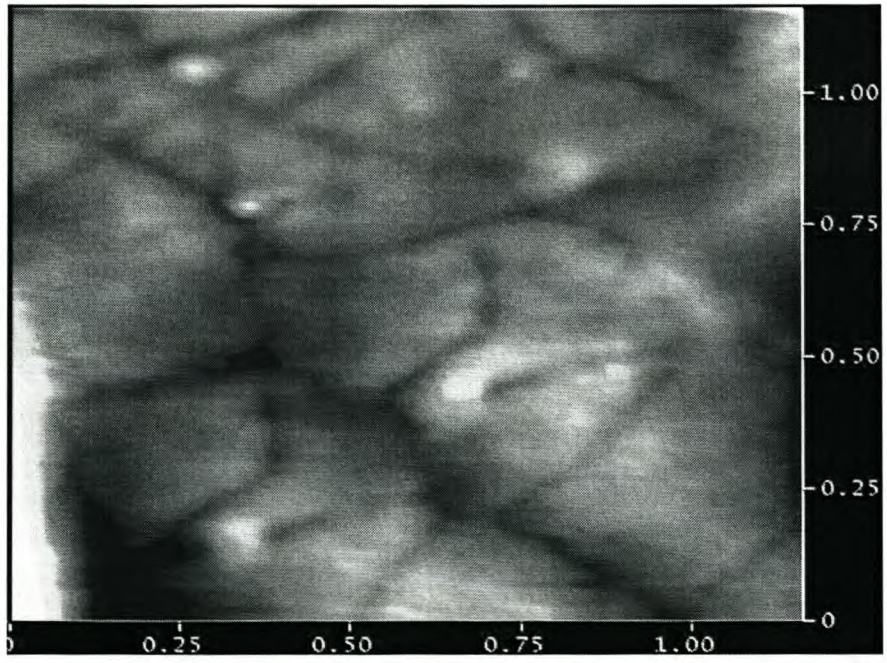

Figure 4.34: Topographic image of AFM, 30 min corona treated sample I after 32 min

The topographic image taken after 32 min corona treatment shows that the corona exposed sample has a cracked surface. This supports to the observation of a brittle SiO_X layer formed upon degradation of the polymer.

4.4 Scanning electron microscopic results

Exposure to excessive corona and surface discharge may cause damage to the PDMS material both chemically and physically [2]. SEM results showed that those PDMS samples that were not exposed to corona discharge exhibited a completely smooth surface structure, whereas samples exposed to a certain dose of corona had different degrees of cracks and increase roughness depending on their formulation.

4.4.1 Formation of cracks at the surfaces

Figure 4.35 a, shows the SEM micrographs of the virgin pure PDMS. The surface is smooth without any signs of cracks or roughness. Figure 4.35 b shows the micrograph of the 30 min desk top corona exposed sample C. It can be clearly seen that there is cracked, brittle surface after corona treatment. Although cracks are formed after 30 min of corona treatment in sample C, these cracks are not deep and broad. Figure 4.35 also shows the micrographs of sample G, where c and d in the figure represent the virgin and 30 min corona treated sample G respectively. Once again the micrograph of the virgin sample was smooth whereas after 30 min of corona treatment, the sample had wider cracks on the surface. This crack formation was observed in all samples. This is, once again, an indication of the degradation of the material. The SEM micrographs are representative and all the un-aged samples have similar smooth surfaces, but different degrees of cracks and roughness after corona treatment.

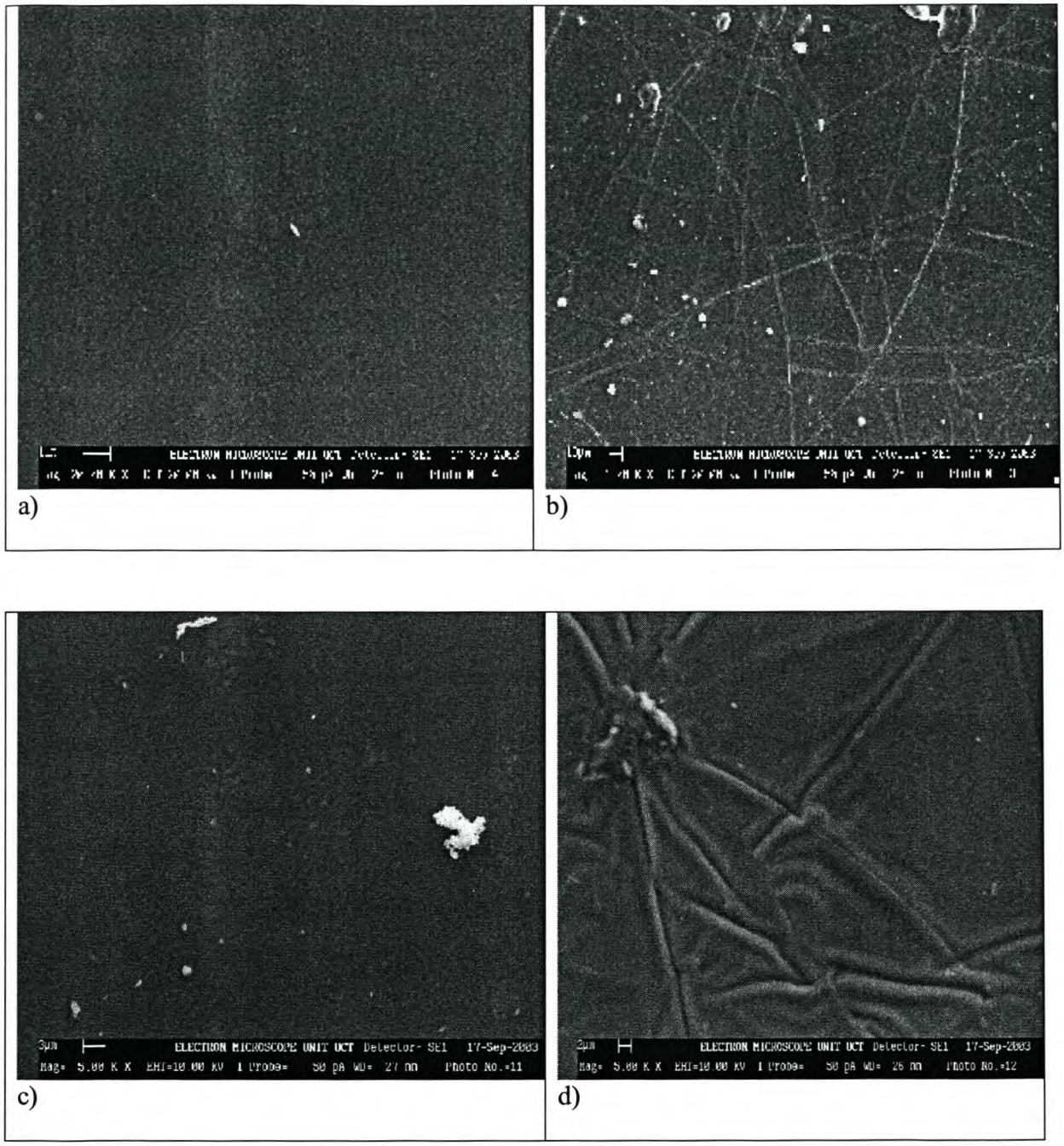

Figure 4.35: SEM result of sample C: virgin (a) and after 30 min corona treatment (b) and sample G, (c) virgin and (d) after 30 min corona treatment.

Figure 4.36 shows the SEM micrographs of a number of samples after 30 mins of corona treatment.

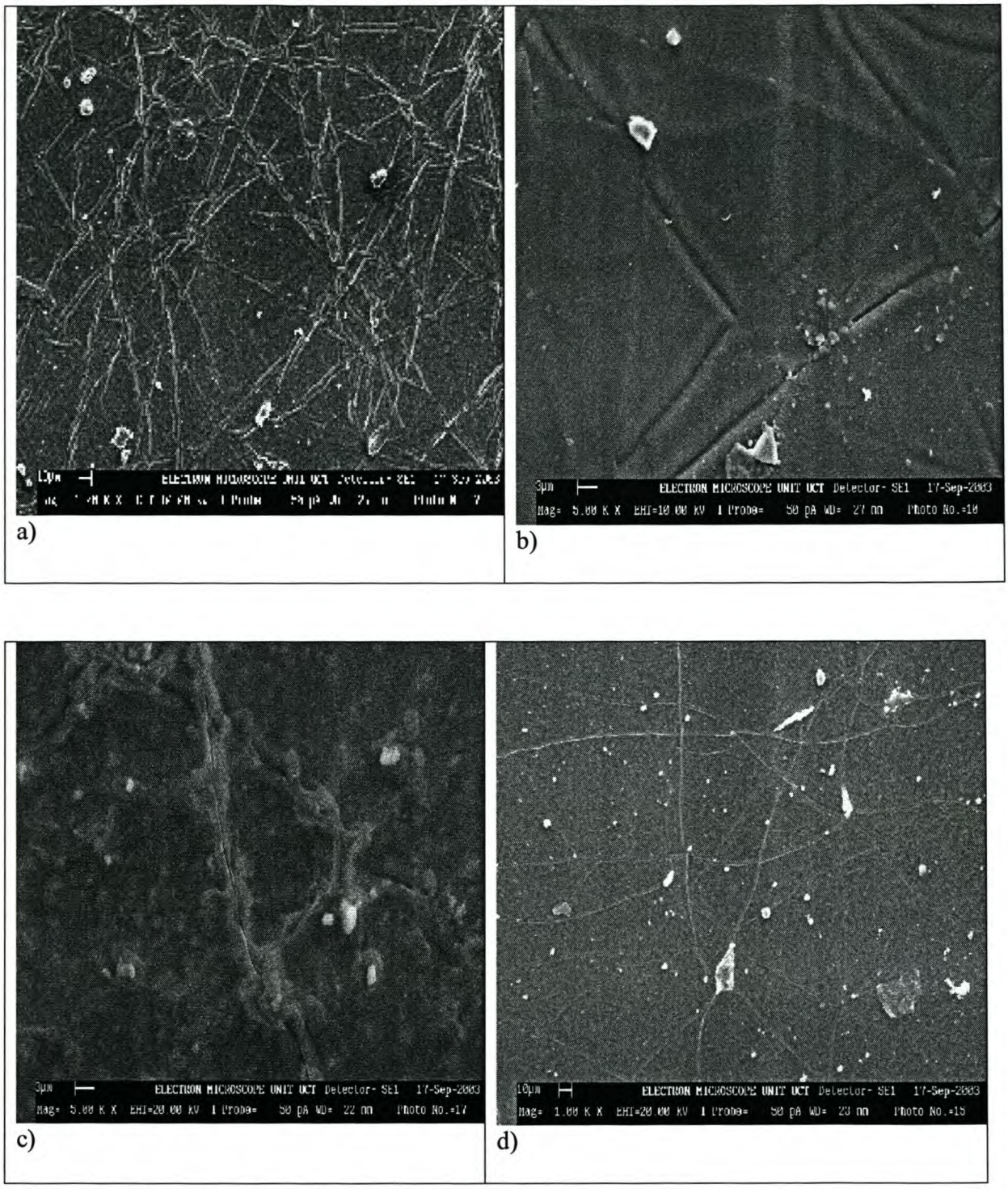

Figure 4.36: SEM result of various samples all after 30 min corona treatment: (a) sample D, (b) sample E, (c) sample J and (d) sample I (where samples D and J have LMW added)

4.4.2 Roughness of the material after corona

The investigation carried out by Deng *et. al.* [29] after salt fog energizing revealed that there is a general increase in surface roughness and the sample prepared with the addition of silicone fluids showed a greater roughness. Similar results were observed in

this study, where the samples with extra LMW oils show significant damage on the surface after corona treatment. This effect can be clearly seen in Figure 4.36 a. The formulation of sample D is similar to that of sample C, except that D was prepared with pre-addition of about 5% low molecular PDMS oils. The 30 min corona treated sample D is highly damaged compared to the 30 min corona treated sample C. Sample I and J also gave similar result, where J (the sample one with the LMW oils) was severely affected compared to sample I. Sample J had wider cracks after 30 min corona.

Figure 4.37 shows the SEM results of HTV commercial samples aged under different conditions.

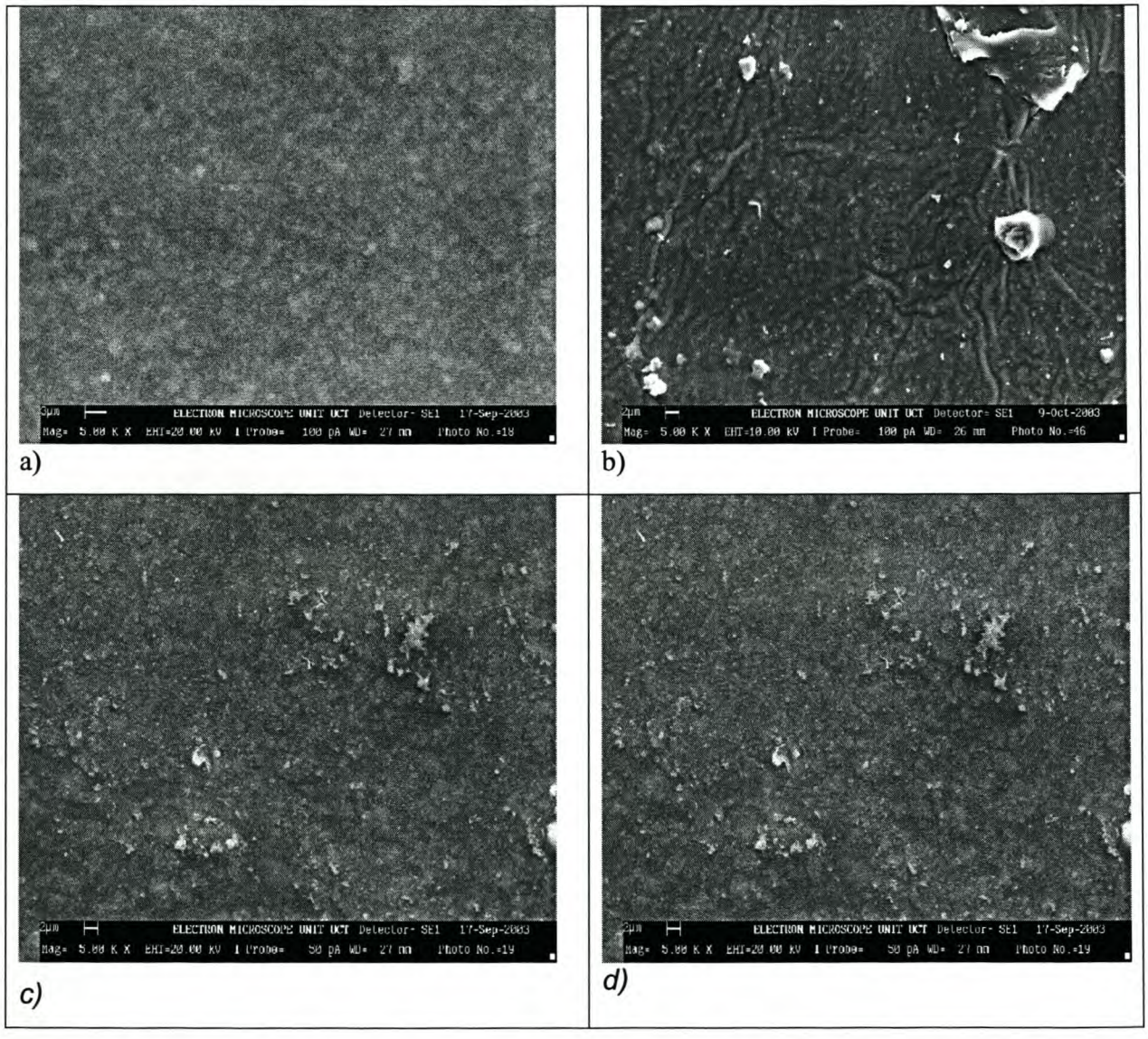

Figure 4.37: SEM results of HTV commercial PDMS (a) virgin (b) 30 min corona treated (c) 120 min coco corona treated and (d) 600 hours UV-C aged.

The virgin sample is relatively smooth compared to the aged samples. There is an increase in roughness of the surface with ageing and white fillers were exposed at the surface after ageing. There is slight formation of cracks after 30 min desktop corona ageing. Compared to the RTV samples, the HTV samples show less surface roughness and only a slight sign of crack formation after corona treatment. This indicates that HTV is more resistant to the effect of corona than the RTV PDMS is. The 120 min French cell type corona treated sample (Figure 3.37c) shows a slight increase in surface roughness. No sign of a brittle cracked surface is observed. This result is consistent with the positron results (Figure 4.20) where it is observed that although material degradation has occurred after 120 min of French cell corona treatments, no SiO_X layer has yet formed. The 600 hrs UV-C aged samples (Figure 3.37d) also only show very small changes.

4.4.3 KIPTS naturally aged insulators

Figure 4.38 shows SEM micrographs of the naturally aged commercial HTV samples, before and after cleaning.

Once again, the effects of pollution are clearly seen in the micrographs. In the aged polluted samples, after cleaning, the contaminants appear as more discrete particles whereas on the sample as received they appear to be coated as a film on the surface. The results indicate that not all the pollution is removed during the cleaning steps. This is due to the adhesion of the pollutants to the surface as a result of them being coated by the LMW silicones.

a)

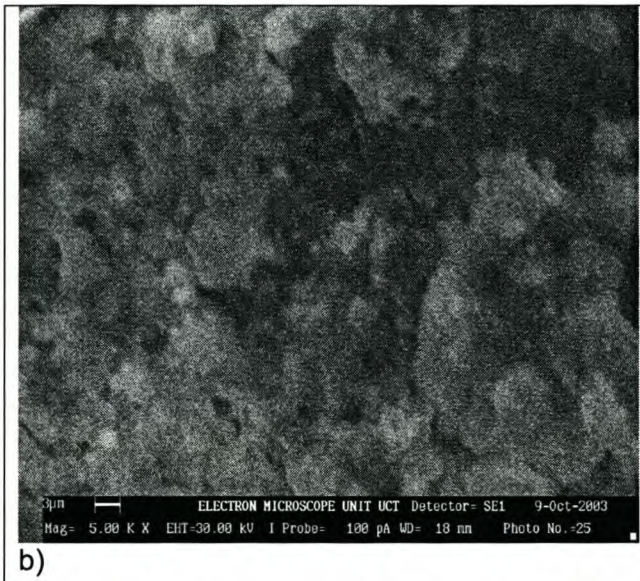

b)

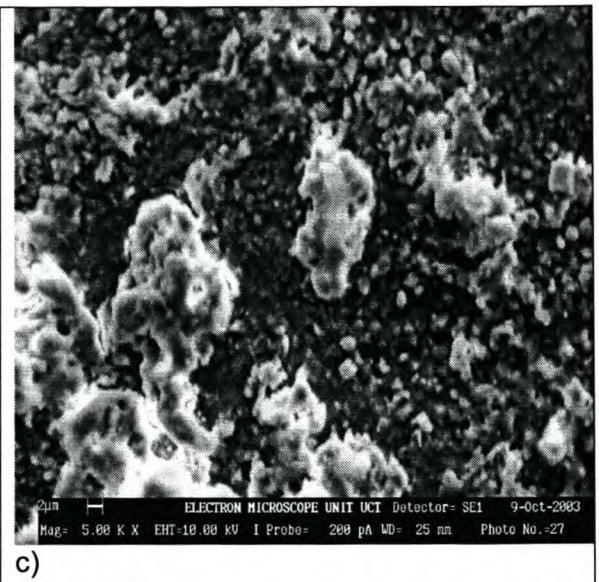

c)

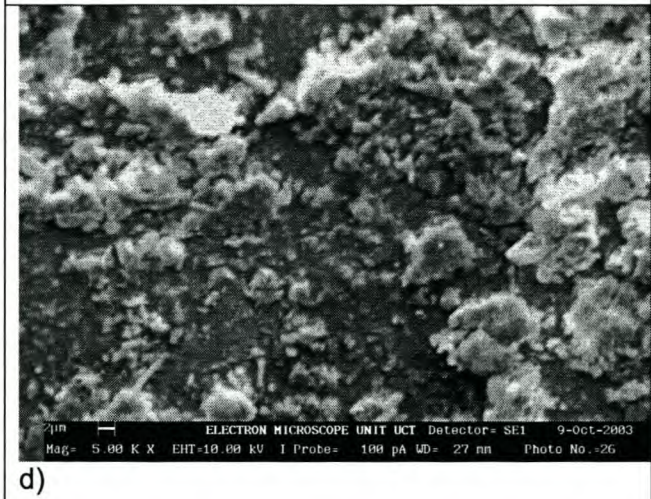

d)

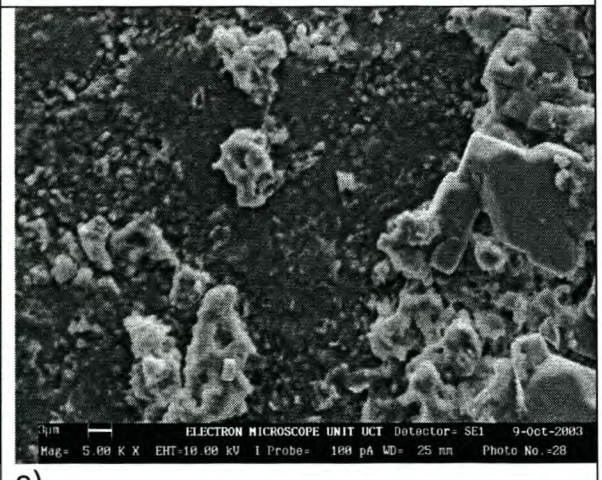

e)

Figure 4.38: SEM micrographs of a) naturally aged Blue HTV, b) un aged c) top as received d) top cleaned e) bottom as received f) bottom cleaned by heat + US.

Comparing the SEM and optical (light) microscopic results (Figure 4.24), the light microscopy seems to give a better indication of the dispersion and the contaminants at the surface.

4.4.4 Energy dispersive X-ray analysis (EDAX)

Sample surfaces were studied in a SEM equipped with an EDAX. This technique is widely used to study the composition of surface topography. The specimens were analysed before and after accelerated ageing. The electron beam that was employed in this study was 5, 10 and 20 keV. The higher the energy of the electron beams the deeper the penetration into the surface. The chemical analyses of different RTV PDMS tabulated below are expressed in percentages of the various elements.

4.4.4.1 Laboratory aged samples

Table 4.1: EDAX result of RTV PDMS formulations

Sample	kV	Virgin sample					desktop corona 30 min					French cell corona 120 min				
		O	Si	Al	Si/Al	Si/O	O	Si	Al	Si/Al	Si/O	O	Si	Al	Si/Al	Si/O
C	5	18.2	81.8			4.5										
	10	12.9	87.1			6.8	17.3	82.7			4.9	14.1	85.9			6.1
D	10	19.5	80.5			4.1	14.2	85.8			3.6					
E	5															
	10	16.9	83.2			4.9	20.8	79.2			3.8	19.5	80.5			4.1
G	5	18	80.6	1.4	57.6	4.5										
	10	23.0	75.4	1.6	47.1	3.8	14.4	84.2	1.4	60.1	5.9					
	20	18.1	74.3	7.6	9.8	4.1	15.0	78.9	6.1	12.9	5.3					
I	10	36.6	57.3	6.1	9.4	1.6	20.9	71.5	7.6	9.4	3.6	21.1	70.6	7.6	8.5	3.4
	20	20.2	68.0	11.8	5.8	3.4	22.0	65.1	12.9	5.1	3	20.7	66.7	12.9	5.3	3.2
J	10	20.0	74.8	5.2	14.4	3.7	60.7	37.7	1.6	23.6	0.6					
	20	19.6	70.3	10.1	7	3.6	31.7	57.8	10.5	5.5	1.8					
							600 Hours UV-C									
M	10	21.5	58.7	16.4	3.6	2.7	22.0	59.5	15.6	3.8	2.7	23.9	56.4	16.6	3.4	2.4
	20	22.8	52.3	21.8	2.4	2.3	22.7	52.9	21.1	2.5	2.3	23.8	52.7	20.2	2.6	2.2

Table 4.1 shows the results of surface analysis by EDAX. Comparing the RTV samples with HTV sample, the Al content of ATH in HTV is closer to the surface. This is consistent with positron results where it was found that the HTV commercial sample had a thinner polymer-rich layer than the RTV samples.

EDAX results showed slight increase in oxygen content ratio at the surface after corona treatment in some of the samples. However, this technique was not found to be as effective as other researchers reported [3].

4.4.4.2 Silicone insulators aged at KIPTS for one year

EDAX analysis was done on the field-aged samples in order to identify the nature of the pollutants present on the polymer surface.

Table 4.2: Light grey silicone insulator aged at KIPS for 1 year

Element	Unaged light grey insulator 5000X		Top polluted as received 5000X		Top cleaned Heat + 2x US $CHCl_3$ 5000X		Bottom polluted as received 5000X		Bottom cleaned Heat + 2x US $CHCl_3$ 5000X	
% Oxide	10KV	20KV	10KV	20KV	10KV	20KV	10KV	20KV	10KV	20KV
0	40.5	24.1	38.8	24.0	38.6	25.7	55.0	32.5	36.0	23.3
Na			1.0	0.7	0.6	0.4	1.4	0.5	0.0	0.5
Mg			1.6	1.3	1.4	1.0	1.6	0.7	1.9	1.2
Al	14.7	23.9	10.6	18.9	10.6	19.5	3.8	8.6	9.7	18.6
Si	43.1	49.8	42.2	48.9	45.4	49.1	29.6	28.4	47.2	51.2
S			1.0	0.8	0.6	0.8	2.0	7.3	1.0	0.7
Cl			2.2	2.3	1.5	2.0	2.2	2.4	2.5	2.1
K			0.5	0.8	0.5	0.5	0.5	0.7	0.5	0.5
Ca			1.1	1.2	0.3	0.6	3.5	17.3		0.6
Si/Al	2.9	2.1	4.0	2.6	4.3	2.5	7.8	3.3	4.9	2.8
Si/O	1.0	2.1	1.1	2.0	1.2	1.9	0.5	0.9	1.3	2.2

Bottom shed polluted surfaces, without cleaning; have oxidized chemical species as pollutants and they are observed to decrease after cleaning as shown in table 4.2.

Comparing the 10 keV and 20 keV results of all three KIPTS aged samples (1 year), Aluminium (Al) content is increase with depth. As the electron-beam increase from 10 keV to 20 keV the Al content increase significantly. This once again, implies that the polymer rich layer decrease with depth due to the ATH effect. However, Blue sample is totally different where the comparison of Al at 10 and 20 keV is not much different.

Although the amounts and the types of contaminants differ from sample to sample (blue, light grey and dark grey), the majority of the pollutants of the insulators aged at KIPTS that were identified by EDAX are, Cl, Na, Mg, Ca, K, and S. These are primarily originated from the ocean and industry. Cl and Ca are among the most dominant pollutants found. The other detailed EDAX result is included in Appendix B.

4.5 Fourier transform infrared spectroscopy

A qualitative analysis of an FTIR-ATR spectrum of a sample aged by corona discharge provides useful information. Figure 4.39 shows the FTIR-ATR spectrum of the pure PDMS compound (sample C) before and after corona treatment. The two FTIR-ATR spectra indicate the formation of hydrophilic silanol groups after 30 min corona exposure time Assignment of the various absorption peaks is tabulated in table 4.3. The absorption from the CH of the methyl group occurs at 2963 cm^{-1} and the broad band around 3377 cm^{-1} is due to the O-H group. The carbonyl (C=O) group and the O-H from water appears at around 1721 cm^{-1} and 1656 cm^{-1} respectively. The absorption band at 1278 cm^{-1} is due to CH deformation in the Si-CH_3 groups. The infrared absorption in the region 1020-1010 cm^{-1} is due to the Si-O-Si bonds in PDMS.

Table 4.3: The characteristic IR absorption bands for PDMS [30-31]

Wave number (cm^{-1})	**Bond**
3700-3200	OH
2962-2960	CH in methyl
1680-1740	C=O
1640	OH in H_2O
1440-1410	CH
1270-1255	Si-CH_3
1100-1000	Si-O-Si
870-850	Si $(CH_3)_3$

Corona treatment leads to the formation of hydrophilic species at the surface of the PDMS material, which is the main cause for the loss of hydrophobicity. After corona treatment of the unaged PDMS sample, there are new absorption bands formed due to oxidation of the surface.

Figure 4.39 shows that, the O-H and carbonyl bands increased and the methyl band at

2963 cm^{-1} decreased after corona ageing. This means that the oxygen content on the surface increased due to oxidation and the carbon content decreased. Similar results have been reported by Kumgai [30].

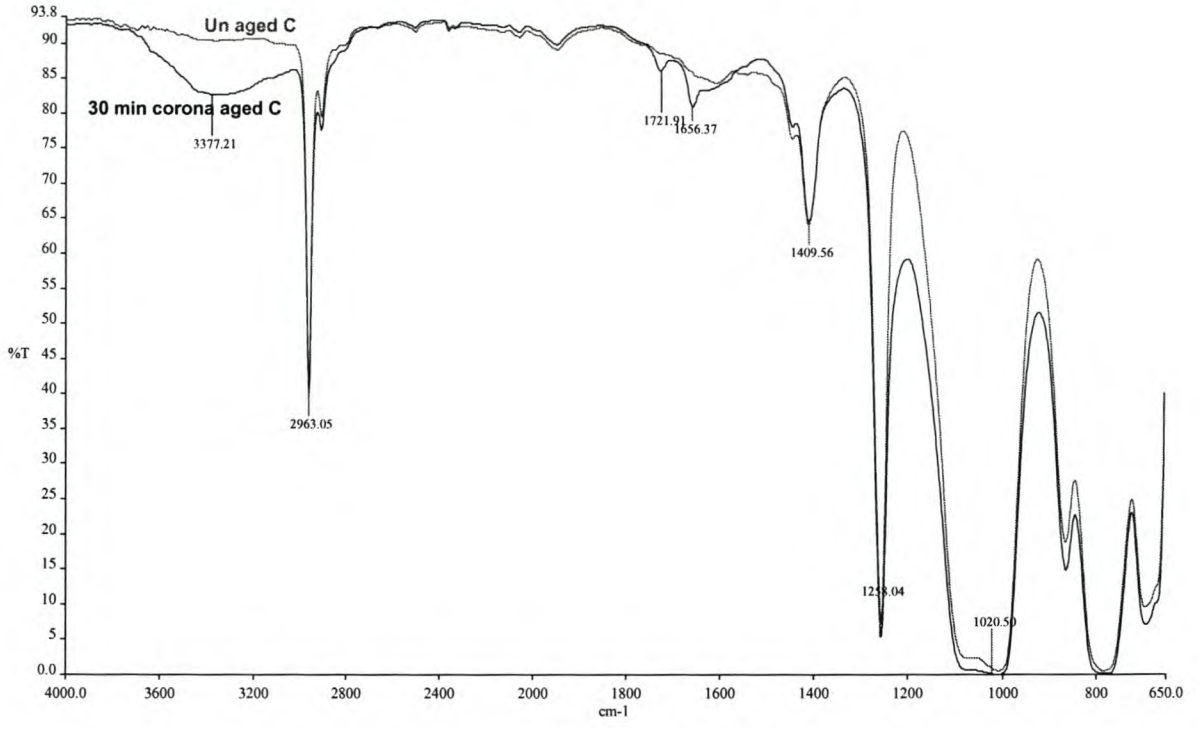

Figure 4.39: FTIR-ATR spectrum of sample C before and after corona treatment

A slight increase in oxygen content after corona treatment was also observed from the result of EDAX analysis (section 4.4.4). This is most probably due to the formation of silanol and carbonyl group by the surface oxidation and the subsequent formation of the SiO_X degradation layer. Therefore, it is possible to conclude that corona discharge produces hydrophilic O-H and C=O groups, thus reducing the amount of hydrophobic methyl groups. In addition, there could be a possibility of crosslinking, branching and interchanging by bridging of oxygen during corona ageing.

Figure 4.40 shows the FTIR-ATR spectra of sample I, J (RTV) and sample M (HTV) before and after corona treatment. The FTIR-ATR spectra of the HTV and RTV compounds show very little difference. The hydroxyl group observed on degradation in the PDMS compound that contained ATH filler is difficult to detect because of the presence of strong O-H bond absorbance due to the presence of ATH in both of the aged and unaged PDMS samples. However, there is a decrease in the intensity of methyl group and a small change in the carbonyl region.

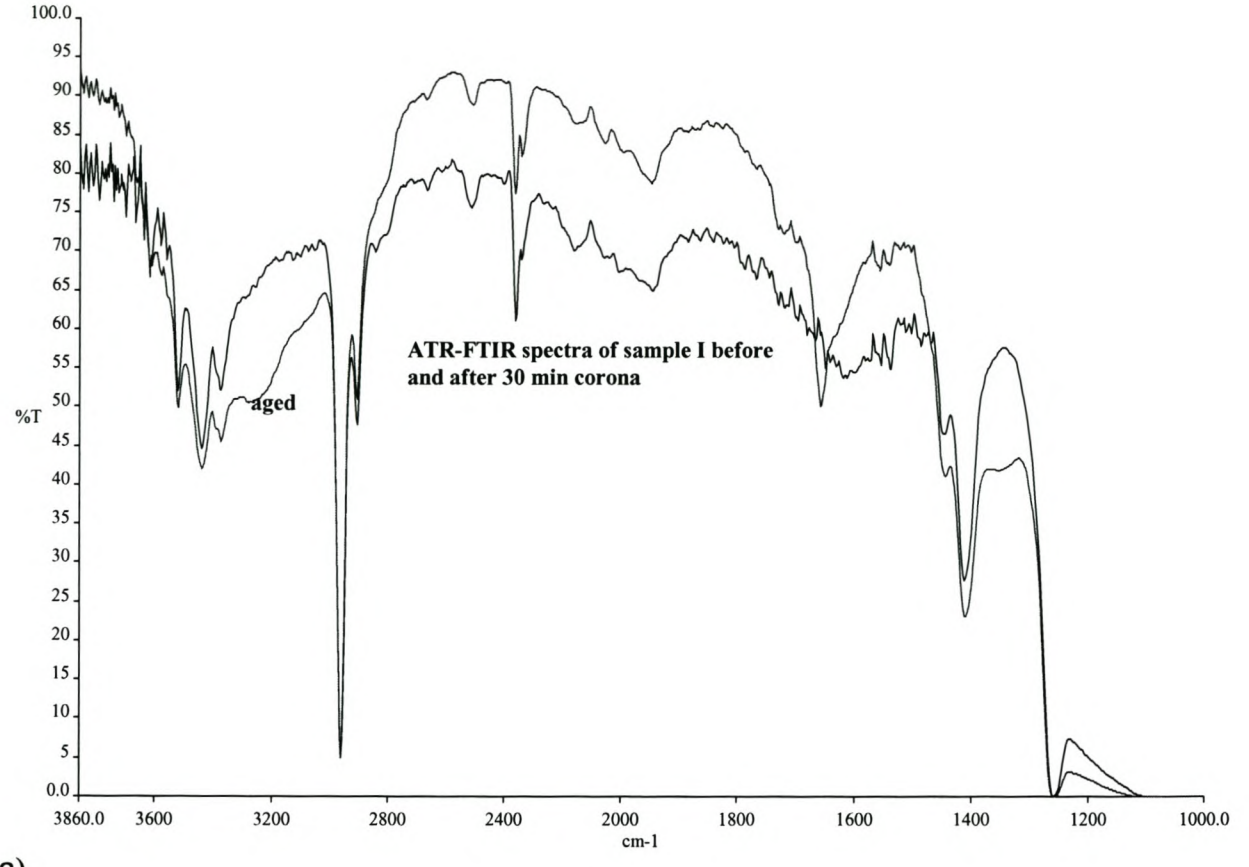

a)

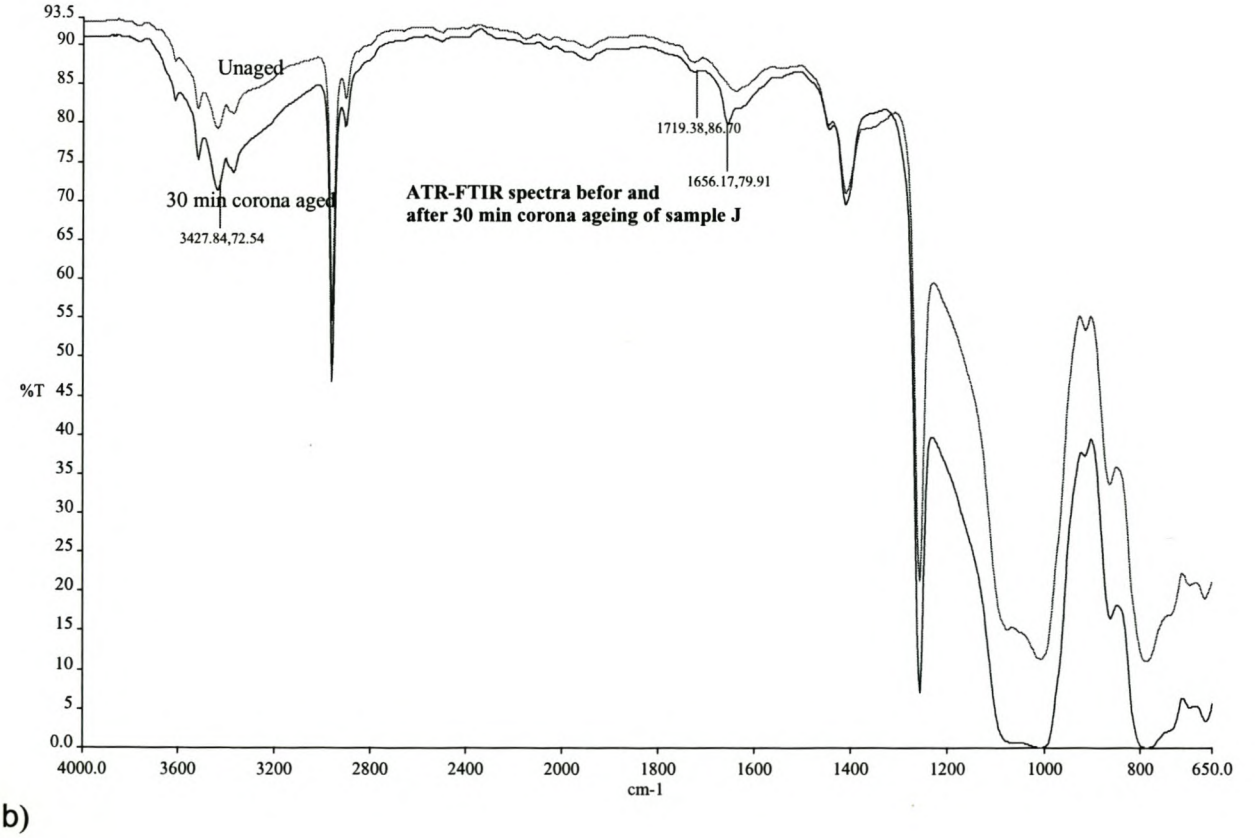

b)

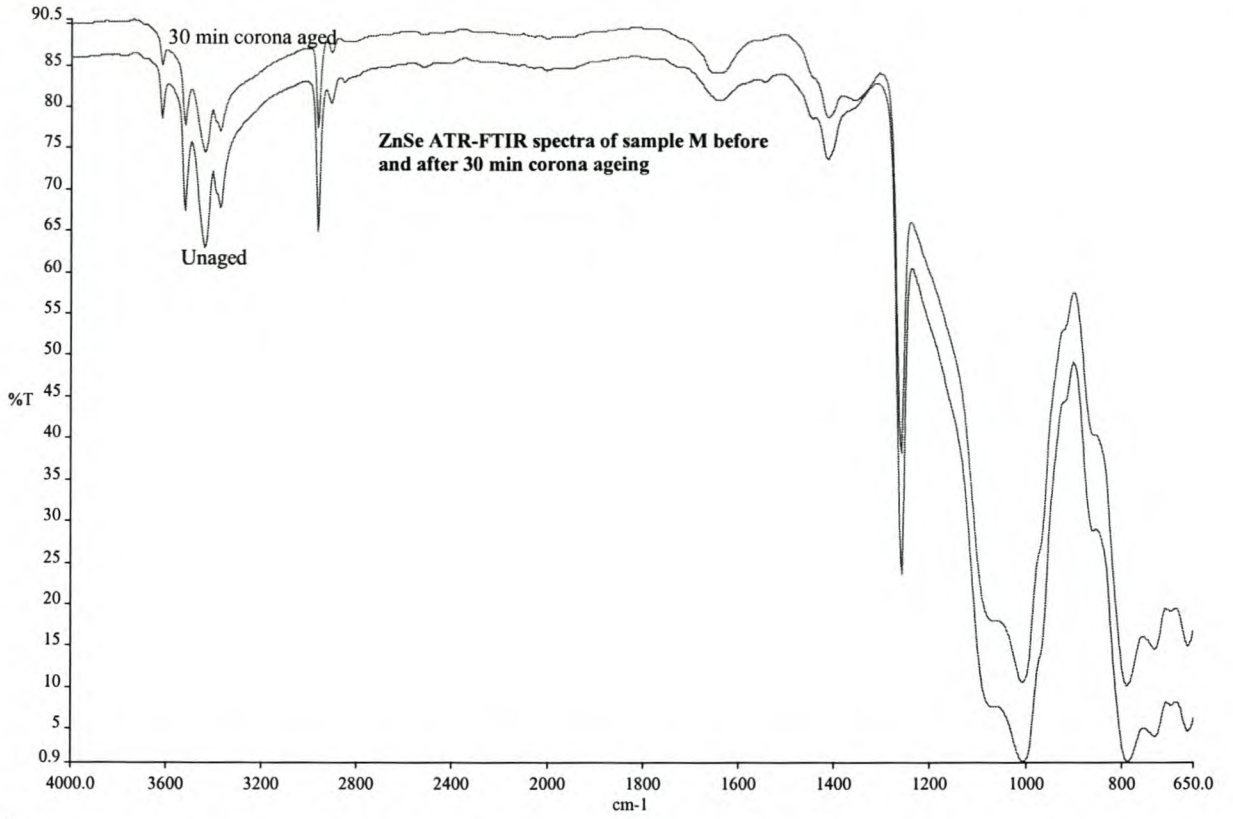

c)

Figure 4.40: FTIR-ATR spectra of a) sample I b) sample J c) sample M before and after 30 min corona ageing.

Comparing the commercial RTV compounds of samples I and J with the commercial HTV sample M, it is seen that the relative intensity of the methyl peak is much higher than the peak of the O-H bands in both the RTV samples, whereas in sample M (HTV) the O-H peak is higher than the methyl peak. This result is consistent with the positron data which shows that the RTV samples have higher polymer rich layer thickness than the HTV sample. In the HTV the O-H from the ATH dominates over the methyl peak intensity, since the amount of ATH in the near surface region is much higher than in the RTV sample.

In a confidential internal Eskom TSI report [32], it has been suggested that it is possible to quantify the degree of degradation from the FTIR-ATR spectra by calculating the ratios of peak height and areas in a similar way as has been done in transmission IR spectra [33]. Measurement of the following ratios have been suggested: peak height in the regions 3690-3036cm^{-1}, and 3010-2930cm^{-1} peak area 1800-1550cm^{-1} and polymer loss index by the ratio of peak height at 1040 and 2924 cm^{-1}. The calculated ratios for various samples are shown in Appendix C. It is observed that the majority of the peak ratios of the O-H and C=O groups increases after corona ageing and the methyl peak

decreases. Some of the results showed the reverse, i.e. the peak height ratios of the O-H and carbonyl decrease and the methyl increase.

The degree of conversion, ß, of PDMS to SiO_X can be determined by the change in peak height and area [33] as follows:

$$\beta = (H_o - H)/H_o \tag{4.3}$$

H_o and H is the peak height before and after exposure to corona, β is the degree of SiO_X formation. (Results of the calculated samples are summarised in Appendix C.)

The results of this study suggest that the various ratios mentioned above are actually not reliable or accurate measures of the degree of degradation due to the corona. In this case the use of an FTIR-ATR spectrum looses the quantitative information contained in a conventional transmission IR spectrum. Unfortunately, however, there is no suitable internal reference peak in these PDMS compounds to enable a quantitative comparison of different samples.

Using ATR one is able to perform surface profiling from 0.2 to 5μm thickness. The ATR penetration depth, d_p, is given by the equation below [34]:

$$d_p = \frac{\lambda}{2\pi n_1 (\sin^2\theta - n_{21}^2)^{1/2}} \tag{4.4}$$

Where n_{21}, is the relative index ratio of the sample and crystal (n_2/n_1), λ is the wavelength of electromagnetic ratio and θ is the beam angle. The estimated average depth penetration of the zinc selenide crystal used in this study is about 1.7 μm at 45°. Unfortunately, the change in surface morphology (both hardness and roughness), makes a direct quantitative analysis, by comparing the intensities of the virgin sample to those of the aged samples, meaningless. These ratios cannot, therefore, be used as a quantitative measure of the degree of degradation when using FTIR-ATR.

4.5.1 Comparison of FTIR-ATR and Pas

Comparing the results of ATR and Pas-FTIR spectroscopy for analysing of aged PDMS samples, the Pas spectra show almost no change after 30 min corona ageing whereas

the ATR spectra clearly show a considerable change. The most likely reason for this could be related to the depth of the Pas analysis. The spectrum of the aged and unaged samples of Pas results have matching spectra without any additional new bond formation as shown in Figure 4.41 a, unlike the ATR aged sample. This could be related to the ability of penetrating deeper i.e. Pas is penetrating deeper beyond the thin silica like layer formed during corona treatment. Similar results was observed for all samples.

The depth of penetration of photoacoustic spectroscopy is given by the equation [35]:

$$d_p = [\alpha\lambda / 2\pi\nu]^{1/2} \qquad (4.5)$$

where d_p is the thickness (depth penetration) at incident wavelength λ, α is the thermal diffusivity of the sample and ν the interferometer mirror velocity. The estimated penetration ability of photoacoustic spectroscopy is about 5-34 μm [36], which is deeper than the ATR.

From the positron annihilation data (section 4.2.1), it was found that the thickness of the silica-like layer formed due to corona ageing (which is our main concern) is about 40-60 nm after an hour of corona treatment. The thickness of the silica-like layer formed during the corona discharge might be much thinner than the probing depth of the Pas technique where the spectrum includes the unaffected part of the sample.

Figure 4.41 shows the comparison of ATR and Pas spectra of samples C and I. As can be seen from the figure below, a number of new absorption bands appeared in the ATR spectra but no new peak in the Pas spectra.

As mentioned above, the spectra of sample I in a, showed no change in the Pas analysis. The relative intensity of the O-H peak is higher than the methyl peak contrary to the ATR result where the methyl peak is much intense than the Pas result. This is due to the deeper penetration of Pas beyond the polymer rich surface.

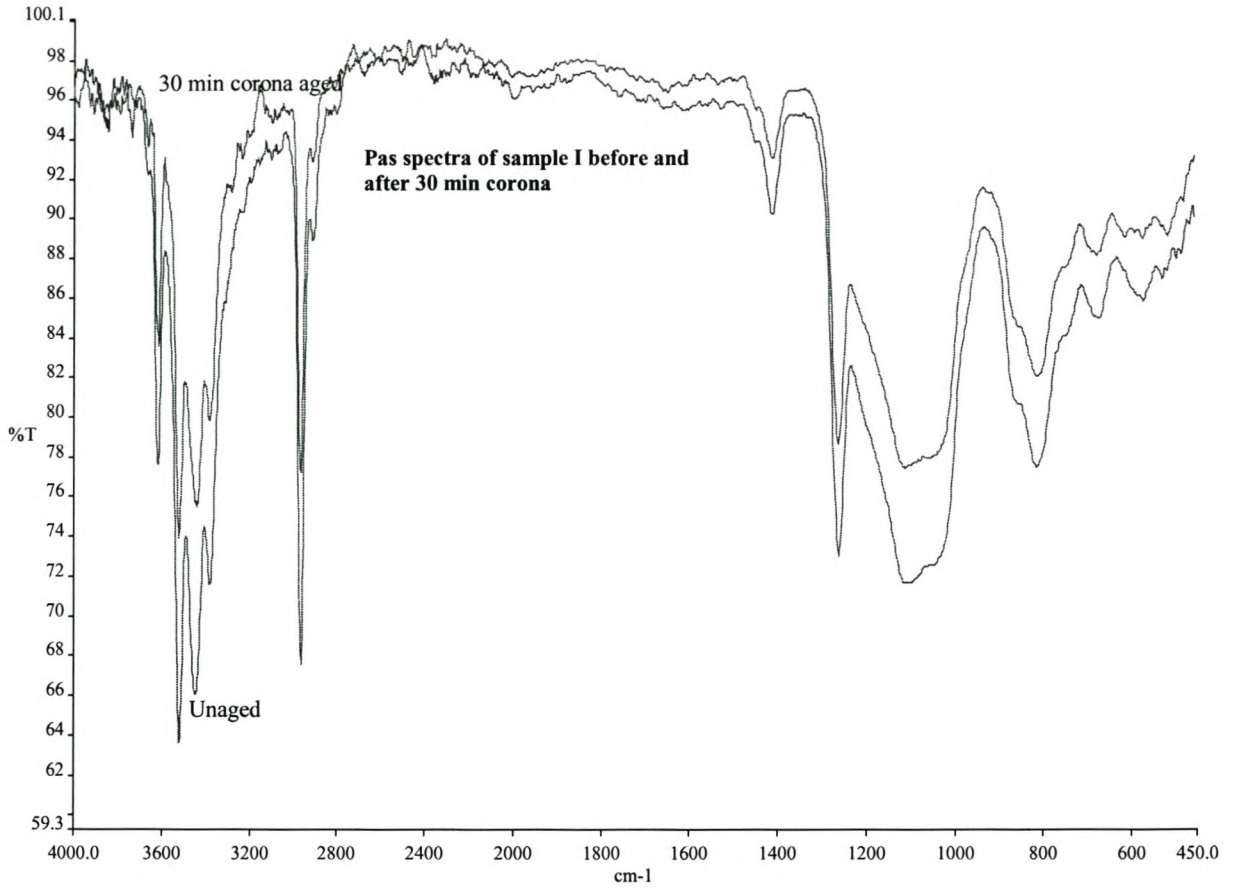

a)

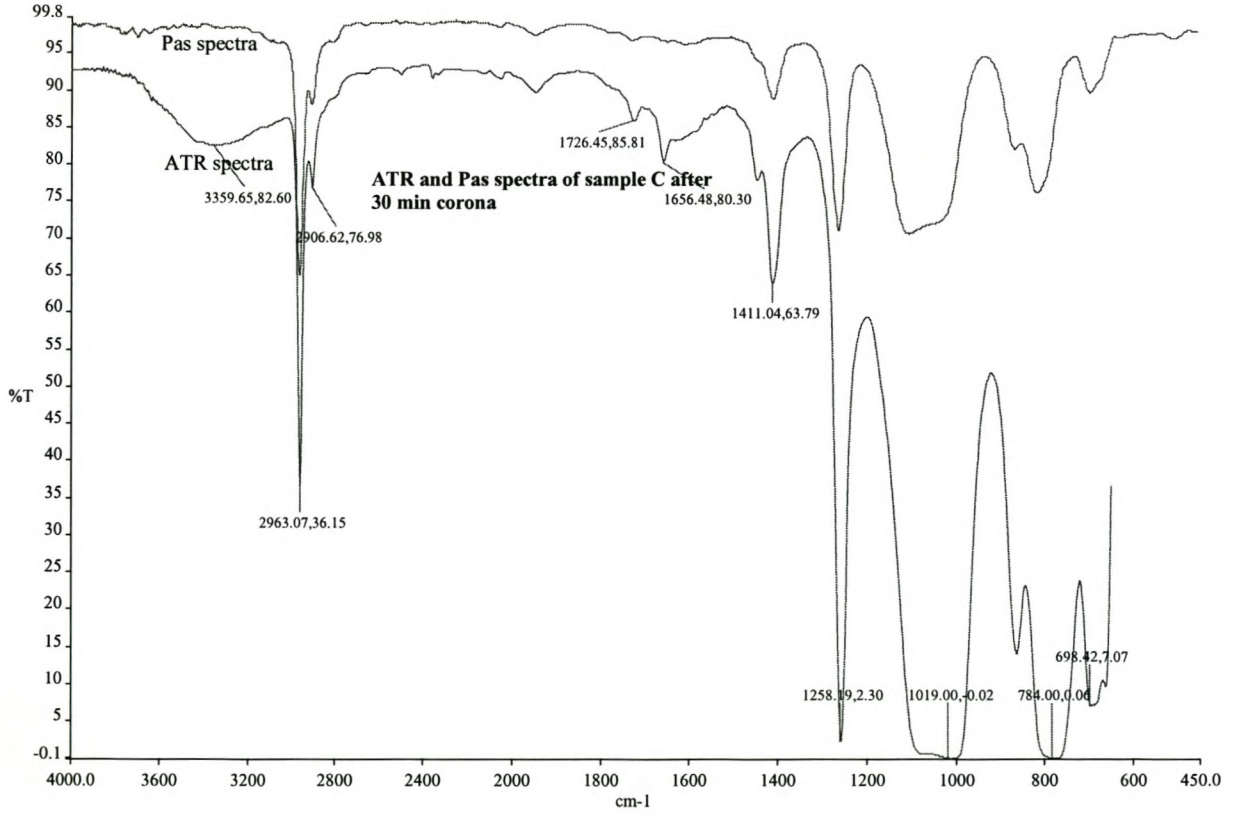

b)

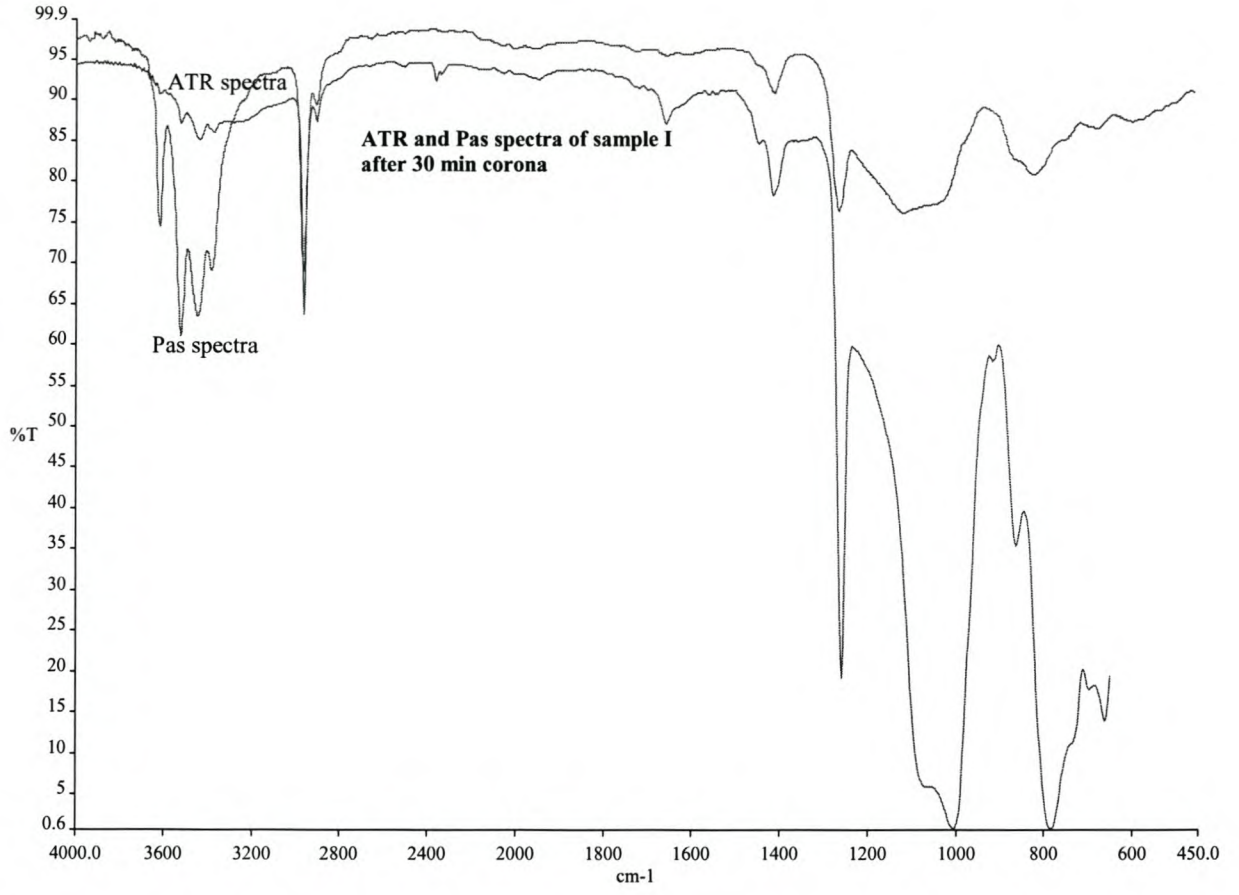

c)

Figure 4.41: a) Pas results of sample I before and after 30 min corona, b) comparison of ATR and Pas after 30 min corona of sample C and c) ATR and Pas result of sample I.

4.6. References

1. J. K. Kim and I. H. Kim, J. Appl. Polym. Sci., Vol. 79, 2251-2257, 2001.
2. S. M. Gubanski and A. E. Vlastós, IEEE. Trans. on Power Delivery, Vol. 5, 1527-1535, 1990.
3. S. Kumagai and N. Yoshimura, IEEE. Trans. on Power Delivery, Vol. 18, 506-515, 2003.
4. ASTM D 2275, May 2001, West Conshohocken, United States.
5. H. Hillborg and U. W. Gedde, Polymer, Vol. 39, 1991-1998, 1998.
6. H. Janssen, A. Herden, and H. C. Kärner, The loss and recovery of hydrophobicity on silicone rubber surfaces, 10th International Symposium on High Voltage Engineering, Montreal, Canada, 1997.
7. J. Kim, M. K. Chaudhury and M. J. Owen, J. Colloid Interface Sci., Vol. 226, 231-

236, 2000.

8. R. S. Gorur, J. W. Chang, and O. G. Amburgey, IEEE. Trans. on Power Delivery, Vol. 5 1990.

9. G. Bar, L. Delineau, A. Häfele and M. H. Whangbo, Polymer, Vol. 42, 3627-3632, 2001.

10. D. H. Han, H. Y. Park, D. P. Kang, H. G. Cho, K. E. Min, K. Takasu and T. Kuroyagi, IEEE. Trans. Diel. Elect. Insul., Vol. 9, 323-328, 2002.

11. A. Toth, I. Bertoti, M. Blazso, G. Banhegyi, A. Bognar and P. Szaplonczay, J. Appl Polym Sci., Vol. 52, 1293-1307, 1994.

12. N. Yoshimura, S. Kumagai and S. Nishimura, IEEE. Trans. Diel. Elect. Insul., Vol 6, 632- 649, 1999.

13. H. Büchener, F. Schmuck, A. Zanetti, R. Bärsch, H. Jahn, and J. Lambrecht, CIGRE regional meeting for the African continent, Cairo, Egypt, 1997.

14. A. E. Vlastós and S. M. Gubanski, IEEE. Trans. on power delivery, Vol. 6,888-900, 1991.

15. M. Abdel-salam, H. Anis, A. Ei-Morshedy and R. Radwan, *High voltage engineering theory and practice*, 2nd edition, Marcel Dekker, Inc., New York, 2000.

16. V. M. Moreno, R. S. Gorur and A. Kroese, IEEE, Trans. Diel. Elect. Insul., Vol. 10, 80-95, 2003.

17. Y. C. Wu, Chia-Ming. Huang, Y. Ll, R. Zhang, H. Chen, P. E. Mallon, J. Zhang, T. C. Sanderczki, Da-Ming. Zhu, Y. C. Jean, R. Suzuki and T. Ohdaira, J. Polym. Sci., Part B, Polym. Phys. Vol. 39, 2290-2301, 2001.

18. H. Cao, J. P. Yuan, R. Zhang, C. M. Huang, T. C. Sandreczki, and Y. C. Jean, Macromolecules, Vol. 32, 5925-5933, 1999.

19. Y. C. Jean, P. E. Mallon, D. M. Schrader, *Principles and applications of positronium and positronium chemistry*, Ed's World Scientific Publishing, Singapore, 2003.

20. P. E. Mallon, T. A. Berhane, C. J. Greyling, W.Vosloo, H. Chen and Y. C. Jean, Mat. Sci. Forum, Vol. 445-446, 322-324, 2004.

21. R. Zhang, H. Cao, C. M. Huang, P. E. Mallon, T. C. Sandreczki, J. R. Richardson, Y. C. Jean, B. Nielsen, R. Suzuki and T. Ohdaira, J. Radiat. Phys. Chem., Vol. 58,

639-644, 2000.

22. H. Chen, Q. Peng, Y.Y. Huang, R. Zhang, P.E. Mallon. J. Zhang, Y.Li, Y. Wu, J. R. Richardson, T. C.Sandreczki, Y. C. Jean, R. Suzuki and T. Ohdaira, Applied Surf. Sci., Vol. 194, 168-175, 2002.

23. R. Zhang, P.E. Mallon, H. Chen, C.M. Huang, J. Zhang, Y.Li, Y. Wu, T. C. Sandreczki and Y. C. Jean, J. Prog. Org. Coatings, Vol. 42, 244-252, 2001.

24. J. P. Renders, I. R. Jandrell and S. M. Reynders, IEEE. Trans. Diel. Elect. Insul., Vol. 6, 620-631, 1999.

25. H. Cao, R. Zhang, C. S. Sundar, J. P. Yuan, Y. He, T. C. Sandrezki and Y. C. Jean, Macromolecules, Vol. 31, 6627-6635, 1998.

26. P. E. Mallon, C. J. Greyling, W. Vosloo, Y. C. Jean, Radiat. Phys. Chem., Vol. 68, 453-456, 2003.

27. H. Hillborg, S. Sandelin and U. W. Gedde, Polymer, Vol. 42, 7349-7362, 2001.

28. H. Hillborg, J.F Ankner, U.W. Gedde, D.D. Smith, H.K. Yasuda and K. Wikstrom, Polymer, Vol. 41, 6851-6863, 2000.

29. H. Deng and R. Hackam, IEEE, Trans. Diel. Elect. Insul. Vol. 8, 84- 94, 1998.

30. N. Yoshimura, S. Kumagai and S. Nishimura, IEEE. Trans. Diel. Elect. Insul., Vol 6, 632- 649, 1999.

31. S. H. Kim, E. A. Cherney, R. Hackam and K. G. Rutherford, IEEE. Trans. Diel. Elect. Insul., Vol.1, 106-122, 1994.

32. Confidential internal Eskom TSI report, *Material test for Eskom HV polymer insulator 2003 part 1*, finger printing and QA materials analysis producedure, C. J Greyling, 2003.

33. M. Ouyang, P.P. Klemchuk, J. T. Koberstein, Polym. Degrad. Stab., Vol, 70, 217-228, 2000.

34. R. A. Meyers, Encyclopedia of Analytical Chemistry, *Application, theory and instrumentation*, John Wiley & Sons, Ltd, New York, P 1758.

35. A. Kumar, S. Commereuc, L. Gonon, V. Verney, Polym. Degra. Stab., Vol. 75, 509-516, 2002.

36. L. Gonon, J. Mallegol, S. Commereuc, V. Verney, Vib. Spec., Vol. 26, 43-49, 2001.

Chapter Five
Conclusions and Recommendations

5.1 Conclusions

It is well known that addition of large amounts of filler to the material formulation of PDMS improves the mechanical strength of the PDMS insulators in outdoor high voltage insulation. However, results of the investigations carried out in this study with different types and amount of fillers proves that fillers have a negative effect on the recovery of hydrophobicity which is crucial factor to suppress electrical discharge. Those samples without filler are observed to recover faster than those with filler, regardless of the types and amounts present. The possible reason given for this is that the filled samples are able to resist de-polymerisation of the polymer to low molecular weight during corona discharge, which has a large effect on the recovery of hydrophobicity.

Furthermore, studies carried out to determine the effect of the addition of LMW silicone oils externally show no major improvement in hydrophobicity recovery. Results obtained in this study indicate, however, that their role is not significant. This is because during corona exposure sufficient LMW silicone oil formation takes place which plays a vital role in the recovery of hydrophobicity. Therefore, the recovery of hydrophobicity by diffusion of LMW species from the bulk to the surface is governed predominantly by the LMW species formed due to de-polymerisation (*in-situ*) in the process of the corona discharge and not by the pre-existing LMW species in the matrix.

UV-C aged HTV PDMS samples showed slight decrease in static contact angle measurement and increase with recovery time.

The time of exposure to corona and the nature of corona treatment strongly affect the rate of hydrophobicity recovery of the PDMS material. The SCA and AFM results indicate that the 10 min desk top corona aged sample recovered faster than the 5 min and 30 min corona treated samples. This result agrees with previously published results, where the short time of corona treatment and low intensity voltage activates the LMW silicone oils to diffuse to the surface of the material. Results of the present study also showed, higher intensity and longer treatment time leads to thicker silica-like SiO_X layer formation and this restrict the fast diffusion of low molecular weight species, which

is most probable means of hydrophobicity recovery.

Analysis by the positron technique can reveal important information on the micro structural changes that occur during corona treatment, including estimation of the thickness of the silica-like layer that is responsible for the loss of hydrophobicity. This technique can detect even the very early stage of degradation of the material.

The corona treatment of PDMS samples results in a decrease of the S parameter. The decrease is observed even at a very short exposure times which once again indicates the unique sensitivity of the PAS technique as a method of material surface analysis. Such a decrease is the result of the formation of a silica-like layer due to oxidation of the polymer by corona discharge. The decrease in S parameter continues until a certain dose of corona (5 min corona exposure), where after it is observed to increase. This increase in the S parameter with further increase of corona dose is proposed to be due to the formation of a highly damaged polymer skin and indicates the point at which the material no longer may considered as a polymer and the silica-like layer has started to form. With an increase in exposure time to corona there is also an increase in thickness of the silica-like inorganic layer at the surface. A pure PDMS RTV sample, after 60 min corona treatment for example has a silica-like layer with an estimated 40-60 nm thickness.

The two PDMS samples, with 15% silica + 26% ATH and the PDMS with only ATH showed sharp decreases in their S parameters with increased implantation energy, unlike samples without ATH filler. The PDMS samples without fillers, however, have a relatively thicker polymer-rich layer. At the very near surface both the silica and ATH filled PDMS samples show similar profiles which indicate the presence of a thin polymer-rich layer at the surface.

In comparison of the positron beam results of RTV PDMS sample I having the same formulation to commercial HTV samples, show a similar profile with sharp maximum peak and significant drop with implementation energy. The results do however indicate that the HTV samples have much thinner polymer surface layers as indicated by a sharp drop in the S parameter of commercial HTV at relatively low depth. The commercial HTV samples cut from insulator sheds show similar results to those of the RTV compounds after corona treatment. Once again, evidence for the formation of a SiO_X degradation layer was found. In the case of the HTV samples the layer appears

thinner than that observed in the RTV compounds. This is ascribed to the fact that the commercial HTV compounds have a much thinner polymer rich layer on the surface.

Comparison of samples treated by French cell type corona and desk top corona similarly showed that the desk top corona has a more severe effect on PDMS material than the French cell corona treatment does, as determined by the static contact angle and PAS result. The short desk top corona treatment (even for as short period as 1 min) is much more severe than the 2 hours French corona exposure. This is due to the effect of direct ion bombardment on the material. Even though the French corona treatment is milder than the desk top corona treatment, permanent material change occurs in the French corona treated samples, as is indicated by PAS results. The positron beam technique has also given unique information on the degradation reaction as a function of corona treatment time.

The naturally aged commercial samples are covered with pollutants, which may interfere with the analyses. The positron beam analysis done for the polluted commercial sample shows a complete drop of S parameter due to the pollutants which cover the surface of the material. However, cleaning in an ultrasonic bath with chloroform after heating for 30 min resulted in an increase of S parameter. Though there is an increase of S parameter, comparing to the unaged sample, the S parameter is low even after cleaning. This could be due to the remaining pollutants on the surface of the material or due to the effect of natural ageing.

Atomic force microscopic studies also confirm the loss and hydrophobicity recovery of the PDMS material after corona treatment. The adhesive force calculated from the pull-off force-distance curves clearly show that the adhesive force between the probe and the sample decrease with increasing time after corona treatment. This decrease in adhesive force indicates the hydrophobicity recovery. The decrease in adhesive force is much greater in the first 30 minutes, which implies that the recovery rate is faster in the first minutes after corona treatment.

The topographic image also confirms the recovery of hydrophobicity by diffusion of LMW from the bulk to the surface after corona ageing. Due to the effect of corona, the fillers are exposed to the surface and, after a certain period of time, this exposed filler decreases gradually because of coverage to by diffused LMW silicone oils.

Furthermore, the AFM study indicates an increase in surface hardness with an increase on corona exposure time. This increase could be related to the formation of an inorganic silica-like layer. With time, the hardness decreases which indicates the recovery of hydrophobicity of the material.

The atomic force distance curves could also be used to track the rate of hydrophobicity recovery by measuring the adhesion force as a function of recovery time and fitting equation (4.2) to calculate the recovery rate.

The usefulness of FTIR-ATR and Pas as quantitative analysis tools with which to track degradation due to corona is limited. This is mainly due to the fact that the material change is limited to the first few nanometers from the surface, whereas the technique probes too deeply beyond the expected surface change. Nevertheless, the techniques do provide qualitative information on the material change.

5.2. Recommendations

Hydrophobicity is good indicator of the insulator surface condition; therefore, it is important to evaluate the dynamic contact angle for better understanding of the degradation mechanism.

The results of this study on RTV compounds of controlled formulation have shown that the formulation have a significant impact on the material behaviour. Further investigation of controlled formulations of high temperature vulcanization (HTV) is there for essential to have good understanding of the mechanisms of ageing of these PDMS materials used in bulk insulators.

The evaluation of field aged insulator material using surface specific techniques is difficult because of the interference of contaminants present at the surface. Therefore, the effects and types of surface cleaning for the naturally aged sample will have to be further investigated before there can be a meaningful comparison between the naturally and laboratory aged samples can be made.

In addition to the applied analytical techniques employed it would be worthwhile to investigate other analytical techniques such as Rutherford Backscattering (RBS), Proton-induced X-ray emission (PIXE)

The results of this study have shown significant difference between the desktop and French cell corona treatment. It is recommended that further studies be done on the comparison of the two techniques particularly in terms of exposure time. For example it would be use full to conduct positron beam studies of the French cell treated samples treated for a very long time, to find the point at which formation of the SiO_X degradation layer will occur when this type of treatment is used.

It would also be useful to attempt to isolate the various component of corona (i.e. UV, ozone, ion bombardment) in order to study the effect of these individual components of PDMS materials.

.

Appendix A

SCA measurements of selected RTV PDMS samples

Sample C: **30 min desktop corona aged**

Recovery time	X1	X2	Y1	Y2	ΔX	ΔY	tan (theta/2)	theta (degrees)	average
1 min								completely flat	
30 min	155	456	196	269	301	73	0.485	51.8	
	154	516	210	269	362	59	0.326	36.1	
	94	412	199	277	318	78	0.491	52.3	
	136	471	245	297	335	52	0.310	34.5	
	150	440	224	315	290	91	0.628	64.2	47.8
1 hour	57	364	230	305	307	75	0.489	52.1	
	121	399	210	291	278	81	0.583	60.5	
	101	356	227	289	255	62	0.486	51.9	
	201	442	206	286	241	80	0.664	67.2	
	143	376	209	288	233	79	0.678	68.3	
	159	426	210	296	267	86	0.644	65.6	
	60	351	212	298	291	86	0.591	61.2	
	158	420	231	300	262	69	0.527	55.6	60.3
3 hours	3	271	206	308	268	102	0.761	74.6	
	340	602	210	308	262	98	0.748	73.6	
	16	302	217	312	286	95	0.664	67.2	
	312	599	212	310	287	98	0.683	68.7	
	2	272	201	308	270	107	0.793	76.8	
	348	601	190	302	253	112	0.885	83.0	
	43	293	187	292	250	105	0.840	80.1	
	348	574	189	294	226	105	0.929	85.8	
	22	272	192	304	250	112	0.896	83.7	
	348	573	197	303	225	106	0.942	86.6	78.0
24 hours	31	245	182	298	214	116	1.084	94.6	
	345	564	190	300	219	110	1.005	90.3	
	84	291	196	303	207	107	1.034	91.9	
	370	585	190	302	215	112	1.042	92.3	
	378	570	203	305	192	102	1.063	93.5	
	13	255	203	336	242	133	1.099	95.4	
	360	592	199	330	232	131	1.129	97.0	
	55	258	218	331	203	113	1.113	96.1	
	180	387	171	288	207	117	1.130	97.0	94.2
virgin	30	248	169	285	218	116	1.064	93.6	
	339	541	176	285	202	109	1.079	94.4	
	179	422	176	291	243	115	0.947	86.9	
	174	385	177	288	211	111	1.052	92.9	
	44	279	183	298	235	115	0.979	88.8	
	65	286	182	296	221	114	1.032	91.8	
	350	581	179	292	231	113	0.978	88.7	
	54	261	185	296	207	111	1.072	94.0	
	323	549	180	289	226	109	0.965	87.9	
	11	237	175	291	226	116	1.027	91.5	91.0

Sample D: **30 min desktop corona aged**

Recovery time	X1	X2	Y1	Y2	ΔX	ΔY	tan (theta/2)	theta (degree)	average
1 min								completely flat	
30 min	26	538	187	254	512	67	0.262	29.3	
	122	478	197	263	356	66	0.371	40.7	
	137	466	198	264	329	66	0.401	43.7	
	134	438	205	260	304	55	0.362	39.8	
	77	435	187	247	358	60	0.335	37.1	
	159	497	181	248	338	67	0.396	43.3	
	1	287	157	248	286	91	0.636	64.9	
	340	599	147	243	259	96	0.741	73.1	46.5
1 hour	154	440	206	288	286	82	0.573	59.7	
	92	386	206	284	294	78	0.531	55.9	
	196	439	210	275	243	65	0.535	56.3	
	143	408	205	277	265	72	0.543	57.0	
	108	387	193	269	279	76	0.545	57.2	
	180	460	201	271	280	70	0.500	53.1	
	1	263	185	263	262	78	0.595	61.5	
	318	541	180	261	223	81	0.726	72.0	
	205	400	168	257	195	89	0.913	84.8	
	87	421	191	284	334	93	0.557	58.2	61.6
3 hours	371	622	188	283	251	95	0.757	74.2	
	36	279	190	281	243	91	0.749	73.7	
	312	549	189	281	237	92	0.776	75.6	
	23	274	185	279	251	94	0.749	73.7	
	351	584	189	278	233	89	0.764	74.8	
	14	262	180	273	248	93	0.750	73.7	
	343	600	173	268	257	95	0.739	73.0	
	115	331	183	260	216	77	0.713	71.0	
	352	573	171	263	221	92	0.833	79.6	
	180	374	173	261	194	88	0.907	84.4	75.4
24 hours	53	277	180	285	224	105	0.938	86.3	
	328	539	184	288	211	104	0.986	89.2	
	94	295	178	284	201	106	1.055	93.1	
	357	561	175	283	204	108	1.059	93.3	
	26	242	166	283	216	117	1.083	94.6	
	305	540	164	282	235	118	1.004	90.2	
	68	274	179	284	206	105	1.019	91.1	
	304	536	172	283	232	111	0.957	87.5	
	74	274	184	285	200	101	1.010	90.6	
	319	523	175	287	204	112	1.098	95.4	90.6
virgin	40	257	127	243	217	116	1.069	93.8	
	317	543	124	246	226	122	1.080	94.4	
	31	277	173	287	246	114	0.927	85.7	
	332	578	169	289	246	120	0.976	88.6	
	47	283	173	287	236	114	0.966	88.0	
	354	593	174	291	239	117	0.979	88.8	
	25	248	176	291	223	115	1.031	91.8	
	370	579	193	293	209	100	0.957	87.5	
	34	255	192	291	221	99	0.896	83.7	
	308	510	189	286	202	97	0.960	87.7	89.0

Sample E: **30 min desktop corona aged**

Recovery time	X1	X2	Y1	Y2	ΔX	ΔY	tan (theta/2)	theta (degrees)	average
1 min								completely flat	
30 min	341	578	251	299	237	48	0.405	44.1	
	180	417	244	299	237	55	0.464	49.8	
	128	414	235	280	286	45	0.315	34.9	
	100	471	203	286	371	83	0.447	48.2	
	103	468	225	280	365	55	0.301	33.5	
	173	464	182	273	291	91	0.625	64.0	
	130	407	196	274	277	78	0.563	58.8	
	146	484	186	282	338	96	0.568	59.2	
	97	438	210	283	341	73	0.428	46.4	48.8
1 hour	20	234	202	279	214	77	0.720	71.5	
	161	446	215	277	285	62	0.435	47.0	
	189	447	219	279	258	60	0.465	49.9	
	3	238	211	284	235	73	0.621	63.7	
	335	593	220	277	258	57	0.442	47.7	
	77	355	174	282	278	108	0.777	75.7	
	77	353	181	281	276	100	0.725	71.9	
	139	412	194	286	273	92	0.674	68.0	
	330	618	177	269	288	92	0.639	65.1	62.3
3 hours	36	247	204	295	211	91	0.863	81.6	
	350	591	194	292	241	98	0.813	78.2	
	9	221	219	298	212	79	0.745	73.4	
	45	259	209	296	214	87	0.813	78.2	
	314	580	194	291	266	97	0.729	72.2	
	24	253	207	290	229	83	0.725	71.9	
	286	540	199	289	254	90	0.709	70.6	
	355	598	158	269	243	111	0.914	84.8	76.5
24 hours	173	391	148	271	218	123	1.128	96.9	
	152	457	172	320	305	148	0.970	88.3	
	15	192	233	316	177	83	0.938	86.3	
	311	587	196	316	276	120	0.870	82.0	
	121	332	197	311	211	114	1.081	94.4	
	20	259	190	313	239	123	1.029	91.7	
	312	562	189	318	250	129	1.032	91.8	
	146	353	193	302	207	109	1.053	93.0	90.8
48 hours	20	268	180	310	248	130	1.048	92.7	
	364	594	192	311	230	119	1.035	92.0	
	23	251	179	305	228	126	1.105	95.7	
	372	575	197	302	203	105	1.034	91.9	
	79	316	189	308	237	119	1.004	90.2	
	361	583	197	309	222	112	1.009	90.5	92.2
virgin	63	286	146	281	223	135	1.211	100.9	
	86	303	156	281	217	125	1.152	98.1	
	349	560	144	283	211	139	1.318	105.6	
	48	267	148	283	219	135	1.233	101.9	
	355	575	162	278	220	116	1.055	93.0	
	338	546	178	309	208	131	1.260	103.1	
	38	260	179	308	222	129	1.162	98.6	
	341	558	175	307	217	132	1.217	101.2	100.7

Sample G: **30 min desktop corona aged**

Recovery time	X1	X2	Y1	Y2	ΔX	ΔY	tan (theta/2)	theta (degrees)	average
1 min								completely flat	
30 min	67	473	217	296	406	79	0.389	42.5	
	92	424	192	299	332	107	0.645	65.6	
	114	448	207	289	334	82	0.491	52.3	
	138	496	230	287	358	57	0.318	35.3	
	101	456	216	284	355	68	0.383	41.9	
	80	479	224	297	399	73	0.366	40.2	
	74	514	232	291	440	59	0.268	30.0	
	83	477	239	287	394	48	0.244	27.4	41.9
1 hour	8	301	202	282	293	80	0.546	57.3	
	335	602	192	281	267	89	0.667	67.4	
	34	283	187	282	249	95	0.763	74.7	
	328	612	195	280	284	85	0.599	61.8	
	156	452	207	277	296	70	0.473	50.6	
	197	467	203	276	270	73	0.541	56.8	
	122	404	214	280	282	66	0.468	50.2	
	116	469	202	274	353	72	0.408	44.4	
	90	473	203	274	383	71	0.371	40.7	
	117	393	188	266	276	78	0.565	59.0	56.3
3 hours	9	271	165	276	262	111	0.847	80.6	
	328	590	173	275	262	102	0.779	75.8	
	11	282	191	265	271	74	0.546	57.3	
	377	598	188	264	221	76	0.688	69.0	
	105	336	192	280	231	88	0.762	74.6	
	361	590	181	278	229	97	0.847	80.5	
	131	415	201	304	284	103	0.725	71.9	
	157	474	207	303	317	96	0.606	62.4	
	30	303	201	294	273	93	0.681	68.5	71.3
	353	604	199	290	251	91	0.725	71.9	71.3
24 hours	24	271	173	297	247	124	1.004	90.2	
	330	597	168	297	267	129	0.966	88.0	
	7	274	159	293	267	134	1.004	90.2	
	314	587	154	288	273	134	0.982	88.9	
	61	312	185	309	251	124	0.988	89.3	
	320	586	177	306	266	129	0.970	88.3	
	334	587	169	296	253	127	1.004	90.2	89.3
48 hours	39	253	193	302	214	109	1.019	91.1	
	52	275	182	302	223	120	1.076	94.2	
	350	587	180	299	237	119	1.004	90.2	
	23	240	196	300	217	104	0.959	87.6	
	347	572	188	298	225	110	0.978	88.7	
	103	299	189	301	196	112	1.143	97.6	
	334	556	185	301	222	116	1.045	92.5	91.5
virgin	25	254	197	329	229	132	1.153	98.1	
	354	582	199	327	228	128	1.123	96.6	
	3	213	199	321	210	122	1.162	98.6	
	51	273	179	308	222	129	1.162	98.6	
	344	548	190	308	204	118	1.157	98.3	
	65	275	193	313	210	120	1.143	97.6	
	351	547	199	311	196	112	1.143	97.6	97.9

Sample I: **30 min desktop corona treated**

Recovery time	X1	X2	Y1	Y2	ΔX	ΔY	tan (theta/2)	theta (degrees)	average
1 min								complete flat	
30 min	95	442	248	318	347	70	0.403	43.9	
	133	437	196	270	304	74	0.487	51.9	
	165	458	191	272	293	81	0.553	57.9	
	106	414	200	268	308	68	0.442	47.6	
	54	500	213	263	446	50	0.224	25.3	
	137	478	189	261	341	72	0.422	45.8	
	124	503	202	256	379	54	0.285	31.8	
	66	444	203	254	378	51	0.27	30.2	
	90	447	203	255	357	52	0.291	32.5	40.8
1hour	133	408	194	270	275	76	0.553	57.9	
	135	462	182	283	327	101	0.618	63.4	
	139	428	195	280	289	85	0.588	60.9	
	101	465	193	276	364	83	0.456	49	
	74	415	202	273	341	71	0.416	45.2	
	116	415	186	265	299	79	0.528	55.7	
	129	534	186	260	405	74	0.365	40.1	
	137	508	182	250	371	68	0.367	40.3	51.6
3 hours	2	271	165	264	269	99	0.736	72.7	
	347	601	168	266	254	98	0.772	75.3	
	22	270	164	264	248	100	0.806	77.8	
	2	262	174	258	260	84	0.646	65.7	
	348	605	179	255	257	76	0.591	61.2	
	4	299	173	263	295	90	0.61	62.8	
	323	599	165	260	276	95	0.688	69.1	
	10	319	169	252	309	83	0.537	56.5	
	340	608	174	247	268	73	0.545	57.2	66.5
24 hours	337	575	168	281	238	113	0.95	87	
	10	284	157	276	274	119	0.869	82	
	323	587	151	280	264	129	0.977	88.7	
	57	300	161	274	243	113	0.93	85.8	
	332	599	166	276	267	110	0.824	79	
	37	275	167	271	238	104	0.874	82.3	
	337	584	163	271	247	108	0.874	82.3	
	229	441	155	258	212	103	0.972	88.4	84.4
48 hours	322	565	145	276	243	131	1.078	94.3	
	40	267	152	281	227	129	1.137	97.3	
	332	566	155	279	234	124	1.06	93.3	
	45	269	159	274	224	115	1.027	91.5	
	317	547	151	272	230	121	1.052	92.9	
	72	280	155	268	208	113	1.087	94.7	
	166	380	136	263	214	127	1.187	99.8	
	92	300	180	301	208	121	1.163	98.6	95.2
virgin	390	589	180	305	199	125	1.256	103	
	372	562	191	301	190	110	1.158	98.4	
	37	236	184	290	199	106	1.065	93.6	
	371	570	182	294	199	112	1.126	96.8	
	57	260	178	296	203	118	1.163	98.6	
	308	486	183	295	178	112	1.258	103.1	
	370	580	179	311	210	132	1.257	103	99.8

Sample J: **30 min desktop corona aged**

Recovery time	X1	X2	Y1	Y2	ΔX	ΔY	Tan (theta/2)	Theta (degrees)	average
1 min								completely flat	
30 min	152	453	198	277	301	79	0.525	55.4	
	118	454	229	284	336	55	0.327	36.3	
	2	582	201	260	580	59	0.203	23.0	
	64	543	204	252	479	48	0.200	22.7	
	6	613	199	257	607	58	0.191	21.6	
	36	514	198	258	478	60	0.251	28.2	31.2
1 hour	114	389	153	253	275	100	0.727	72.1	
	151	447	170	252	296	82	0.554	58.0	
	103	397	178	253	294	75	0.510	54.1	
	128	427	187	251	299	64	0.428	46.4	
	147	453	201	255	306	54	0.353	38.9	
	101	499	205	268	398	63	0.317	35.1	
	144	455	201	260	311	59	0.379	41.6	
	56	450	207	274	394	67	0.340	37.6	47.9
3 hours	10	234	121	222	224	101	0.902	84.1	
	324	557	131	229	233	98	0.841	80.1	
	67	289	205	287	222	82	0.739	72.9	
	320	571	201	291	251	90	0.717	71.3	
	2	280	208	298	278	90	0.647	65.8	
	347	606	230	295	259	65	0.502	53.3	
	170	446	228	304	276	76	0.551	57.7	
	5	278	205	284	273	79	0.579	60.1	
	312	604	209	285	292	76	0.521	55.0	66.7
24 hours	1	258	181	296	257	115	0.895	83.7	
	354	611	186	294	257	108	0.840	80.1	
	340	587	196	312	247	116	0.939	86.4	
	18	258	184	300	240	116	0.967	88.1	
	350	587	200	299	237	99	0.835	79.8	
	6	265	212	322	259	110	0.849	80.7	
	314	577	212	323	263	111	0.844	80.3	
	334	597	207	311	263	104	0.791	76.7	
	132	384	207	313	252	106	0.841	80.1	
	348	590	156	281	242	125	1.033	91.9	82.7
48 hours	35	287	160	289	252	129	1.024	91.3	
	346	584	174	294	238	120	1.008	90.5	
	48	300	166	291	252	125	0.992	89.5	
	325	562	171	290	237	119	1.004	90.2	
	53	286	167	295	233	128	1.099	95.4	
	366	590	176	298	224	122	1.089	94.9	
	21	251	184	298	230	114	0.991	89.5	
	345	586	175	298	241	123	1.021	91.2	91.6
virgin	29	230	172	291	201	119	1.184	99.6	
	180	408	160	284	228	124	1.088	94.8	
	347	577	150	279	230	129	1.122	96.6	
	74	254	171	276	180	105	1.167	98.8	
	353	556	158	275	203	117	1.153	98.1	
	111	299	201	309	188	108	1.149	97.9	
	351	556	195	308	205	113	1.102	95.6	
	73	264	201	312	191	111	1.162	98.6	
	326	537	198	314	211	116	1.100	95.4	97.3

Sample F: **30 min desktop corona aged**

Recovery time	X1	X2	Y1	Y2	ΔX	ΔY	tan (theta/2)	theta (degrees)	average
1 min								completely flat	
30 min	116	502	212	295	386	83	0.430	46.5	
	75	395	207	296	320	89	0.556	58.2	
	60	414	214	298	354	84	0.475	50.8	
	32	600	248	300	568	52	0.183	20.8	
	109	591	263	306	482	43	0.178	20.2	
	192	474	200	282	282	82	0.582	60.4	
	104	416	218	294	312	76	0.487	51.9	47.0
1 hour	2	234	177	275	232	98	0.845	80.4	
	336	595	169	275	259	106	0.819	78.6	
	21	257	188	282	236	94	0.797	77.1	
	316	595	186	279	279	93	0.667	67.4	
	17	273	203	290	256	87	0.680	68.4	
	296	563	203	286	267	83	0.622	63.7	
	89	519	234	293	430	59	0.274	30.7	
	107	514	236	294	407	58	0.285	31.8	
	156	433	204	291	277	87	0.628	64.3	62.5
3 hours	4	251	167	275	247	108	0.874	82.3	
	298	541	167	278	243	111	0.914	84.8	
	41	277	174	286	236	112	0.949	87.0	
	298	546	181	285	248	104	0.839	80.0	
	28	280	187	287	252	100	0.794	76.9	
	331	583	191	287	252	96	0.762	74.6	
	176	423	204	288	247	84	0.680	68.4	
	130	462	234	290	332	56	0.337	37.3	
	151	424	178	286	273	108	0.791	76.7	74.2
24 hours	43	293	174	300	250	126	1.008	90.5	
	361	603	186	304	242	118	0.975	88.6	
	76	320	191	312	244	121	0.992	89.5	
	348	579	207	316	231	109	0.944	86.7	
	25	265	204	314	240	110	0.917	85.0	
	333	585	208	315	252	107	0.849	80.7	
	11	266	217	332	255	115	0.902	84.1	
	319	589	222	331	270	109	0.807	77.8	
	99	470	247	346	371	99	0.534	56.2	
	141	412	213	334	271	121	0.893	83.5	82.3
virgin	32	277	162	286	245	124	1.012	90.7	
	335	576	164	283	241	119	0.988	89.3	
	380	583	187	297	203	110	1.084	94.6	
	64	290	152	283	226	131	1.159	98.4	
	357	574	151	282	217	131	1.207	100.7	
	55	278	150	286	223	136	1.220	101.3	
	105	316	151	282	211	131	1.242	102.3	
	351	565	149	276	214	127	1.187	99.8	97.3

Sample M: **30 min desktop corona aged**

Recovery time	X1	X2	Y1	Y2	ΔX	ΔY	Tan (theta/2)	Theta (degrees)	average
1 min								completely flat	
30 min	147	530	201	272	383	71	0.37	40.7	
	106	511	209	272	405	63	0.31	34.6	
	45	502	207	283	457	76	0.33	36.8	
	63	492	221	287	429	66	0.31	34.2	
	70	478	214	271	408	57	0.28	31.2	
	119	466	217	273	347	56	0.32	35.8	
	153	456	207	269	303	62	0.41	44.5	
	120	418	203	257	298	54	0.36	39.8	37.2
1 hour	20	293	192	260	273	68	0.5	53	
	329	584	192	259	255	67	0.53	55.4	
	37	307	199	259	270	60	0.44	47.9	
	317	602	203	261	285	58	0.41	44.3	
	16	280	202	266	264	64	0.49	51.7	
	325	604	198	263	279	65	0.47	50	
	1	286	200	271	285	71	0.5	53	
	321	614	196	271	293	75	0.51	54.2	51.2
3 hours	12	228	202	280	216	78	0.72	71.7	
	275	517	201	275	242	74	0.61	62.9	
	58	323	212	295	265	83	0.63	64.1	
	337	587	218	296	250	78	0.62	63.9	
	352	594	222	291	242	69	0.57	59.4	
	16	306	201	295	290	94	0.65	65.9	
	311	602	199	299	291	100	0.69	69	
	29	294	201	291	265	90	0.68	68.4	
	313	582	201	291	269	90	0.67	67.6	65.9
24 hours	330	600	167	285	270	118	0.87	82.3	
	38	273	175	283	235	108	0.92	85.2	
	371	600	188	281	229	93	0.81	78.2	
	64	277	195	290	213	95	0.89	83.5	
	346	572	187	288	226	101	0.89	83.6	
	81	299	185	289	218	104	0.95	87.3	
	334	547	187	286	213	99	0.93	85.8	
	202	417	191	284	215	93	0.87	81.7	83.4
virgin	3	220	138	258	217	120	1.11	95.8	
	292	519	141	260	227	119	1.05	92.7	
	281	479	148	257	198	109	1.1	95.5	
	50	283	162	284	233	122	1.05	92.6	
	328	544	170	282	216	112	1.04	92.1	
	81	299	161	276	218	115	1.06	93.1	
	331	529	167	280	198	113	1.14	97.6	
	68	243	190	303	175	113	1.29	104.5	
	323	547	169	302	224	133	1.19	99.8	96

Appendix B

EDAX results of field-aged PDMS samples

EDAX results of blue silicone insulator aged at KIPS for 1 year

Element	Unaged blue insulator 5000X		Top polluted as received 5000X		Top cleaned heat + 2x US $CHCl_3$ 5000X		Bottom polluted as received 5000X		Bottom cleaned heat + 2x US $CHCl_3$ 5000X	
% Oxide	10KV	20KV	10KV	20KV	10KV	20KV	10KV	20KV	10KV	20KV
0	22.3	29.2	37.5	44.5	38.9	27.0	17.5	36.8	38..6	24.2
Na			2.5	2.6	1.4	1.4	0.4	1.0	2.5	1.7
Mg			1.9	2.8	1.2	1.4	0.8	1.2	1.8	1.2
Al	25.8	26.0	7.5	3.6	14.0	20.4	10.5	10.1	8.3	17.3
Si	50.5	44.5	41.2	43.0	39.9	41.5	40.6	36.7	41.5	44.0
S					0.8	0.7	1.7	2.5	0.7	0.8
Cl			1.9	2.8	2.9	5.0	0.8	3.2	4.8	7.7
K			2.1	0.2	0.2	0.6	8.3	1.4	0.5	0.5
Ca			2.1	0.5	0.5	0.6		7.2	0.5	1.0
Ti			3.74	0.1	0.1		19.4			
Si/Al	2.0	1.7	5.5	11.0	2.9	2.0	3.9	3.6	5.0	2.5
Si/O	2.3	1.5	1.1	1.0	1.0	1.5	2.3	1.0	1.1	1.8

EDAX results of dark grey silicone insulator aged at KIPS for 1 year

Element	**Unaged dark grey insulator 5000X**		**Top polluted as received 5000X**		**Top cleaned heat + 2x US $CHCl_3$ 5000X**		**Bottom polluted as received 5000X**		**Bottom cleaned heat + 2x US $CHCl_3$ 5000X**	
% Oxide	10KV	20KV	10KV	20KV	10KV	20KV	10KV	20KV	10KV	20KV
0	42.5	25.1	36.8	22.1	39.7	24.0	46.1	29.3	38.6	26.0
Na			1.5	1.0	1.0	0.4	1.7	1.0	0.9	0.7
Mg			1.6	1.5	2.7	1.9	1.7	0.9	2.8	1.9
Al	14.2	21.3	8.9	18.7	7.8	12.7	7.3	16.0	7.6	14.7
Si	40.6	48.3	40.4	44.7	35.7	40.4	37.5	41.4	42.1	47.7
S			1.1	1.9	3.9	5.6	0.7	1.1	1.3	1.3
Cl			5.9	5.7	4.1	5.2	2.6	4.7	4.3	4.5
K			0.9	0.7	1.2	0.8	0.2	0.6	0.8	0.7
Ca			1.9	2.8	3.0	7.9	1.6	4.1	0.8	1.1
Fe			0.5	0.8	0.6	0.6	0.2	0.8	0.3	0.7
Zn			0.5	0.3	0.2	0.5	0.3	0.2	0.4	0.8
Si/Al	2.9	2.3	4.5	2.4	4.6	3.2	5.1	2.6	5.5	3.2
Si/O	1.0	1.9	1.1	2.0	0.9	1.7	0.8	1.4	1.1	1.8

Appendix C

Degree of degradation of PDMS calculated by the ratio of peak height and area

Integration points	3375		2963		1656	
	3690-3036 Height		3010-2930 Height		1800-1550 Area	
	total	corrected	total	corrected	total	corrected
30 min corona aged C	17.49	2.21	7.23	9.25	9895.73	467.57
Unaged C	23.5	1.15	9.38	12.55	12555.7	290.72
Ratio (Ho-H)/Ho	0.26	-0.92	0.23	0.26	0.21	-0.61
Ratio (H/Ho)	0.74	1.92	0.77	0.74	0.79	1.61
30 min corona aged D	23.92	3.69	13.45	12.96	16393.6	599.66
Unaged D	28.36	1.42	13.59	13.4	13704.8	287.48
Ratio (Ho-H)/Ho	0.16	-1.6	0.01	0.03	-0.2	-1.09
Ratio (H/Ho)	0.84	2.6	0.99	0.97	1.2	2.09
30 min corona aged E	47.47	5.34	37.42	13.88	19030.4	430.97
Unaged E	62.83	3.41	51.98	12.58	20193.2	181.29
Ratio (Ho-H)/Ho	0.24	-0.57	0.28	-0.1	0.06	-1.38
Ratio (H/Ho)	0.76	1.57	0.72	1.1	0.94	2.38
30 min corona aged G	52.76	3.95	41.61	12.66	18363.8	298.47
Unaged G	17.78	1.8	6.97	10.08	11602.4	326.49
Ratio (Ho-H)/Ho	-1.97	-1.19	-4.97	-0.26	-0.58	0.09
Ratio (H/Ho)	2.97	2.19	5.97	1.26	1.58	0.91
30 min corona aged I	30.44	3.75	23.22	9.41	17060.4	359.54
Unaged I	77.26	2.03	70.42	7.33	21767.7	70.34
Ratio (Ho-H)/Ho	0.61	-0.85	0.67	-0.28	0.22	-4.11
Ratio (H/Ho)	0.39	1.85	0.33	1.28	0.78	5.11

Continuation of the table

Integration points	3375		2963		1656	
	3690-3036 Height		3010-2930 Height		1800-1550 Area	
	total	corrected	total	corrected	total	corrected
30 min corona J	12.87	2.978	8.34	6.44	13208	547.98
Unaged J	32.04	4.42	21.88	12.86	16652	381.68
Ratio (Ho-H)/Ho	0.60	0.33	0.62	0.50	0.21	-0.44
Ratio (H/Ho)	0.40	0.67	0.38	0.50	0.79	1.44
10 h French corona J	88.7	5.06	60.01	6.83	20102	219.07
Unaged J	81.78	9.25	20.63	12.12	16652	381.68
Ratio (Ho-H)/Ho	-0.08	0.45	-1.91	0.44	-0.21	0.43
Ratio (H/Ho)	1.08	0.55	2.91	0.56	1.21	0.57
30 min corona M	77.71	11.69	29.71	3.87	16082	386.53
Unaged M	67.43	17.45	14.48	3.91	12992	314.87
Ratio (Ho-H)/Ho	-0.15	0.33	-1.05	0.01	-0.24	-0.23
Ratio (H/Ho)	1.15	0.67	2.05	0.99	1.24	1.23
600 UV-C aged M	86.13	7.98	38.38	1.92	23135.2	145.38
Unaged M	67.43	17.54	14.48	3.91	20886.4	257.93
Ratio (Ho-H)/Ho	-0.28	0.55	-1.65	0.51	-0.11	0.44
Ratio (H/Ho)	1.28	0.45	2.65	0.49	1.11	0.56

Note:

H is peak height before ageing and H_o is peak height after ageing.